Diagnostic Model Study of Seasonal Variation of Global Ozone and Antarctic Ozone Hole

秋吉, 英治
九州大学理学研究科物理学専攻

https://doi.org/10.11501/3088101

出版情報：九州大学, 1991, 博士（理学）, 課程博士
バージョン：
権利関係：

Diagnostic Model Study of Seasonal Variation of Global Ozone and Antarctic Ozone Hole

秋　吉　芙　治

(1)

Diagnostic Model Study of Seasonal Variation of Global Ozone and Antarctic Ozone Hole

by

Hideharu AKIYOSHI

Kyushu University

1991

CONTENTS

ABSTRACT

A simple 2-D model is constructed in order to simulate and understand global ozone distribution and its seasonal variation. In the model, the Chapman cycle parameterized by Hartmann (1978) is used. The time dependence of diffusion coefficients is neglected except in the both polar regions. Effects of the meridional circulation consisting of the following three components are taken into account; 1) an annually varying component due to the annual variation of the ozone, oxygen, and water vapor heating, which is assumed to be anti-symmetric about the equator, 2) a nonseasonal, steady component of the transport circulation which ascends in the tropics and descends in the middle latitudes and high latitudes of the both hemispheres, 3) an annually varying component of the transport circulation which represents the planetary wave activity, strong convection in the tropics and some other seasonally variable factors. Although the employed circulations and diffusion coefficients are empirical, and the various processes behind them are not sufficiently evaluated except for the first component of the circulation, the simple model can well simulate the global ozone distribution and its seasonal variation.

The Antarctic ozone hole is discussed from a global point of view. A possibility of a weak October minimum of the Antarctic total ozone amount without chlorine chemistry is suggested. It is shown that a simple chlorine catalytic chemistry taken into account in the model can induce a depletion of the Antarctic total

ozone amount as low as 150 D.U. at a time scale of 1 month. It is also shown that the dynamical ozone depletion due to the upward motion during the Antarctic spring is thermodynamically impossible.

1. INTRODUCTION

Chubachi (1984) and Farman et al. (1985) found unusual decrease in ozone during Antarctic spring. Analyzing the Dobson spectrophotometer data or the satellite data, many scientists reported the fact that the ozone depletion had occurred every year since 1980 and become severer (Gardiner and Shanklin, 1986; Stolarski et al., 1986; Schoeberl and Krueger, 1986; Chandra and McPeters, 1986; Komhyr et al., 1986, 1987, 1988a, 1989a; Krueger et al., 1988). Now, the ozone depletion is well known as the Antarctic ozone hole. The ozone hole phenomenon has given us an opportunity to rethink about the global ozone distribution and the behavior of the Antarctic ozone from the dynamical, chemical, and radiative view points. At the early stages, three sorts of the hypotheses were proposed in order to explain the sudden decrease in ozone during the Antarctic spring. First, we briefly review them from the point of view of the seasonal variation of ozone.

The first one of the hypothesis is the dynamical hypothesis proposed by Tung et al. (1986). They thought that the Antarctic stratosphere temperature was nearly in a radiative equilibrium in late winter and early spring, and the ozone depletion in spring might be caused by the upward motion of the air due to the sudden increase in the solar heating. The upward motion rather than the local temperature increase tends to occur in the Antarctic atmosphere, because in September, the temperature of the Antarctic atmosphere is prevented from increasing by the flywheel effect of

the middle atmosphere through the thermal wind equation and the continuity equation (Tung et al., 1986; Mahlman and Fels, 1986; Fels et al., 1980). Thus, the local temperature in the Antarctic may be controlled predominantly by a longer dynamical time scale, so that the evolution of temperature may be suppressed. The induced upward motion brings the ozone-poor air from the troposphere up to the lower stratosphere, and carries off the ozone-rich air in the stratosphere out of the polar vortex. Shi et al. (1986) showed that if the aerosol loading in the stratosphere was large, the upward motion due to the solar heating and the thermal heating could occur in the Antarctic spring. However, we should note that there is not so much amount of aerosol during the ozone hole, because PSCs (Polar Stratospheric Cloud) begin to evaporate and disappear in September and October, and we also should note that there is much uncertainty of the optical property of the stratospheric aerosol (McCormick and Trepte, 1987). Akiyoshi et al. (1988, 1989) performed similar radiative calculations more accurately by using the NMC (National Meteorological Center) temperature data and the extinction data derived from SAGE II (Stratospheric Aerosol and Gas Experiment II) observations in 1985. They concluded that the net heating due to the aerosols did not exceed 0.1 K d^{-1}, even if some ambiguous parameters such as the aerosol composition and the size distribution were chosen so that they might magnify the heatings. The results of these calculations are shown in Appendix A. The result of the N_2O observation by Parrish et al. (1988) during the ozone hole is also

against the upward motion hypothesis. In addition, this hypothesis cannot explain such a severe depletion of ozone in the narrow altitude range from 11 km to 23 km as observed in the Antarctic. Thus, all these results suggest that the upward motion hypothesis is irrelevant to the ozone hole.

The second one is a chemical hypothesis based on the solar 11-year cycle, which was proposed by Callis and Natarajan (1986). When the solar activity is high, more odd nitrogen is produced in the polar thermosphere by the reactions of fast electrons with N_2 molecules or by the photodissociation of N_2 molecules. N_2O_5 and NO_3 are produced, while the produced odd nitrogen is transported from the thermosphere into the stratosphere by the downward motion in the polar vortex during the polar night. When the sun comes up, the NO_3 and N_2O_5 are photodissociated, and NO and NO_2 are, as a result, produced. Then, ozone will be destroyed by the anomalous high concentration of NO and NO_2. The downward motion in the polar vortex is a key point of the unusual seasonal variation of ozone in this hypothesis. This hypothesis expects that NO_x will increase within the polar vortex during the polar night, and also expects that ozone will be destroyed severely between the altitude of 16 km and 32 km. However, the results of AAOE (Airborne Antarctic Ozone Experiment) campaign, which was conducted in 1987, were against this hypothesis. It was found that the concentration of NO_x was extremely low within the polar vortex, and the ozone was destroyed severely in the lower stratosphere between 11 km and 23 km (Toon et al., 1989; Hofmann et

al., 1989; Komhyr et al., 1989b). Thus, this hypothesis is not acceptable. And it also seems to be impossible that the decrease in ozone at the middle latitude after the final warming is caused by the high concentration of NO_x flowing out of the polar vortex.

The third one is a chemical hypothesis related to some chlorine catalytic cycles. People pay much attention to this hypothesis, since the production of chlorofluorocarbon has been increasing more and more recently. The chlorofluorocarbons produced at the ground surface ascend slowly in the atmosphere, and are photodissociated and extricate chlorine atoms in the upper stratosphere, which destroy ozone catalytically. A catalytic cycle

$$Cl + O_3 \rightarrow ClO + O_2$$
$$ClO + O \rightarrow Cl + O_2$$

$$\text{net}: \quad O_3 + O \rightarrow 2O_2$$

is well known (e.g. Molina and Rowland, 1974; Cicerone et al., 1974; Crutzen, 1974; Wofsy et al., 1975). However, this cycle does not work effectively in the lower stratosphere, since the number density of atomic oxygen is low there. In addition, the condition of the low sun elevation in the Antarctic spring may prevent the production of the atomic oxygen. Hence, some other catalytic cycles must be considered in order to explain the destruction of ozone between 11 km and 23 km high. Today, three

catalytic cycles are considered to be effective in the lower stratosphere. The first one is the chlorine catalytic cycle with OH and HO_2, which was proposed by Solomon et al. (1986).

$$OH + O_3 \rightarrow HO_2 + O_2$$
$$Cl + O_3 \rightarrow ClO + O_2$$
$$HO_2 + ClO \rightarrow HOCl + O_2$$
$$HOCl + h\nu \rightarrow OH + Cl$$

$$\text{net} : \quad 2O_3 \rightarrow 3O_2$$

ClO reacts with HO_2 in stead of atomic oxygen in this cycle, and it is assumed that HO_2 is produced dominantly by the reaction of OH with O_3. Austin et al. (1989) reported that this cycle could contribute only about 10 % to the net ozone destruction in their model. The second one is the chlorine-bromine catalytic cycle proposed by McElroy et al. (1986).

$$Br + O_3 \rightarrow BrO + O_2$$
$$Cl + O_3 \rightarrow ClO + O_2$$
$$BrO + ClO \rightarrow Cl + O_2 + Br$$

$$\text{net} : \quad 2O_3 \rightarrow 3O_2$$

The reaction of BrO with ClO is the rate limiting step in this cycle. This cycle works effectively in very high concentrations

of both ClO and BrO. Actually, extremely high concentration of ClO (about 1000 ppbv at 18 km) was observed within the Antarctic polar vortex (Brune et al., 1989b). But, the concentration of BrO was not so high, and about 5 pptv (Brune et al., 1989a). And hence, this cycle also can contribute only about 10 % to the net ozone destruction (Austin et al., 1989; Ko et al., 1989). The third one is the Cl_2O_2 (ClO dimer) catalytic cycle proposed by Molina and Molina (1987).

$$2\,(\,Cl + O_3 \rightarrow ClO + O_2\,)$$

$$ClO + ClO + M \rightarrow Cl_2O_2 + M$$

$$Cl_2O_2 + h\nu \rightarrow Cl + ClOO$$

$$ClOO + M \rightarrow Cl + O_2 + M$$

$$\text{net}: \quad 2\,O_3 \rightarrow 3\,O_2$$

ClO forms the dimer in the low temperature field within the Antarctic polar vortex. This cycle has been believed to be the most effective one since AAOE campaign. And many calculations were performed based on this catalytic cycle in order to simulate the Antarctic ozone hole (e.g. Ko et al., 1989; Austin et al., 1989). McGrath et al. (1988) calculated thermochemical stabilities and vibrational spectra of the isomers of Cl_2O_2 using ab-initio molecular orbital calculations. They concluded that an isomer ClOOCl, which can produce chlorine atom more easily, is more stable than ClOClO, showing the validity of the above ozone

destruction catalytic cycle. Eberstein (1990), however, pointed out the possibility that more ClO rather than ClOO might be produced by the photodissociation of Cl_2O_2 in the Antarctic spring lower stratosphere, even if the molecular structure of Cl_2O_2 was ClOOCl. In order to determine accurately the destruction rate of ozone by the ClO dimer catalytic cycle, it seems to be important to investigate the molecular structure of Cl_2O_2, and the strength of the Cl-O bond and O-O bond empirically and theoretically.

These chlorine catalytic cycles work efficiently, if abundant chlorine atom is supplied by the photolysis of Cl_2, $ClNO_2$, or HOCl, which easily release chlorine atom only by absorbing a weak solar radiation just after the polar night. In the normal situation of winter lower stratosphere, however, there is not enough amount of Cl_2, $ClNO_2$, or HOCl for the ozone destruction, because the chlorine atoms are stored in the form of so called reservoirs such as HCl and $ClNO_3$. These reservoirs are chemically stable, and hard to release the chlorine atoms. Thus, some other mechanisms are necessary for changing the reservoirs to some sorts of more chemically active species such as Cl_2, $ClNO_2$, and HOCl. Today, some heterogeneous reactions of the reservoir species with water, ice, or hydrochloric acid on PSCs are known as the mechanisms. These are;

$$ClNO_3 + H_2O(\text{aerosol}) \rightarrow HOCl + HNO_3$$

$$ClNO_3 + HCl(\text{aerosol}) \rightarrow Cl_2 + HNO_3$$

$$N_2O_5 + H_2O(\text{aerosol}) \rightarrow 2HNO_3$$

$$N_2O_5 + HCl(\text{aerosol}) \rightarrow ClNO_2 + HNO_3$$

(Tung et al., 1986; Solomon et al., 1986; McElroy et al., 1986; Rodriguez et al., 1986). Sticking coefficients of these heterogeneous reactions were measured by Tolbert et al (1987, 1988) and by Leu (1988). One problem is that they used much larger and much more plain ice surface than the real PSC for the measurement, which will give a smaller value than the real value of it.

The sudden ozone depletion in the Antarctic spring can be explained as follows by the chlorine catalytic cycle; Within the cold polar vortex during the Antarctic winter, the reservoir species are transformed into more chemically active substances such as Cl_2, $ClNO_2$, and HOCl by the heterogeneous reactions on the PSCs, while NO_x is decreased by the heterogeneous reactions which produce HNO_3 in the PSCs. When the sun returns in the Antarctic in September, Cl_2, $ClNO_2$, and HOCl are photodissociated, and chlorine atoms are released. These chlorine atoms destroy ozone catalytically in the low concentration of NO_x, because in the normal concentration of NO_x in the stratosphere a quick reaction of ClO with NO_2 prevents the catalytic cycle from destroying ozone effectively.

The results of AAOE (1987) support the hypothesis. In this experiment, unusually high concentration of ClO, low concentration of NO_x, and nitric acid aerosols were detected within the

polar vortex where ozone was depleted severely.

All these dynamical and chemical hypotheses try to explain the sudden ozone decrease in the Antarctic during September, based on the local return of the sunlight in the Antarctic spring: The local, sudden increase in the solar energy input is an important factor to explain the unusual seasonal variation of the Antarctic ozone.

Next, we review these hypotheses again from a point of view of year-to-year variation.

The upward motion hypothesis expected that the increase in the stratospheric aerosols due to the eruption of Mt. El Chichon in 1982 had caused a larger heating in the spring of the Antarctic stratosphere since 1982, and thereby, caused stronger upward motion there (Tung et al., 1986). However, this explanation is not acceptable, because in spite of the fact that the stratospheric loading of aerosols in the Antarctic has been decreasing since 1983, severer ozone hole events occurred in 1985 and 1987.

On the other hand, the solar 11-year cycle hypothesis stressed that the solar activity, which can be estimated with the sun spot number, caused the year-to-year variation of the ozone depletion. This hypothesis, however, cannot explain the severer ozone hole in 1985 and 1987, when the solar activity was near a minimum, than in 1980 when the solar activity reached a maximum. Moreover, the ozone hole in 1990 was much severer than the 1980 ozone hole, although the magnitudes of the solar activity of these years are almost same.

According to the chlorine catalytic hypothesis, it is deduced that the increase in the use of chlorofluorocarbon has caused the ozone hole for the last 10 years. So far, this is consistent with the observations, which show chlorofluorocarbons in the stratosphere have been increased in the Antarctic (Cronn et al., 1986), and still increasing (Aoki et al., 1990). However, the relationship between the amount of the Antarctic ozone and the chlorofluorocarbons before 1980 is not evident because of the lack of the observations.

More comprehensive insight into the year-to-year variation of the ozone hole was first obtained by Mahlman and Fels (1986). They showed quantitatively some expected stratospheric consequences, under the necessary requirement of a recent substantial reduction of the wintertime planetary-scale disturbance activity in the southern hemisphere troposphere. This requirement is based on the measurement of Eliassen-Palm flux convergence (Nagatani and Miller, 1987). And the most important consequence of them is an increase in the length of the Antarctic winter, that is, longer duration of the cold polar vortex. The longer existence of the polar vortex in spring makes various unusual stratospheric conditions: It may strengthen westerly wind in October and November, and the temperature consequently may remain cold, under the thermal wind relationship. Besides, the stable polar vortex may prevent the diffusion of heat, ozone, NO_x and other chemical constituents from the middle latitude region. In the lower temperature environment formed like this, PSC may be

formed easily, and some heterogeneous reactions and the chlorine catalytic cycles may destroy ozone more and more effectively. In addition, a GCM (General Circulation Model) experiment shows that the ozone depletion over the Antarctic may extend the period of the Antarctic winter, and may delay the breakdown of the Antarctic polar vortex, because less ozone amount prevents the increase in temperature during the Antarctic spring (Kiehl et al., 1988). Thus, it is possible that both less planetary wave activity and less ozone amount accelerate further the depletion of the Antarctic ozone by enhancing the activity of heterogeneous chemistry through the lower temperature. It seems that the increase in the amount of chlorofluorocarbons and the decrease in the planetary scale wave activities are the key points of the year-to-year variation. Many observations and analyses have been performed on these issues (Chandra and McPeters, 1986; Komhyr et al., 1986; McCormick and Trepte, 1987; Kawahira and Hirooka, 1989).

The year-to-year variation of ozone is, moreover, related to QBO (Quasi-Biannual Oscillation) (Hasebe, 1983; Lait et al., 1988; Gray and Pyle, 1988; Garcia and Solomon, 1987; Dunkerton, 1988). During the westerly phase of QBO, the induced downward motion at the equator causes an upward motion in the subtropics. Since the descending arm of the Hadley cell extends to middle latitude, the suppression of the strength of the Hadley circulation during the westerly phase of the QBO results in a negative anomaly of ozone in the middle latitudes. The ozone anomaly is

then transferred farther poleward by the eddy motions, so that the polar ozone shows a negative anomaly in the westerly phase of QBO. In addition to this mechanism, a QBO signal in temperature in polar region modulates the formation of PSC, and consequently, modulates the destruction rate of ozone.

The understanding of the year-to-year variation of ozone is very important, since it makes the prediction of the future trend of ozone distribution possible. But we have not yet completely solved the problem. At least, a two-dimensional interactive dynamical chemical radiative models are necessary for the study of the year-to-year global ozone trend. The ozone molecules absorb the solar energy, heat the atmosphere, and induce the air motion. A feedback of the induced motion to the ozone distribution changes the ozone radiation process, so that an accurate calculation of radiation transfer will be necessary.

Tung and Yang (1988) formulated a nonlinear and non-geostrophic model in an isentropic coordinate. Although they used observed temperature as the input data, both advective transport and diffusive transport were determined in a self-consistent manner from the temperature data, together with the prediction of ozone and other radiatively important gases. Brasseur et al. (1990) also developed a nonlinear interactive chemical dynamical radiative two-dimensional model. They used the log-pressure coordinate and specified the vertical wind velocity at 15 km high as a function of latitude and season. These interactive type models are called as the third generation model (Tung, 1987).

These phenomena tell us how directly the polar ozone is influenced by the middle latitude ozone and middle latitude dynamical processes, and how indirectly influenced by the equatorial wind. The amount of polar ozone is more dynamically controlled than that in the middle latitude and in the equatorial region, because of the less amount of sunlight and the smaller area. The difference in the severity of ozone depletion between in the Arctic and in the Antarctic reveals these factors. It was reported by AASE (Airborne Arctic Stratospheric Expedition) Campaign that the Arctic ozone hole was not so severe, not so extended, and did not last so continuously as the Antarctic ozone hole, because of more active atmospheric disturbances due to the planetary waves in the northern hemisphere stratosphere (e.g. Turco et al., 1990). The AASE campaign and AAOE campaign have revealed that the severe ozone depletion over the Antarctic is an extreme case which is caused by the combined effects of the strong, local chemical ozone sink and the weakened ozone transport from the middle latitude region. Thus, in order to understand the Antarctic ozone hole correctly, we have to understand how the global ozone is produced and distributed latitudinally, vertically, and seasonally.

A theoretical study of the distribution of global ozone was recently done by Hou et al. (1991). They explained the difference in the distribution of the total ozone amount between the both hemispheres, using an interactive 2-D model of Schneider et al. (1989). Performing various numerical experiments on some ideal-

ized hypothetical conditions, they showed that the chemistry and dynamics in the lower stratosphere produced a subpolar maximum of the total ozone amount in the absence of planetary wave forcing, and also showed that a polar maximum of the total ozone amount in the winter and spring of the northern hemisphere appeared as a result of the stronger wave driving in the northern hemisphere.

The purpose of this study is to understand the seasonal variation of global ozone and in particular to understand the seasonal variation of the Antarctic ozone, and to make the first step for the dynamical-chemical-radiative comprehensive understanding of the Antarctic ozone hole from a global point of view.

The model used in this study belongs to the second generation 2-D model, mentioned by Tung (1987) in which the transformed Eulerian mean circulation and a symmetric diffusion tensor are specified independently on the calculated ozone distribution. However, in some aspects, our model is different from the second generation model. In this study, we shall concentrate to understand the seasonal cycle of global ozone and the Antarctic ozone hole by introducing a seasonal variation of meridional circulations, eddy diffusion, and chemical reactions.

In the next chapter, the basic theoretical framework of our simple 2-D model is described. In Chapter 3, simulations are carried out, in which various factors such as vertical and horizontal eddy diffusions and meridional circulations are introduced one by one to the model. Discussing the discrepancy between the simulated distributions of ozone and the observation, we try

to get essential roles of these factors to the seasonal variation of global ozone distribution. In Chapter 4, based on the results of the previous section, we focus on the seasonal variation of ozone in the Antarctic, and show how dramatically the Antarctic spring ozone decreases if we consider the effect of ozone destruction due to the chlorine catalytic cycle. In Chapter 5, we discuss the Antarctic ozone hole from a global point of view. The capacity of our model and its limitations are also mentioned. Chapter 6 is devoted to the conclusion and remarks.

2. THEORETICAL FRAMEWORK AND GENERAL MODEL DESCRIPTION

The mixing ratio of odd oxygen (= $O+O_3$) following the motion of an individual air parcel is expressed by the following equation,

$$\frac{d\chi}{dt} = S, \tag{2.1}$$

where, χ is the volume mixing ratio of the odd oxygen, and S the source and sink of the odd oxygen. In Eulerian framework, equation (2.1) is expressed as follows,

$$\frac{\partial\chi}{\partial t} + u\frac{\partial\chi}{\partial x} + v\frac{\partial\chi}{\partial y} + w\frac{\partial\chi}{\partial z} = S, \tag{2.2}$$

where $dx=a\cdot\cos\phi\cdot d\lambda$, $dy=a\cdot d\phi$, a is the radius of the earth, λ longitude, ϕ latitude, and z altitude. The continuity equation of the atmosphere for the synoptic scale motions on log-pressure coordinate is

$$\frac{\partial u}{\partial x} + \frac{\partial v}{\partial y} + \frac{1}{P}\frac{\partial}{\partial z}(Pw) = 0. \tag{2.3}$$

Combining equation (2.2) and (2.3), the equation written by a flux form,

$$\frac{\partial \chi}{\partial t} + \frac{\partial}{\partial x}(\chi u) + \frac{\partial}{\partial y}(\chi v) + \frac{1}{P}\frac{\partial}{\partial z}(P\chi w) = S$$

is obtained. Separating χ into the zonally averaged part $\bar{\chi}$ and the deviation from it χ', and taking the zonal average of the above equation, we get the following zonal-mean equation,

$$\frac{\partial \bar{\chi}}{\partial t} + \bar{v}\frac{\partial \bar{\chi}}{\partial y} + \bar{w}\frac{\partial \bar{\chi}}{\partial z}$$

$$= \bar{S} - \frac{1}{\cos\phi}\frac{\partial}{\partial y}\left(-\cos\phi\, K_{yy}\frac{\partial \bar{\chi}}{\partial y} - \cos\phi\, K_{yz}\frac{\partial \bar{\chi}}{\partial z}\right)$$

$$- \frac{1}{P}\frac{\partial}{\partial z}\left(-P\, K_{zy}\frac{\partial \bar{\chi}}{\partial y} - P\, K_{zz}\frac{\partial \bar{\chi}}{\partial z}\right), \qquad (2.4)$$

where second order correlation terms, $\overline{\chi' v'}\cos\phi$ and $P\overline{\chi' w'}$, are expressed by an eddy diffusion form,

$$-\cos\phi\, K_{yy}\frac{\partial \bar{\chi}}{\partial y} - \cos\phi\, K_{yz}\frac{\partial \bar{\chi}}{\partial z},$$

and

$$-P\, K_{zy}\frac{\partial \bar{\chi}}{\partial y} - P\, K_{zz}\frac{\partial \bar{\chi}}{\partial z},$$

respectively. K_{yy}, K_{yz}, K_{zy}, and K_{zz} are eddy diffusion coefficients. In the presence of planetary waves, most part of the anti-symmetric part of the eddy diffusion tensor can be expressed by the Stokes' drift (Matsuno, 1980). Thus, in the transformed Eulerian framework, in which the mean meridional circulation is replaced by the residual mean circulation defined by Andrews and McIntyre (1976), only the symmetric part of the eddy diffusion tensor is needed. The residual mean circulation can be estimated directly from the knowledge of the Eulerian mean diabatic heating and static stability (Dunkerton, 1978). In this model, in addition to the Eulerian mean meridional circulation we consider transport meridional circulations, so that only the symmetric eddy diffusion tensor is considered. The value of eddy diffusion coefficients and the meridional circulations in the present model will be described specifically in each numerical experiment in Chapter 3.

If the residual mean circulation, the eddy diffusion coefficients, and the zonally averaged chemical source term are given as a function of latitude, altitude, and time, we can calculate numerically the odd oxygen mixing ratio $\overline{\chi}$ as a function of latitude, altitude, and time. In the real atmosphere, the circulation and the eddy diffusion are closely related each other, and related to the ozone distribution. In the present model, however, the circulation and the eddy diffusion are prescribed as some external parameters, and hence, this model is not a consistently closed system. But, this model is adequate to the present

purpose.

We shall solve equation (2.4) on the uniform grid points with horizontal resolution of 5 degrees of latitude and vertical resolution of 2.5 km. The region of the numerical integration is between -90 degrees and +90 degrees of latitude and between the surface and 70 km high on the log-pressure coordinate. The equation (2.4) is solved every 20 minutes. However, the sun elevation and the duration of sun shine are calculated and renewed every 10 days. The eddy diffusion coefficients are renewed every month. These time-intervals are sufficient to study the seasonal variation of ozone. The horizontal fluxes of the odd oxygen at the both poles are assumed to be zero. At the ground level, a fixed (latitudinally independent) deposition velocity of ozone is used (=0.08 cm s^{-1}; Cunnold et al., 1975). It can be assumed that this value is nearly equal to the deposition velocity for odd oxygen, since the concentration of atomic oxygen is much smaller than that of ozone at the ground surface. Above 70 km, the concentration of ozone is fixed at the calculated value by a one-dimensional radiative convective photochemical model (Brasseur and Solomon; 1986, Appendix D), because the chemistry used in the present model is not applicable to the simulation of ozone at the higher altitude. The diurnal variation of the photochemistry is not considered. But, the diurnal average of the photon number absorbed by ozone and oxygen molecules is calculated.

3. SIMULATIONS OF SEASONAL VARIATION OF GLOBAL OZONE DISTRIBUTION

In this chapter, we show the results of some simulations which are performed by introducing some factors one by one which control ozone distribution. Comparing them to the observations, we try to understand the seasonal variation of ozone comprehensively.

3-a) Photochemical Equilibrium

Model Description

Although there are many chemical reactions in the atmosphere which are involved with ozone production or destruction (e.g. Brasseur and Solomon, 1986), only the Chapman cycle is considered. That is,

$$O_2 + h\nu_2 \rightarrow 2\,O \qquad (q_2)$$

$$O_3 + h\nu_3 \rightarrow O_2 + O \qquad (q_3)$$

$$O + O_2 + M \rightarrow O_3 + M \qquad (k_{12})$$

$$O + O_3 \rightarrow 2\,O_2 \qquad (k_{13}),$$

Where h is Planck's constant, ν_2 the spectral frequencies of Schumann-Runge continuum absorption (126 nm$<\lambda<$175 nm), Schumann-Runge bands absorption (175 nm$<\lambda<$205 nm), and Herzberg continuum absorption (205 nm$<\lambda<$240 nm), and ν_3 the spectral frequencies

of Hartley continuum absorption (175 nm<λ <320 nm), Huggins bands absorption (320 nm<λ <350 nm), and Chappius bands absorption (450 nm<λ <750 nm).

The ozone mixing ratio in photochemical equilibrium is estimated by the formula

$$\chi_{O_3} = n_{O_2}\sqrt{\frac{q_2\, k_{12}}{q_3\, k_{13}\, n_m}}\,, \tag{3a.1}$$

where n_m and n_{o2} are the number density of any arbitrary atom or molecule, and oxygen molecule, respectively, and q_i (i=1, 2, 3) the photon number absorbed by a molecular O_i (i=1, 2, 3) per unit time. q_i is expressed as

$$q_i(\phi, z, t, \lambda) = F_o(\lambda, t)\,\frac{hc}{\lambda}\,\sigma_{Oi}(\lambda)$$
$$\cdot \exp\left[-\int_z^\infty \sigma_{O_2}(\lambda)\, n_{O_2}(\phi, z, t)\, dz - \int_z^\infty \sigma_{O_3}(\lambda)\, n_{O_3}(\phi, z, t)\, dz\right]$$
$$+ (\text{reflection from the surface})\,, \tag{3a.2}$$

where $F_o(\lambda, t)$ is the solar flux at the top of the atmosphere at wavelength λ and time t, $\sigma_{o_i}(\lambda)$ (i=1, 2, 3) the absorption cross section of a molecular O_i (i=1, 2, 3) at wavelength λ, and $n_{oi}(\phi, z, t)$ the number density of O_i at latitude ϕ, altitude

z, and time t. The data of $F_o(\lambda)$, $\sigma_{O_2}(\lambda)$, and $\sigma_{O_3}(\lambda)$ are taken from Strobel (1978). The quantities of $\sigma_{O_2} \cdot n_{O_2}$ and $\sigma_{O_3} \cdot n_{O_3}$ are integrated over the light path between the point in question and the top of the model atmosphere (100 km), and the integration depends on the zenith angle as well as altitude. The first term of equation (3a.2) is written in a more practical form as follows,

$$q_i(\phi, z_\ell, t, \lambda) = F_o(\lambda, t) \frac{hc}{\lambda} \sigma_{Oi}(\lambda)$$

$$\cdot \exp\left[-\sigma_{O_2}(\lambda) \sum_{i=\ell+1}^{N} (n_{O_2}(\phi, z_i, t)\, \Delta z_i/\mu_i) - \sigma_{O_3}(\lambda) \sum_{i=\ell+1}^{N} (n_{O_3}(\phi, z_i, t)\, \Delta z_i/\mu_i)\right] \times CF,$$

$$CF = \frac{1. - \exp\left[-\sigma_{O_2}(\lambda)\, n_{O_2}(\phi, z_\ell, t)\, \Delta z_\ell/\mu_\ell - \sigma_{O_3}(\lambda)\, n_{O_3}(\phi, z_\ell, t)\, \Delta z_\ell/\mu_\ell\right]}{\sigma_{O_2}(\lambda)\, n_{O_2}(\phi, z_\ell, t)\, \Delta z_\ell/\mu_\ell + \sigma_{O_3}(\lambda)\, n_{O_3}(\phi, z_\ell, t)\, \Delta z_\ell/\mu_\ell},$$

(3a.3)

where l is the layer number of the homogeneous atmospheric layer in question, μ_l cosine of the zenith angle of the direct solar beam at the lth layer, and N the total number of the layers. CF in equation (3a.3) is the correction factor for the optical thick layers in which the solar beam is extinguished seriously. Equation (3a.3) gives accurately the layer-averaged number of photons absorbed by an ozone molecule or an oxygen molecule in the lth uniform layer per unit time. (See Appendix B.)

The effect of the reflection of the sunlight at the surface is also considered. At first, photochemical equilibrium ozone concentration without the reflection is predicted from the top of the atmosphere to the surface. Then, the ozone concentration is corrected by considering the reflection light at the surface and the optical depth from the surface to the altitude in question which can be temporarily estimated by the first approximation of ozone concentration. And the correction is iterated until the value converges. We assume that the surface is a Lambertian reflector and the albedo is fixed at 0.3. Integration over the zenith angle is executed by using 3-point Gaussian integral formula, for the sake of saving CPU time. The value of 0.3 is a little high for the globally averaged surface albedo, but more appropriate for the planetary albedo, which includes the effects of the reflection by the ground surface, sea surface, clouds, the atmosphere, etc. Although we use the value as a surface albedo in this model, the calculated values of the ozone heating and ozone photochemical source term will not be so seriously different from the values which are calculated by using a more realistic value of the surface albedo (a lower value than 0.3) and by using a complex radiative transfer scheme which includes the cloud effect, because most of clouds exist below 10 km high, while most of ozone exists above that altitude, and the ozone below 10 km is predominantly controlled by dynamics. For the ozone calculation, it is possible to consider the value of 0.3 as a planetary albedo including the effects of cloud reflection.

We consider the dependence of the zenith angle on altitude, but sunrise and sunset occur simultaneously at all altitudes. The diurnal variation of q_1 is not considered, but the diurnal average of q_1 is used. The diurnal average is obtained by averaging the number of the absorbed photons over four zenith angles spaced between sunrise and noon, multiplying the double of this average by the proportion of daytime to 24 hours. And this value is applied over the entire day.

Although the Chapman cycle is very simple and useful for the qualitative understanding of the ozone photochemistry, it is known that the predicted ozone concentration is twice or three times larger than the observed value in the stratosphere and mesosphere. In order to avoid this quantitative defect of the Chapman cycle, we use the Chapman cycle parameterized by Hartmann (1978), in which the catalytic destructions of ozone due to HO_x and NO_x are included. In the parameterization, the rate constant k_{13} is adjusted such that the following conditions are satisfied;

1) The temperature dependence of ozone concentration is approximately that expected from more complete chemistry and from observations.

2) Ozone and temperature distributions of the radiative photochemical equilibrium state are realistic.

The normal value of $1.5\times 10^{-11}\cdot e^{-2218/T}$ cm^3 s^{-1} for k_{13} is replaced by the larger value of $3.5\times 10^{-12}\cdot e^{-1300/T}$ cm^3 s^{-1}. Then, the value of $1.1\times 10^{-34}\cdot e^{510/T}$ cm^6 s^{-1} is used for k_{12}. The photochemical equilibrium profile is consequently much better

than the profile of the normal Chapman cycle as shown in Figure 3.1.

Solar elevation angle α at the ground surface and the duration of sunshine T are calculated by considering the day of year and the latitude, and by using the formula

$$\sin\alpha = \sin\phi \cdot \sin\delta + \cos\phi \cdot \cos\delta \cdot \cos h ,$$

and

$$T = \frac{24}{\pi} \cos^{-1}\left(-\frac{\sin\phi}{\cos\phi}\frac{\sin\delta}{\cos\delta}\right),$$

where ϕ is latitude, δ declination angle, and hour angle h is expressed by

$$h = 15\frac{\pi}{180}\,(\text{local time} - 12\ \text{hours}).$$

In order to calculate the seasonal variation of the photochemical equilibrium ozone, we need the seasonal variation of temperature. Seasonal variation of temperature and the zonal-mean circulation are calculated by the linear quasi-geostrophic system on the log-pressure coordinate. That is,

$$\frac{\partial\bar{u}}{\partial t} - f\bar{v} = -\frac{1}{\rho}\frac{\partial}{\partial z}\left(-\nu\rho\frac{\partial\bar{u}}{\partial z}\right) - k_M\bar{u}, \qquad (3a.4)$$

$$f\bar{u} = -\frac{\partial \bar{\Phi}}{\partial y}, \tag{3a.5}$$

$$\frac{1}{\cos\phi}\frac{\partial}{\partial y}(\cos\phi\,\bar{v}) + \frac{1}{\rho}\frac{\partial}{\partial z}(\rho\bar{w}) = 0, \tag{3a.6}$$

$$\frac{\partial}{\partial t}\left(\frac{\partial \bar{\Phi}}{\partial z}\right) + N^2\bar{w} = \bar{Q}_{ext} - k_H\frac{\partial \bar{\Phi}}{\partial z}, \tag{3a.7}$$

where $\bar{u}$, $\bar{v}$, and $\bar{w}$ are eastward, northward, and upward wind velocity, respectively. $\bar{\Phi}$ the perturbation of geopotential height which is related to the atmospheric temperature $\bar{T}$ by $d\bar{\Phi} = -R\cdot\bar{T}\cdot d\ln P$, $\bar{Q}_{ext}$ the external heating function by the absorption of the solar radiation, f Coriolis parameter, N Brunt-Väisälä frequency, ν vertical eddy diffusion coefficient, k_M Rayleigh friction coefficient, and k_H Newtonian cooling coefficient. Hereafter, the zonal-mean symbol "-" is omitted for simplicity and convenience. Figure 3.2a illustrates the vertical profile of N(z) used in this model, while Figure 3.2b illustrates the profiles of ν (z) and k_H(z), respectively. Note that ν (z) is a global representative of vertical eddy diffusion coefficient and it is different from the latitudinally dependent vertical eddy diffusion coefficient $K_{zz}(\phi, z)$ which will be used to calculate ozone transport. The values of k_H(z) above 30km are the same as those of Matsuno (1982), which were taken from Dickinson (1973)

except for the upper part above 70 km high where a constant value of 0.03 K d^{-1} is used. Below 30 km, the values are similar to those used by Trenberth (1973). The linear expression of infrared cooling is questionable in the troposphere. However, considering the perturbation from the radiative-convective equilibrium temperature due to latent heat, boundary layer heating, and radiation, we use the vertical profile with the minimum value of 0.02 K d^{-1} at 120 mb and the value of 0.08 K d^{-1} at 600 mb. The value of 0.08 K d^{-1} is assumed below 600 mb. Rayleigh friction coefficient $k_M(z)$ which is the same value as Matsuno (1982) is used to decelerate the zonal wind near the mesopause.

Eliminating u, v, and w from equations (3a.4)-(3a.7), and using the quasi-geostrophic approximation, we obtain the well-known quasi-geostrophic potential vorticity equation,

$$\frac{\partial}{\partial t}\left[\frac{1}{\rho}\frac{\partial}{\partial z}\left(\frac{\rho}{N^2}\frac{\partial \Phi}{\partial z}\right)+L(\Phi)\right]=\frac{1}{\rho}\frac{\partial}{\partial z}\left(\frac{\rho}{N^2}Q_{ext}\right)$$

$$-\frac{1}{\rho}\frac{\partial}{\partial z}\left(\frac{\rho}{N^2}k_H\frac{\partial \Phi}{\partial z}\right)-k_M L(\Phi)+\frac{1}{\rho}\frac{\partial}{\partial z}\left(\nu\rho\frac{\partial}{\partial z}L(\Phi)\right),$$

where

$$L(\phi)=\frac{1}{4\omega^2a^2}\frac{1}{\cos\phi}\frac{\partial}{\partial\phi}\left(\frac{\cos\phi}{\sin\phi}\frac{\partial}{\partial\phi}\right).$$

Then $\Phi(\phi, z, t)$ can be solved by a method of separation of vari-

able in ϕ , z, and t (Matsuno, 1982), if we assume a sinusoidal time-dependence in Φ , and expand the external heating function Q_{ext} in terms of the eigenfunctions of the operator $L(\phi)$, which are well known as Hough Functions. Since we are interested in the annual oscillation, the time-dependent parts of Φ and Q_{ext} are assumed to be $\exp(i\sigma t)$, where $\sigma = 2\pi$ /year. This is a zonal-mean, annual oscillation version of the tidal equation (Sawada and Matsushima, 1964; Plumb, 1982; Garcia, 1987). Each mode of anti-symmetric eigenfunction of $L(\phi)$ and its equivalent depth are calculated by applying the tidal theory (Lindzen and Chapman, 1969) to the annual zonal-mean oscillation. They are tabulated in Table 3.1.

The altitude-dependent parts of the external heating functions $Q_n(z)$ corresponding to the nth mode are obtained as follows: First, we calculate the atmospheric heating rate due to the absorption of the solar radiation by the ozone, oxygen, and water vapor as a function of time, latitude, and altitude. The calculation of the ozone heating rate is performed in the same way as the calculation of photon number described in this section, in which we consider the reflection sunlight from the surface, and we use SBUV (Solar Backscattered UltraViolet) global ozone data in 1979 above 100 mb (McPeters et al, 1984) and ECC (Electrochemical Concentration Cell) ozone sonde data in 1985-1987 below 100 mb (obtained by Komhyr et al.) in order to avoid the inaccurate satellite ozone data in the troposphere. The solar heating due to water vapor is roughly estimated by using the

results of Yamamoto (1962), and the solar heating due to oxygen molecules is calculated by using oxygen partial pressure and its absorption cross section data (Strobel, 1978). Then, we calculate the amplitude of annual component of the heating rate as a function of latitude and altitude by using Fourier transformation. The heating rate is subjected to Fourier expansion by using Hough modes, and $Q_n(z)$ are obtained as the Fourier coefficients. In Figure 3.3a, the distributions of the annual component of the ozone heating at 15 km at the northern summer solstice are shown. The top panel shows the original heating rate, the middle is the heating rate represented by the gravest anti-symmetric Hough mode alone, and the bottom is the one represented by the sum of the 10 anti-symmetric Hough modes. And Figure 3.3b shows the distributions of the annual component of the ozone heating at 50 km. As shown in these figures, the expansion using up to 10 anti-symmetric modes is sufficient to the present heating.

Above 65.0 km, we assume $Q_{ext}(\phi, z)=HOU_{o1}(\phi)\cdot Q_{o1}(z)/HOU_{o1}(\phi=90^{\circ})$, where $HOU_{o1}(\phi)$ is the gravest mode of the anti-symmetric Hough function and $Q_{o1}(z)=8\cdot\exp(-((z-50\ km)/17\ km)^2)$, because if we use $Q_n(z)$ obtained from the SBUV ozone data or from the ozone concentration of a one-dimensional radiative convective photochemical model, unusually large amplitude of the annual variation of temperature is obtained above 65.0 km, as shown in Figure 3.4. Figure 3.4 also shows the revised $Q_{o1}(z)$ (solid line) which includes the effect of the water vapor heating below 37.5 km. And Figure 3.5 shows the latitudinal distribution of $\sum_{n=1}^{10} Hou_n($

ϕ)$\cdot Q_n(z)$ at 15 km which includes the effect of the water vapor heating. We use the revised $Q_n(z)$ for the following calculations.

Using the $Q_n(z)$, the altitude-dependent part of the nth mode of Φ_n ($=A\cdot U_n(z)$) can be determined by the equation

$$\frac{1}{P}\frac{d}{dz}\left\{\left(\frac{i\sigma+k_H}{N^2}+\frac{\nu}{gh_n}\right)P\frac{dU_n(z)}{dz}\right\}-\frac{i\sigma+k_M}{gh_n}U_n(z)$$
$$=\frac{1}{A}\frac{1}{P}\frac{d}{dz}\left(\frac{P}{N^2}Q_n(z)\right),$$

where h_n is the equivalent depth of mode n, and A is the normalization factor which is chosen $2\omega a/1.6$ (=580.6; Matsuno, 1982). Finally, Φ , T, u, v, and w are expressed as follows;

$$\Phi(\phi,z,t)=A\sum_{n=1}^{10}Hou_n(\mu)\,|U_n(z)|\cos(\sigma t+\theta_n),$$

$$T(\phi,z,t)=T_0(z)+\frac{H_0}{R}A\sum_{n=1}^{10}Hou_n(\mu)\frac{d}{dz}|U_n(z)|\cos(\sigma t+\theta_n),$$

$$u(\phi,z,t)=-\frac{A}{2\omega a}\frac{\cos\phi}{\sin\phi}\sum_{n=1}^{10}\frac{d}{d\mu}(Hou_n(\mu))\,|U_n(z)|\cos(\sigma t+\theta_n),$$

$$w(\phi,z,t)=\frac{1}{N^2}\left\{\sum_{n=1}^{10}Hou_n(\mu)\,Q_n(z)\cos(\sigma t)\right.$$
$$\left.+(\sigma-k_H)A\sum_{n=1}^{10}Hou_n(\mu)\frac{d}{dz}|U_n(z)|\cos(\sigma t-\theta_n)\right\},$$

$$v(\phi,z,t) = \frac{a}{\cos\phi}\int_{-90^\circ}^{\phi}\left\{\frac{\cos\phi}{H_o}w(\phi,z,t) - \cos\phi\,\frac{\partial w(\phi,z,t)}{\partial z}\right\}d(a\phi),$$

where H_o is the scale height of the atmosphere (=7 km), R the gas constant of the dry air, and $T_o(z)$ the vertical temperature profile of U. S. Standard Atmosphere (1962). The calculated temperature T is used to calculate the seasonal variation of the photochemical equilibrium of ozone concentration. v and w in the above equations will be used in subsection 3-c).

Results and Discussion

The temperature distribution calculated by the anti-symmetric Hough functions mentioned above is used for the calculation of the seasonal variation of the photochemical equilibrium ozone in this experiment. The calculated temperature distribution at the northern hemisphere summer solstice is shown in Figure 3.6. The temperature in the stratosphere and mesosphere is well simulated, while in the troposphere, the discrepancy between the real temperature and the calculated one is large. But, this is not a serious problem in order to simulate ozone in the troposphere, because real distribution of ozone in the troposphere is far from the photochemical equilibrium, and predominantly con-

trolled by some dynamical processes (e.g. see Figure 3.1 and Figure 1 of Solomon et al., 1985).

Figure 3.7 illustrates the time-latitude cross section of the calculated total ozone amount in Dobson unit. The calculated total ozone amount varies in accordance with the seasonal variation of the amount of the solar radiation at each latitude. Figure 3.8 shows the total ozone amount for 1986 in Dobson unit observed by TOMS (Total Ozone Mapping Spectrometer). The observed total ozone amount shows more complicated behavior, implying the importance of dynamical effects: In the northern hemisphere, there is a spring maximum of the total ozone amount in the high latitude region. The annual component of the seasonal variation of the total ozone amount is dominant except in the tropics. On the other hand in the southern hemisphere, there is a spring maximum in the middle latitude, and the annual component of the seasonal variation in the high latitude is not clear.

Figure 3.9 shows the latitudinal distributions of the calculated total ozone amount and the observed ones in January, April, July, and October. The observed SBUV data in 1979 are quoted from McPeters et al. (1984). The excessive ozone (about 320 D.U.) is obtained in the equatorial region, and much less ozone (less than 100 D.U.) is obtained in the both Polar regions(*), while the ob-

---

(*)Non-zero ozone amount during the polar night is due to the rather coarse time resolution Δt=10 days used for the calculation of the seasonal variation of the solar elevation angle and the duration of sunshine in this model, since the time scale of ozone production/loss in the Chapman cycle during the polar night is infinite, and a small amount of ozone during that time is the one at a day between 10 days and 1 day before the polar night begins.

servation shows the peaks of the total ozone amount (350 D.U.~ 450 D.U.) in the middle or high latitude regions.

Figure 3.10 shows the seasonal variations of the calculated total ozone amount and the observed ones at 85°S, 75°S, the equator, and 75°N. We can see that the seasonal variation of the total ozone amount at each latitude is considerably different from the observation except at the equator. And the amount of ozone is far from the observed value in the middle and high latitude regions.

Figure 3.11 illustrates the vertical distributions of the calculated ozone concentration and the observed ones in October at 85°S, 45°S, the equator, and 75°N. The calculated ozone concentration in the troposphere is much lower than the observed one, because the Chapman cycle is inactive in this region and the vertical transport of ozone is neglected in this calculation. On the other hand, the ozone between 10 km and 25 km high is overestimated in the low latitudes. The calculated ozone concentration in the lower stratosphere of the high latitude regions is much less than the observed one.

The ozone concentration in the middle and upper stratosphere is well simulated at all latitudes. As shown in Figure 3.12, the seasonal variation is also well simulated in this region. For example, a summer minimum and a winter maximum of the ozone concentration at 50 km, and a winter minimum at 35 km are well simulated. The ozone variation at 50 km predominantly results from the seasonal variation of temperature at that altitude, and the

ozone variation at 35 km results from the seasonal variation of the amount of the solar ultraviolet radiation at that altitude.

Based on the results of the present calculation, it is considered that Hartmann's parameterization is adequate up to 60 km. The large discrepancy between the observed ozone and the calculated ozone at the troposphere and the lower stratosphere shows the importance of the dynamical effects.

To close this subsection, it is noteworthy that the reflection of the solar radiation from the surface reduces the ozone amount. If the reflection from the surface is neglected, the ozone amount increases a little as shown in Figure 3.13. The solar radiation at the wavelength less than 240 nm, which can produce ozone, is absorbed in the atmosphere and does not reach the surface. Thus, the reflected light consists of the spectra which cannot produce ozone through the oxygen photodissociation, but can photodissociate ozone molecules. Therefore, the surface reflection causes the net reduction of the ozone amount.

3-b) Vertical Transport

The photochemical equilibrium calculation shown above shows the importance of dynamical effects on the ozone distribution in the troposphere and lower stratosphere. In this subsection, the effect of the vertical eddy transport of ozone is considered.

Model Description

The odd oxygen mixing ratio is calculated by integrating the following equation numerically over 3 years.

$$\frac{\partial \chi_{Ox}(\phi,z,t)}{\partial t} = S_{Ox}(\phi,z,t) - \frac{1}{P}\frac{\partial}{\partial z}\left(-P K_{zz}(\phi,z)\frac{\partial \chi_{Ox}(\phi,z,t)}{\partial z}\right), \quad (3b.1)$$

where $\chi_{ox}(\phi,z,t)$ is the zonal-mean odd oxygen (O_x=O+O_3) mixing ratio, $S_{ox}(\phi,z,t)$ the photochemical source term of odd oxygen, and $K_{zz}(\phi,z)$ vertical eddy diffusion coefficient which is assumed to be independent of time. The photochemical source term is calculated by the same method used in the previous subsection. As the vertical eddy diffusion coefficients below 30 km, we use the annually averaged values of $K_{zz}(\phi,z,t)$, of which monthly values were calculated by Plumb and Mahlman (1987) with GFDL (Geophysical Fluid Dynamics Laboratory) 11-level GCM. The meridional distribution of the annual average of K_{zz} is shown in Figure 3.14. Above 30 km, where no $K_{zz}(\phi,z,t)$ data are obtained by the GCM, K_{zz} is assumed to have the same value as ν (z) in subsection 3-a) which is used to calculate the seasonal variation of temperature.

Ozone mixing ratio is estimated by assuming photochemical equilibrium in atomic oxygen below 60 km and photochemical equilibrium in ozone between 60 km and 70 km. Above 70 km, atomic oxygen and ozone concentration is fixed at a constant value

(Brasseur and Solomon, 1986; Appendix D). At the surface, the vertical diffusive flux of odd oxygen is specified as a boundary condition. Since the odd oxygen concentration at the ground level is nearly equal to the ozone concentration, we can use there the value of the vertical diffusive flux of ozone in stead of the value of the odd oxygen. The boundary condition is obtained by equating the downward flux of ozone to the surface destruction rate, which is assumed to be proportional to the ozone concentration,

$$K_{zz} \frac{\partial \chi_{O_3}}{\partial z} = f \chi_{O_3}, \quad at \ z=0 . \tag{3b.2}$$

We use a globally averaged value of 0.08 cm s^{-1} for f (Cunnold et al., 1975).

Results and Discussion

Figure 3.15 shows time-latitude cross section of the calculated total ozone amount. In this experiment, the total ozone amount is mainly controlled by the amount of the solar radiation and the height of tropopause which is parameterized by the height of K_{zz} minimum. A higher tropopause causes less total ozone amount on the same photochemical condition, because the ozone is rapidly diffused from the high concentration region into the troposphere and destroyed at the surface. Thus, the ozone amount

in the low latitude region (220 D.U.) is less than that of the photochemical equilibrium case (320 D.U.) due to the higher tropopause there. On the other hand, the total ozone amount is more than the photochemical equilibrium case in the high latitude region, because ozone is mainly produced at the high altitude and diffused downward to the lower stratosphere where photochemical equilibrium concentration of ozone is very low.

Figure 3.16 shows latitudinal distributions of the calculated total ozone amount and the observed ones in the four different months. The rather rough latitudinal distribution of the total ozone amount is a direct manifestation of the latitudinal distribution of the K_{zz} used in the model. The excess of ozone in the low latitudes in the photochemical equilibrium case (Figure 3.9) is improved by including the eddy transport of ozone and the dissipation process at the ground. In the middle and high latitude regions, however, the total ozone amount is still much less than the observed value. The latitudinal local maximum of the total ozone amount corresponds to the latitudinal local minimum of the tropopause height, and vice versa.

Figure 3.17 shows seasonal variations of the calculated total ozone amount and the observed ones at the some latitudes. The pattern of the seasonal variation at each latitude is basically similar to the photochemical equilibrium case, and is not improved by including the vertical transport except at the equator. The amplitude of the seasonal variation of the total ozone amount is smaller than that of the photochemical equilibrium case. This

is due to the use of nonseasonal vertical eddy transport and a constant ozone deposition velocity at the surface.

Figure 3.18 shows the vertical distributions of the calculated ozone concentration and the observed ones at the some latitudes in October. As shown in this figure, the lack of the total ozone amount is due to the lack of ozone below 20 km in the middle latitudes and below 30 km in the high latitudes. The value of the vertical eddy diffusion coefficient used in this model is considered to be adequate, so that the lack of ozone in these regions must be supplied horizontally from the low latitude region. It is also shown that the calculated vertical distribution of ozone concentration at the equator are generally improved. The result shows, as the first approximation, that the ozone distribution in the tropics is explained by a photochemical ozone source in the stratosphere and an ozone sink at the ground.

3-c) Meridional Circulation and Horizontal Diffusion

Model Description

In this model, we consider the horizontal transport of ozone by the meridional circulation due to the ozone, oxygen, and water vapor heating, and by the horizontal diffusion. The zonal-mean continuity equation of the odd oxygen mixing ratio is expressed by the following equation (see (2.4)),

$$\frac{\partial \chi_{Ox}(\phi,z,t)}{\partial t} + v(\phi,z,t)\frac{\partial \chi_{Ox}(\phi,z,t)}{\partial y} + w(\phi,z,t)\frac{\partial \chi_{Ox}(\phi,z,t)}{\partial z}$$

$$= S(\phi,z,t) - \frac{1}{\cos\phi}\frac{\partial}{\partial y}\left\{-\cos\phi\, K_{yy}(\phi,z)\frac{\partial \chi(\phi,z,t)}{\partial y} - \cos\phi\, K_{yz}(\phi,z)\frac{\partial \chi(\phi,z,t)}{\partial z}\right\}$$

$$-\frac{1}{P}\frac{\partial}{\partial z}\left\{-P K_{zy}(\phi,z)\frac{\partial \chi(\phi,z,t)}{\partial y} - P K_{zz}(\phi,z)\frac{\partial \chi(\phi,z,t)}{\partial z}\right\},$$

(3c.1)

where $K_{yy}(\phi,z)$, $K_{yz}(\phi,z)$ (= $K_{zy}(\phi,z)$), and $K_{zz}(\phi,z)$ are the time-independent eddy diffusion coefficients which are obtained by averaging annually the Plumb and Mahlman's monthly $K_{yy}(\phi,z,t)$, $K_{yz}(\phi,z,t)$ (=$K_{zy}(\phi,z,t)$), and $K_{zz}(\phi,z,t)$. The annually averaged $K_{yy}(\phi,z)$ in the stratosphere is modified as follows: The values of $K_{yy}(\phi,z)$ less than 1×10^6 m^2 s^{-1} in the stratosphere are set at 1×10^6 m^2 s^{-1}, because the K_{yy} of the order of 10^6 m^2 s^{-1} is necessary at least at the middle latitudes to simulate a realistic distribution of the total ozone amount, and because the high values of K_{yy} at the middle latitude were obtained by Yang et al. (1990) from an analysis using their model. The meridional distributions of K_{yy} and K_{yz} used in this model are shown in Figure 3.19.

In this experiment, as the first approximation, we only con-

sider the anti-symmetric circulation caused by the atmospheric heating due to the ozone, oxygen, and water vapor. The quasi-geostrophic meridional circulations $v(\phi, z, t)$ and $w(\phi, z, t)$ are calculated by the method mentioned in subsection 3-a). Figure 3.20 illustrates the circulation at the summer solstice. The air ascends in the summer hemisphere, crosses the equator, descends in the winter hemisphere, and comes back to the summer hemisphere in the lower altitude. The representative values of u, v, w, and T at the summer solstice are tabulated in Table 3.2.

The calculation method of photochemical term and boundary conditions are the same as those of the previous subsections.

Results and Discussion

The time-latitude cross section of the calculated total ozone amount is shown in Figure 3.21. Compared to the vertical transport case, the maxima in the spring at the middle latitudes and the minima in the fall at the both polar regions are clearly seen. It is also noted that in the both polar regions ozone in the winter increases due to the downward motion of the circulation, while in summer hemisphere, the no ozone decrease due to the upward motion of the circulation is appreciable, since the ozone is controlled photochemically as well as dynamically in summer.

The observed and calculated latitudinal distributions of the total ozone amount in the four different months are shown in

Figure 3.22. The latitudinal distribution of the total ozone amount is smoother than the vertical transport case because of the inclusion of the horizontal diffusion. The ozone amount around 25°N and 25°S is reduced, while the ozone at the equator and in the high latitude is increased instead. As a result, it has weak local maxima around 45°N and 45°S. In the tropics, the calculated total ozone amount is in good agreement with the observed values, while there is still serious discrepancy between them especially in the high latitudes.

The observed and calculated seasonal variations of the total ozone amount at the some latitudes are shown in Figure 3.23. As shown in this figure, the total ozone amount and its seasonal variation is in fairly good agreement with the observation over the equator. The total ozone amount at the polar region shows the fall minimum, while the total ozone amount is very low as mentioned earlier. A weak "October minimum" of the total ozone amount occurs between the summer maximum due to the active photochemistry and the winter maximum due to the enhanced downward motion of the anti-symmetric circulation. But, this minimum is very small even at 85°S, that is, only about 20 D.U. lower than the winter maximum and only about 5 D.U. lower than the summer maximum.

The observed and calculated vertical distributions of ozone concentration at the some latitudes in October are shown in Figure 3.24. The calculated vertical distributions of ozone concentration at the equator and 45°S are generally improved, while

the ozone concentration in the lower stratosphere at the high latitudes is still lower than the observed one.

The present results clearly show that the ozone in the high latitudes is insufficient if we consider the global circulation alone which is caused by the differential heating of the atmosphere between the summer hemisphere and the winter hemisphere due to the ozone, oxygen, and water vapor. We conclude that the antisymmetric circulation caused by the ozone, oxygen, and water vapor heating is not the primary factor of the global ozone transport.

3-d) Annual-Mean Transport Circulation

In the previous section, we have shown that the combination of the ozone photochemistry with the circulation due to the ozone, oxygen, and water vapor heating and the horizontal and vertical diffusion fails to explain the amount of ozone and its seasonal variation below the lower stratosphere (below 20-30 km high) except the equatorial region. At the lower altitude, where the ozone is predominantly controlled by dynamics, the meridional circulation due to the ozone, oxygen, and water vapor heating is less effective to cause the observed seasonal variation of ozone. The accurate simulation of the low altitude ozone is indispensable for the simulation of the total ozone amount and its seasonal variation, because the ozone amount below 30 km accounts for the almost 90 % of the total ozone amount.

Model Description

In this experiment, in addition to the meridional circulation used in the previous subsection, we add nonseasonal, steady circulation (V_T, W_T) below 30 km which ascends in the tropics and descends at the high latitudes in the both hemispheres. However, it is not easy to estimate this circulation, because not only the global heat balance but also very complex processes such as the cumulus convections due to the latent heat released in the tropics, sea surface temperature, and non-stationary planetary wave activities at the middle latitudes and high latitudes may have a considerable influence on the circulation (Kida, 1983). It is impossible to calculate the circulation in the present simplified 2-D model, so that the transport velocity obtained by Plumb and Mahlman (1987) from a 3-D model is used.

At first, using their monthly, global data of the transport velocity and symmetric diffusion tensor, a simulation is performed. The calculated time-latitude cross section of the total ozone amount is shown in Figure 3.25. The result shows the less total ozone amount in the tropics and at the middle latitude in the southern hemisphere. Although Plumb and Mahlman obtained a realistic N_2O distribution (of which main source region is considered to be at the ground surface) using their transport velocity and diffusion coefficients, there are some questions about the applicability of the original monthly data of the

transport velocity and the diffusion coefficients for the simulation of the seasonal variation of global ozone (of which main source region is in the equatorial stratosphere), as shown by the above result; The monthly transport velocity cannot give us the reasonable seasonal variation of ozone. So, their transport velocity is used with some modifications.

As shown in Figure 3.26, the annually averaged transport velocity has relatively stronger upward motion near the tropics (region A) and relatively weaker downward motion at the middle latitude in the southern hemisphere (region B). In addition, it has unusual downward motion over the tropics (region C). Thus, the annually averaged transport velocity is modified at those latitudes; We weaken the upward motion in the tropics and strengthen the downward motion at the middle latitude in the southern hemisphere. The actual modification is done as follows: The factor 0.5 is multiplied to the values of $W_T(\phi, z)$ in the low latitude region (region A), and in the southern hemisphere middle latitude region B, the values of W_T are set to -0.5 mm s^{-1} if the absolute value is less than 0.5 mm s^{-1}. Finally the values of $W_T(\phi, z)$ at the grid points in the equatorial region C are adjusted so that $W_T(\phi, z)$ can satisfy the following condition

$$\int_{-90^\circ}^{+90^\circ} W_T(\phi, z) \cos\phi \, dy = 0.$$

$V_T(\phi, z)$ is calculated by integrating the continuity equation

(3a.7) from the South Pole. The resulting circulation ($V_T(\phi, z)$, $W_T(\phi, z)$) is shown in Figure 3.27.

In this experiment, we calculate the odd oxygen mixing ratio by using equation (3c.1), but, $v(\phi, z, t)$ and $w(\phi, z, t)$ are replaced by $v(\phi, z, t)+V_T(\phi, z)$ and $w(\phi, z, t)+W_T(\phi, z)$, respectively. The seasonal variation of the transport velocity is neglected in this simulation.

Results and Discussion

Figure 3.28 shows time-latitude cross section of the calculated total ozone amount, and the observed and calculated latitudinal distributions of the total ozone amount in the four different months are shown in Figure 3.29, and the observed and calculated seasonal variations of the total ozone amount at the some latitudes are shown in Figure 3.30.

As shown in these figures, the ozone amount in the middle latitudes and high latitudes of the both hemispheres is increased by adding the steady transport circulation ($V_T(\phi, z)$, $W_T(\phi, z)$). But there still remain some discrepancies between the calculated result and the observation. In the high and middle latitudes of the northern hemisphere, and in the middle latitude of the southern hemisphere, the amplitude of the seasonal variation of the total ozone amount is still insufficient. In the higher latitudes than 70°S, the pattern of the observed seasonal variation is different from that at the other latitudes. And the dis-

crepancies exist not only in the amplitude but also in the phase. The more irregular variation (containing higher frequency components) (Bowman and Krueger, 1985) is also seen. This is related to the fact that the ozone advection cannot reach the southern hemisphere high latitude, because of less activity of planetary wave in the southern hemisphere.

In this experiment, we use the horizontal diffusion coefficient $K_{yy}(\phi, z)$ of the values more than 1×10^6 m^2 s^{-1} everywhere in the stratosphere. The values seem too large for the Antarctic region, since the calculated Antarctic ozone continues to increase during the winter, corresponding to the increase in the middle latitude ozone as shown in Figure 3.28. In the other experiment, K_{yy} in the stratosphere of the latitude between 75°S and 50°S is reduced to 2×10^5 m^2 s^{-1}. In this case shown in Figure 3.31, the ozone variation in the Antarctic is more independent of that at the southern hemisphere middle latitude, and more realistic during the winter.

The results of this subsection show that both the seasonal variation of the transport velocity and the seasonal variation of the horizontal diffusion are necessary for the explanation of the observed data.

3-e) Time-dependent Transport Circulation and Horizontal Eddy Diffusion

Model Description

As shown in the previous subsection by taking into account the transport velocity, the total ozone amount in the middle and high latitudes is increased. However, the amplitude of the seasonal variation is still smaller than the observed one. In order to explain larger amplitude of the seasonal variation of ozone in the middle and high latitudes, we consider the effect of the seasonal variation of the transport velocity ($V_T'(\phi, z, t)$, $W_T'(\phi, z, t)$). $W_T'(\phi, z, t)$ is assumed to have a variable separation form in ϕ, z, and t, as follows;

$$W_T'(\phi, z, t) = W_{TY1}'(\phi)\, W_{TZ1}'(z)\, e^{i\sigma t - \delta_1} + W_{TY2}'(\phi)\, W_{TZ2}'(z)\, e^{i\sigma t - \delta_2}, \qquad (3e.1)$$

where σ is 2π /year, δ phase lag from the summer solstice when the atmospheric heating due to the ozone, oxygen and water vapor takes its maximum. δ_1 and δ_2 are $2\pi \times (40/365)$ and $2\pi \times (10/365)$, respectively. The first term of equation (3e.1) is the seasonal variation up to 10 km high, and the second term is that in the region higher than 10 km. $W_{TY1}'(\phi)$, $W_{TZ1}'(z)$, and δ_1 are

determined by considering the results of Fourier transformation of Plumb and Mahlman's transport velocity ($V_T(\phi, z, t)$, $W_T(\phi, z, t)$). They are illustrated in Figures 3.32 and 3.33. The positive peak of $W_{TY1}'(\phi)$ near 20°N is caused by the shift of the strong convection area to the north in summer. The next negative peak near 50°N is also caused by the same effect, as a reaction on the intensified upward motion near 20°N. The positive peak near the North Pole in summer is regarded as an upward perturbation of transport relative to the negative one in winter when the activities of planetary waves are large and intensify the poleward and downward transport. In the southern hemisphere, these seasonal variations are also seen with somewhat smaller amplitude and with almost reversed phases. The 40 day phase lag δ_1 corresponds to the phase of the seasonal variation of sea surface temperature.

In the upper atmosphere between 10 km and 30 km, as mentioned earlier, the applicability of the transport velocity is questionable, and neither the latitudinal structure of the variation nor the phase is clear. Therefore we assume $W_{TY2}'(\phi)$ rather empirical so that it can well simulate the observed variation of ozone. The assumed $W_{TY2}'(\phi)$ is also illustrated in Figure 3.32. It has positive perturbation in the summer hemisphere and negative perturbation in the winter hemisphere. This means that the negative perturbation of W_T' may be caused by the intensified planetary wave activities in the winter hemisphere and the shift of the equatorial strong upward motion to the summer hemisphere.

But in the Antarctic region, a positive perturbation of W_T' in winter is added to simulate the seasonal variation of ozone more realistically. This issue will be discussed later. These vertical components are imposed the constraint

$$\int_{-90^\circ}^{+90^\circ} W_T'(\phi,z,t)\cos\phi\, dy = 0.$$

The altitude-dependent parts, $W_{Tz1}'(z)$ and $W_{Tz2}'(z)$ are determined by averaging the vertical structure of Plumb and Mahlman's transport velocity at each latitude, weighted by the amplitude of the annual component at the latitudes, but the data which have evidently unusual amplitude or phase are excluded. Figure 3.34 illustrates the assumed component of seasonal variation of transport velocity ($V_T'(\phi,z,t)$, $W_T'(\phi,z,t)$) on June 20.

Replacing $v(\phi,z,t)$ and $w(\phi,z,t)$ in equation (3c.1) by $v(\phi,z,t)+V_T(\phi,z)+V_T'(\phi,z,t)$ and $w(\phi,z,t)+W_T(\phi,z)+W_T'(\phi,z,t)$, respectively, we simulate the odd oxygen mixing ratio as a function of latitude, height, and time. Figures 3.35a and 3.35b illustrate the composite circulation on June 20 and December 19, respectively. The lower panel of each Figure is the magnification below 30 km of the upper panel.

Since the time dependence of K_{yy} seems to be essential for the seasonal variation of ozone in the polar region of the northern hemisphere and in the high latitude region of the southern hemisphere, we take into account the time-dependence of K_{yy} in

this experiment at the altitudes between 16.25 km and 28.75 km in 70°N-90°N and 55°S-75°S, which is shown in Figure 3.36. The small value of K_{yy} at 55°S-75°S during the southern hemisphere winter is due to the formation of the Antarctic polar vortex, and the following sudden increase in K_{yy} on October 18 corresponds to the breakdown of the polar vortex. The large value in the winter of the northern hemisphere is due to the intensified planetary wave activities. The other conditions such as the photochemistry, boundary conditions, etc. are all the same as the previous calculations.

Results and Discussion

Before going to the simulation of the odd oxygen, the distribution of N_2O of which source region exists at the ground surface is simulated in order to examine the validity of the circulation and diffusion coefficients in the model, in particular, to examine the circulation in the lower atmosphere. The N_2O mixing ratio at the surface is set at a constant value of 300 ppbv, and the value in the atmosphere is calculated numerically by

$$\frac{\partial \chi_{N_2O}}{\partial t} = \chi_{N_2O} J_{N_2O} - (k_{N_2O1} + k_{N_2O2}) \chi_{N_2O} [O(^1D)] + (\text{dynamical term}),$$

where $k_{N2O1}=6.7\times 10^{-11}$ cm^3 s^{-1}, and $k_{N2O2}=4.9\times 10^{-11}$ cm^3 s^{-1}, and J_{N2O} is the photon number absorbed by a N_2O molecule per unit time. The simulated latitude-altitude cross sections of N_2O mixing ratio are shown in Figure 3.37. We can see that the ridge of the contour in the low latitude and middle latitude regions tilts to the summer hemisphere. The result is consistent with the observation. (e.g. see Jones and Pyle, 1984.)

Figure 3.38 shows the time-latitude cross section of the calculated total ozone amount. The observed and calculated latitudinal distributions of the total ozone amount in the four different seasons are shown in Figure 3.39. The observed and calculated seasonal variations of the total ozone amount at the some latitudes are shown in Figure 3.40. The seasonal variation and latitudinal distribution of the global total ozone amount are considerably improved. The spring maximum of 410 D.U. and the fall minimum of 240 D.U. in the northern hemisphere high latitude, the spring maximum of 340 D.U. in the southern hemisphere middle latitude, the fall minimum of 220 D.U. in the south polar region, and the almost constant value of 200 D.U. at the equator are well simulated, although these values are a bit smaller than the observed values.

The observed and calculated vertical distributions of ozone concentration at the some latitudes in October are shown in Figure 3.41. The vertical distributions in the high latitudes are improved.

We use two different latitudinal components of W_T' below and

above 10 km, as mentioned previously, because we obtain a quite different seasonal variation of ozone from the observation when we use $W_{TY1}'(\phi)$ alone between the surface and 30 km high. The time-latitude cross section of the total ozone amount is shown in Figure 3.42. The result tells us that $W_{TY2}'(\phi)$ predominantly controls the seasonal variation of the total ozone amount. However, $W_{TY1}'(\phi)$ is also necessary in order to simulate the circulation of the lower atmosphere.

The positive perturbation of W_T' in the Antarctic winter which is shown in Figure 3.36 seems to be necessary, because an unusual deep fall minimum in the Antarctic appears in some numerical experiments in which a negative or zero perturbation of W_T' in the south of 70°S in winter is assumed. It should be noted that the positive perturbation of W_T' nearly cancels out the anti-symmetric circulation almost all the year in the Antarctic. (See Figures 3.35a and 3.35b.) We have not completely yet understood the necessity and cause of the positive perturbation in the Antarctic winter. It may be due to some defects of the model such as the insufficient modeling of the photochemistry in the Antarctic atmosphere, the use of the constant ozone deposition velocity at the Antarctic ground surface, incorrect values of the steady component of the transport velocity in the Antarctic, or insufficient diffusion process of the ozone from the middle latitude in that season. It may be possible that the particularity of the circulation involved with the transient, local radiative process within the isolated polar vortex or the strong

downward motion at the southern hemisphere middle latitude due to the planetary wave activities causes the necessity of the positive perturbation in the Antarctic winter in this model. This is a limitation of the global ozone simulation using the annual component of the anti-symmetric global circulation caused by the ozone, oxygen, and water vapor heating. Then, we must construct and use more sophisticated, consistent, and interactive 2-D model in order to study the dynamics and chemistry in the Antarctic region.

Figure 3.43 shows the time-latitude cross section of the total ozone amount which is calculated by using a constant value of K_{yy} ($=1\times 10^{6}$ m^{2} s^{-1}). The Antarctic ozone unrealistically continues to increase according to the ozone increase at the middle latitude. Considering this result, we understand that the inclusion of the time dependence of K_{yy} leads to the more realistic seasonal variation of the total ozone amount in the Antarctic region, especially leads to the more realistic rapid increase in ozone in October as shown in Figure 3.38. In the northern hemisphere, the inclusion of the time dependence of K_{yy} in the high latitude leads to a little more amount of the total ozone in the Arctic region.

According to the estimation of K_{yy} by Yang et al. (1990) using NMC temperature data and SBUV ozone data, K_{yy} in January and April at the high latitude in the northern hemisphere is a factor of 2 or 3 lager than that in July. At the latitudes between 55°S and 75°S, however, the significant seasonal difference

in K_{yy} cannot be seen. Our assumption that the value of K_{yy} significantly increases after the breakdown of the polar vortex is inconsistent with the Yang et al.'s result. Although both advective and diffusive ozone transport from the middle latitude into the Antarctic region may actually occur after the breakdown of the polar vortex, it is possible to simulate the observed ozone increase in the Antarctic region only by a large horizontal diffusion coefficient, because in the southern hemisphere, a maximum of the total ozone amount exists at the middle latitude in spring, and a steep down gradient of the total ozone amount from the middle latitude to the Antarctic region is formed at that time. Thus, in the southern hemisphere, we cannot conclude whether or not the diffusion transport is more dominant than the advection transport after the breakdown of the Antarctic polar vortex, only by judging from the variation of the zonal-mean ozone distribution. On the other hand, in the northern hemisphere the maximum of the total ozone amount exists at higher latitude than in the southern hemisphere. This is still one of the evidence that in the northern hemisphere ozone is effectively transported to the middle latitude and farther to the high latitude by advection rather than by diffusion, even if the effect of the more total ozone amount due to the lower tropopause in the higher latitude is taken into account.

The total ozone amount in October calculated in this section is much more than the observed one during the ozone hole (about 150 D.U.). Hence we must consider some other processes such as

heterogeneous chemistry on PSCs and the following chlorine catalytic cycle in order to simulate a severe ozone depletion in the Antarctic spring.

4. SIMULATION OF THE ANTARCTIC OZONE HOLE IN THE 2-D MODEL

In Chapter 3, we tried to simulate the global ozone distribution and its seasonal variation using a simple 2-D model, and we could simulate them well except for the lack of severe depletion of the Antarctic ozone in September and October by employing the seasonally varying transport velocity and horizontal eddy diffusion. In this Chapter, the effect of a chlorine catalytic cycle is taken into account in order to simulate the sudden and severe depletion of the Antarctic ozone in September and October.

Model Description

The catalytic process of ozone destruction considered in this model is very simple one;

$$Cl_2 + h\nu_{Cl2} \rightarrow 2\,Cl \qquad (4.1)$$

$$2(\,Cl + O_3 \rightarrow ClO + O_2\,) \qquad (4.2)$$

$$ClO + ClO + M \rightarrow Cl_2O_2 + M \qquad (4.3)$$

$$Cl_2O_2 + h\nu_{Cl2O2} \rightarrow Cl + ClOO \qquad (4.4)$$

$$ClOO + M \rightarrow Cl + O_2 + M \qquad (4.5)$$

$$HNO_3 + h\nu_{HNO3} \rightarrow OH + NO_2 \qquad (4.6)$$

$$ClO + NO_2 + M \rightarrow ClNO_3 + M \qquad (4.7)$$

$$ClNO_3 + h\nu_{ClNO_3} \rightarrow Cl + NO_3 \qquad (4.8)$$

where ν_{Cl_2} is the spectral frequencies at which the photodissociation of Cl_2 into two chlorine atoms occurs (240 nm< λ <450 nm), $\nu_{Cl_2O_2}$ the photodissociation frequencies of Cl_2O_2 (200 nm< λ <360 nm), ν_{HNO_3} the photodissociation frequencies of HNO_3 (190 nm< λ <330 nm), and ν_{ClNO_3} photodissociation frequencies of $ClNO_3$ (190 nm< λ <450 nm). HNO_3, Cl_2, and Cl_2O_2 have their absorption bands in the ultra violet and visible spectra where the absorption bands of ozone and oxygen molecule exist. The extinction effect of HNO_3, Cl_2, and Cl_2O_2 on the solar radiation is very small compared to the effects of the ozone and oxygen molecules, even if the zenith angle approaches to 90°. Therefore, we neglect the extinction effects of these minor species when we calculate the photon number absorbed by O_3, O_2, HNO_3, Cl_2, and Cl_2O_2. Of course, the extinction effects of ozone and oxygen molecules are taken into account when we calculate the photon number absorbed by these minor species. It is estimated, on the condition of the normal concentration of the minor species, that the neglect of the extinction effects of the minor species leads to at most a few percent excessive photon number at each spectrum at the altitudes above 10 km.

Cl_2 is not the only substance which can supply chlorine atoms in the Antarctic spring. Increased $ClNO_2$ and HOCl by some heterogeneous reactions may also supply a considerable amount of chlorine atoms through their photodissociation in the Antarctic

spring. (Tung et al., 1986; Solomon et al., 1986; McElroy et al., 1986; Rodriguez et al, 1986; Salawitch et al., 1988). In spite of this rather complicated situation, we assume that Cl_2 is a representative substance which supplies abundant chlorine atom in the Antarctic spring.

We neglect the reaction

$$ClO + NO \rightarrow Cl + NO_2,$$

which may decrease concentration of ClO. But the produced Cl atom reacts with ozone and produces ClO again. In addition, NO_x concentration in the Antarctic polar vortex is very low. These may be enough reasons for the neglect of the above reaction.

The reactions (4.2)-(4.5) represent the catalytic destruction of ozone due to Cl_2O_2 (ClO dimer), which was proposed by Molina and Molina (1987). As the time goes on from early spring to late spring, more HNO_3 are photolyzed and consumed only to produce NO_2 in this model. The NO_2 reacts rapidly with ClO, and produces $ClNO_3$. (See reactions (4.6) and (4.7).) Then, the ClO concentration is decreased and the efficiency of the ozone destruction by the ClO dimer cycle is weakened. Thus, HNO_3 in this model controls the ClO dimer cycle. We include these reactions at the altitude grid points of 12.5 km, 15.0 km, 17.5 km, and 20.0 km, and at the latitude grid points of 90°S, 85°S, 80°S, 75°S, and 70°S in the model.

In order to calculate the seasonal variation of ozone

including the chlorine chemistry, a ClO_x family is defined as follows,

$$ClO_x = Cl + ClO + ClOO + 2\,Cl_2O_2.$$

We calculate the mixing ratio of O_x, ClO_x, NO_2, Cl_2, and $ClNO_3$ by the numerical integration of the following equations with respect to time,

$$\frac{d\chi_{ClO_x}(\phi,z,t)}{dt} = 2J_{Cl_2}\chi_{Cl_2} + 0.9J_{ClNO_3}\chi_{ClNO_3} - k_{12}\chi_{ClO}\chi_{NO_2}n_m ,$$

$$\frac{d\chi_{NO_2}(\phi,z,t)}{dt} = J_{HNO_3}\chi_{HNO_3} - k_{12}\chi_{ClO}\chi_{NO_2}n_m ,$$

$$\frac{d\chi_{Cl_2}(\phi,z,t)}{dt} = -J_{Cl_2}\chi_{Cl_2} ,$$

$$\frac{d\chi_{ClNO_3}(\phi,z,t)}{dt} = k_{12}\chi_{ClO}\chi_{NO_2}n_m - J_{ClNO_3}\chi_{ClNO_3} ,$$

where J_i represent the photon number received by an i-molecule per unit time, and χ_i the volume mixing ratio of i, n_m the number density of any arbitrary atom or molecule, and 0.9 the quantum yield of $ClNO_3$ photolysis into Cl and NO_3 (reaction (4.8)); The rest 10 % of $ClNO_3$ photolyzes into O and ClONO.

(DeMore et al., 1990).

The concentration of Cl, ClO, ClOO, and Cl_2O_2 is estimated by assuming their photochemical equilibrium, and by solving the following set of linear simultaneous equations,

$$\frac{[Cl]}{[ClO]} = \frac{k_{13}[O]}{k_9[O_3]},$$

$$\frac{[Cl_2O_2]}{[ClO]} = \frac{k_{10}[ClO]}{J_{Cl_2O_2}},$$

$$\frac{[ClOO]}{[ClO]} = \frac{[Cl_2O_2]}{[ClO]} \times \frac{J_{Cl_2O_2}}{k_{11}[M]},$$

$$\frac{[ClO]}{[ClO_x]} = \frac{1}{1 + \frac{[Cl]}{[ClO]} + \frac{[ClOO]}{[ClO]} + \frac{2[Cl_2O_2]}{[ClO]}}.$$

Here, [Cl], [ClO], [ClOO], and $[Cl_2O_2]$ are unknowns to be solved. J_1 are calculated by using the absorption cross section data recommended by DeMore et al. (1990), and by considering the extinction effects of the solar radiation due to the ozone and oxygen in the upper atmospheric layers. The reaction coefficients k_1 are tabulated in Table 4.1. These values are the same as DeMore et al. (1990).

Ozone destruction due to the chlorine catalytic cycle is expressed by

$$\left(\frac{d\chi_{O_3}}{dt}\right)_{catalytic} = -2\,k_{10}\,[ClO]\,[ClO]\,[M]\,, \qquad (4.9)$$

because one cycle of reactions (4.2)-(4.5) can destroy two ozone molecules. And the above expression is based on the assumption that most of ClO and Cl_2O_2 may be produced by reaction (4.2) and (4.3), respectively.

Equation (4.9) is combined with the chemical term of equation (3c.1), assuming that concentration of atomic oxygen is negligible compared to the concentration of ozone in the lower stratosphere of the Antarctic spring. The diffusion and advection of the constituents except for O_x are neglected.

The initial conditions of the chlorine chemistry are set on June 19. They are;

χ_{Cl_2} at 12.5 km = 0.30 ppbv,

χ_{Cl_2} at 15.0 km = 0.45 ppbv,

χ_{Cl_2} at 17.5 km = 0.60 ppbv,

χ_{Cl_2} at 20.0 km = 0.60 ppbv,

χ_{HNO_3} at 12.5 km, 15.0 km, and 17.5 km = 2.0 ppbv,

χ_{HNO_3} at 20.0 km = 3.0 ppbv,

and $\chi_{NO_2} = \chi_{ClNO_3} = \chi_{Cl} = \chi_{ClO} = \chi_{ClOO} = \chi_{Cl_2O_2} = 0$ at all altitudes. The initial latitudinal distributions of all the above

chemical species are assumed to be constant between 90°S and 67.5°S.

The assumed value of Cl_2 (0.6 ppbv) is too high for the stratosphere in the normal situation. However, heterogeneous chemistry on PSCs may easily lead to the high concentration of Cl_2 in the stratosphere during the polar night (Salawitch et al., 1988). The heterogeneous chemical reactions on the PSCs are not included in this model, because the experimentally determined reaction coefficients have large uncertainty, and hence, may have large error. Another reason is that our model cannot simulate very low temperature within the Antarctic polar vortex which is essential to the formation of the PSCs. Thus, we have to start our photochemical calculations by assuming the high concentration of Cl_2.

The value of 2 ppbv of HNO_3 mixing ratio much lower than the normal value in the stratosphere is used in the model, since HNO_3 in the polar vortex may freeze in the very low temperature, and then, the concentration of gas phase HNO_3 may be reduced. The concentration of the gas phase HNO_3 is in equilibrium with solid phase HNO_3, and the low concentration will continue until the Antarctic polar vortex breaks down and HNO_3 outside the polar vortex flows or diffuses into the Antarctic stratosphere. Hence, the mixing ratio of HNO_3 is fixed artificially at the initial low value in spite of its photodissociation during spring. And the HNO_3 mixing ratio is increased artificially on September 28.

The ozone destruction process due to the ClO dimer cycle is

set off from the model on October 18 when the Antarctic polar vortex breaks down.

Results and Discussion

Figure 4.1 shows time-latitude cross section of the calculated total ozone amount. The total ozone amount in the Antarctic decreases to 150 D.U. in mid-October due to the chlorine catalytic cycle included in this model.

In order to see more clearly the total ozone depletion in the latitude section and in the time section, we show the observed and calculated latitudinal distributions of the total ozone amount in August, September, October, and November in Figure 4.2, and the observed and calculated seasonal variations of the total ozone amount at 85°S, 75°S, 65°S, and 55°S in Figure 4.3. As soon as the chlorine chemistry is switched on, the ozone in the Antarctic begins to decrease rapidly and the steep gradient of the total ozone amount in the southern hemisphere high latitude is formed.

The observed and calculated vertical distributions of ozone concentration at 85°S, 75°S, 65°S, and 55°S in October are shown in Figure 4.4. The concentration of ozone between 11.25 km and 21.25 km on October 17 falls quite less than 50 % of the observed normal value shown in this figure. These results are consistent with the recent observations at the ozone hole event. (e.g. see Figure 1 of Hofmann et al.; 1987, or Figure 13 of

Komhyr et al.; 1988b.)

If the Antarctic ozone between 11.25 km and 21.25 km were completely destroyed, the total ozone amount would be about 100 D.U., because the Antarctic ozone amount between 11.25 km and 21.25 km is about 170 D.U. in August, 1987 (Komhyr et al. 1988a), and the total ozone amount in the Antarctic is about 270 D.U. at that time. Since the chlorine chemistry is considered only within the altitude range between 11.25 km and 21.25 km in this model, it is no wonder that the total ozone amount in the Antarctic of the model reaches such a low value as 150 D.U. due to an effective ozone destruction mechanism.

The maximum reduction rates of the total ozone amount are 5.7 D.U. d^{-1} at 90°S, 3.1 D.U. d^{-1} at 85°S, 2.0 D.U. d^{-1} at 80°S, 1.4 D.U. d^{-1} at 75°S, and 0.6 D.U. d^{-1} at 70°S in mid-September. The latitude dependence of the total ozone destruction rate is mainly due to the diffusion of ozone from the middle latitude. In this model, a large part of the ozone between 11.25 km and 21.25 km is destroyed at the time scale of 1 month.

Tables 4.2a and 4.2b show the mixing ratio of ClO, Cl_2O_2, NO_2, and HNO_3 at 85°S and 75°S, respectively. Figures 4.5a-4.5d also show the time evolutions of ClO and Cl_2O_2 mixing ratio calculated at 85°S and 75°S. The ClO mixing ratio is increased as high as 700 pptv at 20 km high in late September, while Cl_2O_2 continues to decrease due to its photodissociation after reaching its maximum concentration earlier than ClO. Comparing the results with those of more sophisticated models which include the

heterogeneous chemistry (Salawitch et al., 1988; Rodriguez et al., 1989; Rodriguez et al., 1990), we see that the increase in ClO and Cl_2O_2 just after the polar night is too fast. We think that the omission of the heterogeneous chemistry, that is, the omission of the simultaneous progress of both the heterogeneous reactions and the dimer cycle leads to such a fast increase in ClO and Cl_2O_2 just after the polar night. We also see that the concentration of ClO and Cl_2O_2 is kept high until just before the breakdown of the polar vortex, because NO_2, which reacts with ClO and decreases ClO concentration, is produced only by the photodissociation of HNO_3 in this model. In the actual situation, it is also considered that NO_2 is produced from NO_3 and HO_2NO_2, and diffused from the outside of the polar vortex. Thus, in this model, the mixing ratio of NO_2 is so low that the ClO concentration remains high, and hence, the ClO dimer cycle can work effectively during the period, even though the concentration of HNO_3 is artificially increased on September 28.

The results also show that Cl_2 mixing ratio of 0.6 ppbv is necessary for the decrease in the total ozone amount to 150 D.U. at the time scale of 1 month if the ozone depletion during the the Antarctic spring is limited between 11.25 km and 21.25 km and if the ozone is destroyed by the catalytic cycle (4.2)-(4.5). However, there is a question about the ClO dimer catalytic cycle. Eberstein (1990) shows that the photolysis of Cl_2O_2 at wavelength longer than 250 nm may produce ClO as the primary product rather than Cl and ClOO, although the Cl_2O_2 absorption spectrum in the

visible region has not been well known yet. In the Antarctic spring, the photodissociation at the longer wavelength which may produce more ClO is important, since the path length of the sunlight through the atmosphere is larger at that time, and the ultraviolet radiation may be extremely extinguished. In that case, the destruction of ozone will be much reduced than expected by our calculation, and then, in order to simulate the Antarctic ozone hole realistically, we will have to assume a higher concentration of Cl_2 or $ClNO_2$, or will have to assume some other catalytic cycles.

Our model cannot simulate the very low temperature during the Antarctic polar night, because the Newtonian cooling approximation is used in the dynamics. In the model, temperature falls at most to 211 K at 15 km and to 205 K at 20 km in mid-winter, and temperature in the spring equinox in the Antarctic region at 12.5 km, 15.0 km, 17.5 km, and 20.0 km where the chlorine chemistry is taken into account is about 217 K. The temperature dependence of the reaction coefficient of the time-limiting step k_{10} is rather large, for example, the value at 170 mb (=12.5 km when the scale height is 7 km) increases from 2.55×10^{-13} cm^3 $molecule^{-1}$ sec^{-1} (at 217 K) to 4.08×10^{-13} (at 192 K, which is a representative temperature in the cold Antarctic polar vortex). Similarly, the value at 120 mb (=15 km) increases from 1.87×10^{-13} to 3.04×10^{-13}, the value at 80 mb (=17.5 km) increases from 1.35×10^{-13} to 2.24×10^{-13}, and the value at 60 mb (=20 km) increases from 9.68×10^{-14} to 1.63×10^{-13}. An additional

experiment is performed to examine the sensitivity of the reduction of ozone to the temperature. Temperature at 12.5 km, 15.0 km, 17.5 km, and 20.0 km at the latitudes of 90°S, 85°S, 80°S, 75°S, and 70°S is fixed at 192 K from June 19 to October 18, which is about 25 K lower than the values of the previous experiment.

Figure 4.6 shows the time-latitude cross section of the total ozone amount and the seasonal variations of the total ozone amount at 85°S and 75°S. Contrary to our expectation, the ozone reduction rates calculated in this model are not so sensitive to the forced low temperature; The maximum reduction rates of the total ozone amount are just about 10 % or 20 % larger than those in the previous normal temperature experiment, for example, 5.7 D.U. d^{-1} at 90°S, 3.4 D.U. d^{-1} at 85°S, 2.4 D.U. d^{-1} at 80°S, 1.7 D.U. d^{-1} at 75°S, and 0.8 D.U. d^{-1} at 70°S in mid-September. The reason is as follows: The value of the reaction coefficient of the time-limiting step is larger at 192 K than that at 217 K, while the ClO concentration in this model at 192 K is smaller than that at 217 K (compare Tables 4.3a and 4.3b to Tables 4.2a and 4.2b, respectively) because of the temperature dependence of the reaction coefficients involved with the ClO production and consumption considering in this model, so that the ozone destruction rate of (4.9) increases at most by 10 % or 20 % at those altitudes except at 20 km, where the increase reaches about 40 % . The relatively large ozone destruction rate at 20 km also does not lead to a severer ozone reduction there, because the

ozone is supplied by diffusion from just above altitude where the chlorine chemistry is not taken into account. Hence, it is concluded by this model that the relatively low temperature in the Antarctic polar vortex is not essential for the reduction rate of ozone due to the ClO dimer cycle. But, the chemistry in the model is so simple that the conclusion about the temperature dependence may not be directly applicable to the real atmosphere. For instance, the uncertainty of the NO_2 concentration in this model will lead to the uncertainty of ClO concentration, and hence will lead to the uncertainty of O_3 concentration through the reaction (4.7) and the ClO dimer cycle (reactions (4.2)-(4.5)).

It should be noted that the temperature dependence of the amount of PSC, that is, the formation of more PSC at the lower temperature, is very important for the appearance of the unusual high ClO concentration in the Antarctic stratosphere and for the ozone destruction in the high ClO concentration due to the ClO dimer cycle. And this is the most dominant temperature dependence of the Antarctic ozone depletion.

Two other experiments are performed in order to examine the Antarctic spring ozone depletion resulting from the competition between the local chemical ozone sink and the ozone transport from the middle latitude into the Antarctic. In these experiments, the seasonal variation of K_{yy} between 55°S and 75°S is changed from that of the previous experiments. In the first experiment, K_{yy} is increased to 3×10^6 m^2 s^{-1} on September 19,

about a month earlier than the previous experiment, and at the same time, the ozone destruction due to the ClO dimer cycle is stopped. This situation simulates the earlier breakdown of the polar vortex. Figure 4.7 shows the time-latitude cross section of the calculated total ozone amount, and also shows the observed and calculated seasonal variations of the total ozone amount at 85°S and 75°S. The results show that the total ozone amount in the Antarctic region keeps the value above 200 D.U.. And it is evident that the earlier breakdown of the polar vortex prevents the severer ozone destruction due to the chlorine chemistry.

In the second experiment, K_{yy} is increased to 3×10^{6} m^2 s^{-1} on November 17, about a month later than the original experiment, and at the same time, the chlorine chemistry is stopped. The results are shown in Figure 4.8. The minimum total ozone amount is little changed, since most of the ozone between 11.25 km and 21.25 km was already destroyed by the time of mid-October. The recovery of ozone before the breakdown of the polar vortex is due to the increase in NO_2 which is produced by the photodissociation of HNO_3. But the effect is small.

5. DISCUSSION

Although we have already mentioned the results and discussions of each numerical experiment, we will discuss in this section our model more comprehensively, and also discuss the ability of our model and its limitation. We will also speculate the ozone depletion in the polar region.

1) The use of annually averaged Plumb and Mahlman's K_{zz} in stead of the original monthly K_{zz} data little changes the distribution and seasonal variation of ozone. We have also tried to simulate the global ozone by using more idealized K_{zz} distribution which has the vertical distribution similar to ν (z) in Figure 3.2b, but the altitude of minimum K_{zz} is changed at each latitude. For example, the minimum is located at 17.5 km in the tropics and at 10.0 km in the polar regions (Miller et al., 1981). However, we cannot obtain a realistic value of the global total ozone distribution. The more complex distribution of K_{zz} shown in Figure 3.14 seems to be very important for the simulation of the globally realistic total ozone amount. On the other hand, the use of annually averaged K_{yy} changes seriously the seasonal variation of the total ozone amount in the high latitudes. This shows the importance of the seasonal variation of the horizontal diffusion, which is closely related to the planetary wave activities.

2) The calculated zonal-mean temperature perturbation is independent on the variation of K_{yy}. In the actual situation,

zonal-mean temperature is affected by planetary wave activity. In this sense, the present model is not self-consistent. However, the temperature change may not seriously affect the ozone distribution.

3) The calculated seasonal variations of the global temperature and the global circulation are not completely consistent with the ozone distribution calculated in the model, because we do not use the model ozone distribution for the calculation of $Q_n(z)$, but use the observed ozone data. In order to examine the difference between the heating by the simulated ozone and the heating by the observed ozone, and also in order to examine the effect of the difference on the calculated seasonal variation of ozone, we have calculated again the annual component of ozone heating rate using the ozone distribution shown in Figure 3.38 which is calculated by the present model in subsection 3-e). Then, we recalculate the seasonal variation of ozone using this heating. And this procedure is iterated until $Q_n(z)$ converges.

Figures 5.1a and 5.1b show the $Q^{annual}(\phi, z)$ of ozone at 15 km and 50 km, respectively, which are consistent with the calculated ozone distribution. Comparing Figure 5.1a to Figure 3.3a, we see that the latitudinal distributions of the ozone heating are different at 15 km, while comparing Figure 5.1b to Figure 3.3b we see that the latitudinal distributions are similar at 50 km although there is a difference in the absolute value. The $Q_{o1}(z)$ obtained from the ozone distribution of Figure 3.38 is also represented by the black triangle marks in Figure 3.4. The

large difference above 65 km between $Q_{o1}(z)$ obtained from the observed ozone and $Q_{o1}(z)$ obtained from the model ozone is due to the poor ozone chemistry at the higher altitudes. So, as mentioned in subsection 3-a), $Q_n(z)$ above 65 km is corrected so that we can simulate a realistic seasonal variation of temperature at these altitudes. We can also see that there is considerable difference between the model ozone $Q_{o1}(z)$ and the observed ozone $Q_{o1}(z)$ around 50km. It is evident that the model underestimates the ozone concentration there.

Figure 5.2 shows the seasonal variation of the total ozone amount which is calculated by using the $Q_n(z)$ consistent with the calculated ozone distribution. The amplitude of the seasonal variation is a little smaller than that of Figure 3.38 in the middle and high latitudes. But the global pattern is hardly changed. The result shows that the feedback of the anti-symmetric annual cycle circulation to the global ozone distribution is small.

4) We conclude that the anti-symmetric global circulation which is driven by the annually oscillating ozone and water vapor heating is not crucially important to the seasonal variation of ozone. On the other hand, however, there are some numerical results which show the importance of the ozone heating to the circulation and heat budget over the Antarctic region. Kiehl et al. (1988) showed by their GCM simulation that the ozone depletion over the Antarctic prolonged the duration of the Antarctic polar vortex and delayed the breakdown of it.

Chipperfield and Pyle (1988) predicted the maximum temperature fall of 10 K at 50 mb if the ozone hole was artificially imposed over the Antarctic in their 2-D model. These results may be caused by a local and transient decrease in the ozone heating due to the ozone depletion over the Antarctic. The local, transient radiative-dynamical interaction cannot be simulated by our simple model, because the anti-symmetric global circulation is calculated by prescribing the anti-symmetric annually sinusoidally oscillating heating and some latitudinally constant parameters such as eddy viscosity ν (z), Newtonian cooling coefficient α (z), Rayleigh friction coefficient $k_M(z)$, and Brunt-Väisälä frequency N(z). This is the most serious defect in our simple model. The predicted ozone reduction may induce the change of the mean meridional circulation of the same order of the perturbation of the transport velocity. This feedback mechanism should be included in order to simulate realistically the local circulation over the Antarctic region.

5) Recent 2-D models use the diffusion coefficients consistent with the meridional transport circulation in order to calculate the transport of the minor constituents in the atmosphere (Tung and Yang, 1988; Brasseur et al, 1990). Since the diffusion coefficients and the transport velocity in our model are determined independently, there is some uncertainty or arbitrariness between them. Although in this paper we have only showed the ozone distributions which are calculated using a combination of the time-independent diffusion coefficients except

in the polar regions and the annually sinusoidally oscillating meridional circulation, we have also calculated ozone distribution using time-dependent diffusion coefficients. Generally speaking, the time-dependence of the diffusion coefficients does not seriously change the results. It just adds a small amount of irregular ozone variation to the smoother dominant variation which is obtained by using the time-independent diffusion coefficients and the annually oscillating meridional circulation. Even if the effect of the more total ozone amount in the high latitudes due to the lower tropopause is taken into account, the ozone maximum apart from the ozone source region (the tropics) is evidently formed by the advective transport, not by the diffusive transport. However, in the polar regions, more precisely, in the higher latitude regions than the maximum total ozone latitudes in the both hemispheres, the time-dependence of the diffusion coefficients affects the seasonal variation of ozone as seriously as the advection. The above conclusions are derived from the results using the empirically modified transport velocity and diffusion coefficients which were originally calculated by Plumb and Mahlman from the GFDL 11-level GCM. It is not sure whether the modification of the diffusion coefficients and meridional circulation in this model is unique or not.

Since the transport velocity used in this model is somewhat empirically modified to simulate the global ozone distribution realistically, the physical origin of the variation of the

transport velocity is not fully understood. The inconsistency of this model prevents us from studying the year-to-year variation of the global ozone distribution. For this purpose, more comprehensive understanding of the atmospheric system by a more sophisticated model will be necessary. But it should be noted that by this simple model the seasonal variation of global ozone has been well simulated and understood more clearly, and the local ozone depletion in the Antarctic has been understood from a global point of view.

6. CONCLUSIONS

Using a two-dimensional dynamical chemical model, we have simulated the distribution and seasonal variation of global ozone, and the Antarctic ozone hole. The results are summarized as follows:

1. The photochemical equilibrium experiment and the vertical transport experiment predict the total ozone amount less than 150 D.U. in the both polar regions all the year. These results show the importance of horizontal ozone transport into the polar regions.

2. The height of tropopause is an important factor to simulate the realistic distribution of global ozone. This is parameterized by the profile of $K_{zz}(\phi, z)$ in the model. The parameterization causes less total ozone in the tropics and more total ozone at the high latitudes than those estimated by the photochemical equilibrium calculation. The rather complex K_{zz} distribution seems to be very important for the simulation of the globally realistic total ozone amount.

3. The vertical distribution of ozone in the tropics is well simulated only by the photochemistry and the vertical diffusion.

4. The fall minimum of the total ozone amount in the both polar regions, especially in the North Pole region, is caused by less amount of the solar radiation in fall than in summer, the upward motion during the summer, and the ozone accumulation during winter by the downward motion due to the planetary wave

activities.

5. The seasonal variation of global circulation which is induced by the differential heating of the atmosphere between the summer hemisphere and the winter hemisphere due to the ozone, oxygen, and water vapor is not crucially important to the seasonal variation of global ozone. The net effect on the amplitude of the variation of the total ozone amount is at most 10 D.U.~ 20 D.U. at the high latitudes.

6. The steady transport circulation from the tropics to the high latitudes is important to the transport of ozone from the low latitude to the high latitude. This causes more total ozone amount at the high latitudes than that calculated by the photochemical and vertical transport experiment in subsection 3-b).

7. In addition to the ozone-inducing anti-symmetric circulation and the steady transport circulation mentioned above, the seasonally varying transport velocity is considered. The time-dependent transport velocity between 10 km and 30 km predominantly controls the seasonal variation of the total ozone amount at the middle latitudes of the both hemispheres and the high latitude in the northern hemisphere. This component represents the seasonal variation of the planetary wave activities and the seasonal variation of the upper branch of the cumulus convections in the tropics.

8. Our simple model can simulate the seasonal variation of ozone in the upper and middle stratosphere as well as in the

lower stratosphere and in the troposphere. Although there is a little discrepancy of the absolute concentration of ozone, the summer minimum and the winter maximum of the ozone concentration at 50 km, and the winter minimum at 35 km are well simulated. The former results mainly from the seasonal variation of temperature at 50 km, and the latter results mainly from the seasonal variation of the amount of the solar ultraviolet radiation at 35 km.

9. The seasonal variation of the horizontal diffusion of ozone as well as the seasonal variation of the advection of ozone is important to the seasonal variation of the ozone amount in the Antarctic. On the other hand, in the middle and high latitudes in the northern hemisphere, and in the middle latitude in the southern hemisphere, the seasonal variation of the ozone advection is more crucial than the ozone diffusion.

10. An ozone hole simulation without the heterogeneous chemistry has been tested by including the ClO dimer cycle at the altitude between 11.25 km and 21.25 km in the Antarctic region of the model, and by assuming unusually high concentration of Cl_2 before the polar dawn. The result shows that the Antarctic ozone rapidly decreases to 150 D. U. by the mid-October at the time scale of 1 month.

11. It was shown by our one-dimensional radiative transfer calculation (Appendix A) that the upward motion to cause the severe ozone depletion in the Antarctic region could not occur during September and October in 1985, even if the aerosol heating

in the lower stratosphere was taken into account.

In this study, we have obtained some important natures of the seasonal variation of global ozone and the Antarctic ozone hole. We have also discussed the global transport circulation from a view point of the global ozone distribution. Although our model has some inconsistencies in itself, we believe that the results and the revealed natures of the ozone transport will supply the insight for the further study of ozone. In the future we have to study the three-dimensional transport problem using a more complicated radiative dynamical chemical interaction model.

we have only concentrated on the ozone transport in this study, using a very simplified parameterization of ozone production. The distribution of HNO_3 and HCl is assumed in order to calculate the ozone destruction around the Antarctic. However, it is necessary to investigate the transport of these chemical constituents in the atmosphere in order to develop more comprehensive ozone model. For this purpose, we need observational studies as well as theoretical investigations of transport and chemical processes of these constituents.

Acknowledgments.

I would like to express my sincere thanks to Prof. M. Uryu for his kind and useful suggestions, discussions, and continuous encouragements. Sadly, he passed away on 21 August 1990. I wish he could be alive more, read this thesis, and comment on it. I would like to dedicate this volume to his soul in token of gratitude.

I especially thank Prof. S. Miyahara for his careful reading of this thesis and many helpful discussions. I also express my thanks to Prof. M. Fujiwara and Prof. T. Takahashi for their discussions.

I also would like to thank Dr. S. Solomon for her useful suggestions and discussions. She suggested the framework of the chlorine photochemistry to introduce into our model. Discussions and comments on dynamics by Dr. J. C. Gille, Dr. R. R. Garcia, Dr. K. K. Tung, and Dr. H. Yang were very useful. Dr. R. A. Plumb sent us the useful transport velocity data and Dr. W. D. Komhyr gave us helpful ozone data. Thanks are also due to Drs. M. Takahashi, Y. Wakata, T. Sasaki, and Mr. Chubachi for their helpful comments and Mr. Y. Hashiguchi for his programming of an interpolation scheme.

This work was partly supported by the Grant-in-Aid for Scientific Research of the Ministry of Education of Japan. The numerical computations were performed by using the FACOM-M780 and FACOM-VP200 computers at Kyushu University.

Appendix A

Results of 1-D Radiative Transfer Calculation: An evaluation of the upward motion hypothesis

In this section, results of 1-D radiative transfer calculation of the Antarctic atmosphere containing aerosols are shown (Akiyoshi et al.; 1988, 1989) to evaluate the upward motion hypothesis of the ozone hole. A two-stream approximation (Modified Eddington-delta function method) proposed by Meador and Weaver (1980) is used in order to include the scattering effects of the atmospheric molecules, aerosols and the surface; The dependence of radiance $I(\tau, \cos\theta)$ W m^{-2} sr^{-1} on zenith angle θ is assumed by considering the amount and optical properties of aerosols in the layer in question. The deviation of the assumed scattering property of the layer from Rayleigh scattering property is parameterized by using asymmetric factor g and the factor β (see Meador and Weaver, 1980) of the turbid atmospheric layer. Then, the assumed $I(\tau, \cos\theta)$, of which absolute value is not still determined, is substituted for $I(\tau, \cos\theta)$ to be solved in the radiative transfer equation, and integrating the equation with respect to μ ($=\cos\theta$), the upward and downward fluxes of the radiation in the atmosphere and the heat budget of the layer are obtained. The number of the linear simultaneous differential equations to be solved is reduced to as few as the double of the number of the atmospheric layer without any serious error.

The possibility of the upward motion is estimated by the first low of thermodynamics;

$$C_p \frac{dT}{dt} = \frac{dQ}{dt} - gw,$$

and this is also written as follows;

$$\Gamma w = Q - \frac{\partial T}{\partial t} - u\frac{\partial T}{\partial x} - v\frac{\partial T}{\partial y}, \qquad \text{(A.a1)}$$

where Γ $(= \frac{\partial T}{\partial z} + \frac{g}{C_p})$ is the static stability parameter, Q $(= \frac{1}{C_p}\frac{dQ}{dt})$ is the net heating rate due to radiation, conduction, and latent heat release. In this model, the net heating rate is approximated by the radiative heating alone, because the other terms are much smaller than the radiative heating. If equation (A.a1) is averaged zonally, the following zonal-mean equation is derived;

$$\Gamma \bar{w} = \bar{Q} - \overline{\frac{\partial T}{\partial t}} - \overline{v\frac{\partial T}{\partial y}}. \qquad \text{(A.a2)}$$

Since v is very small during the ozone hole event, the term $-\overline{v\frac{\partial T}{\partial y}}$ is neglected. Equation (A.a2) may give us a fairly good measure of the possibility of the upward motion (Tung et al., 1986), if the observed, in-situ temperature data is used for the radiative transfer calculation, and if the calculation has enough accuracy.

Although some of the calculation were performed by using equation (A.a2) (e.g. Tung et al., 1986), we use equation (A.a1) instead. The reasons are as follows: The center of the polar vortex does not completely coincide with the South Pole, and usually the shape of the vortex is not a perfect circle. The SAGE II satellite observed the aerosol extinction at 4 wavelengths by the solar occultation method (Limb sounding), and the observation was limited in the lower latitude than 73°S, so that even the data at the most southern latitude consists of the data both inside and outside of the polar vortex. Hence, the zonal-mean temperature data and the zonal-mean aerosol extinction data are not a good representative of the data inside of the polar vortex where the ozone hole occurs.

We choose one point inside the polar vortex, where the temperature is lowest and the PSC is densest between 11 km and 23 km high, out of 15 data on the same latitude on a day. Then, the term $-u\frac{\partial T}{\partial x}$ and $-v\frac{\partial T}{\partial y}$ can be neglected, and the calculation will give a good measure of the possibility of the upward motion within the polar vortex. We calculated Q in equation (A.a1) as accurately as possible by using the NMC temperature data and the SAGE II aerosol extinction data in 1985. The calculated heating rates Q are less than 0.1 K d^{-1} in the Antarctic stratosphere during the ozone hole, as shown in Figure A.1, even if the aerosol heating effect is added, and even if some ambiguous parameters such as the aerosol composition and the size distribution are chosen so that they magnify the heating effect.

The net heating effect of the aerosol in 1985 is also shown in Figure A.2. Furthermore, even if $\frac{\partial T}{\partial t}$ is assumed to be zero (actually, it has a positive value in spring to have a tendency to decrease w), w is estimated to be less than 0.07 mm s^{-1} when Γ =9.8 K km^{-1} ($\frac{\partial T}{\partial z}=0$). The value of w is too small to cause the sufficient upward motion for the ozone depletion. The result is evidently against the upward motion hypothesis.

Appendix B

The Derivation of the Correction Factor

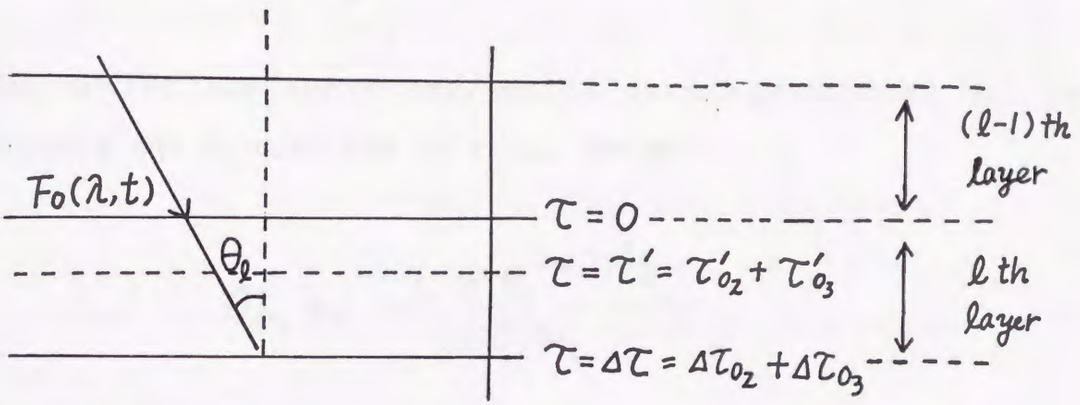

The energy absorbed by an ozone molecule at the optical depth $\tau'=\tau'_{o3}+\tau'_{o2}$ (see the above figure) in the lth layer per unit time is $\sigma_{o3}\cdot F_o\cdot\exp(-\tau'/\mu_l)$, where σ_{o3} is the absorption cross section of an ozone molecule, F_o is the solar flux at the top of the lth layer, and $\mu_l=\cos\theta_l$. Because $d\tau'_{o3}$ is proportional to the number of ozone, the absorption energy per an ozone molecule averaged over the lth layer can be obtained by averaging $\sigma_{o3}\cdot F_o\cdot\exp(-\tau'/\mu_l)$ on τ'_{o3},

$$\frac{1}{\Delta\tau_{o_3}}\int_0^{\Delta\tau_{o_3}}\sigma_{o_3}F_o\,e^{-(\tau'_{o_2}+\tau'_{o_3})/\mu_l}\,d\tau'_{o_3}\,. \qquad \text{(A.b1)}$$

When the layer is uniform, the ratio of the oxygen number density to the ozone number density is constant. That is,

$$\frac{\tau_{O_2}'}{\tau_{O_3}'} = R \,.$$

Substituting the above expression into equation (A.b1) and executing the integration on τ'_{O_3}, we get

$$\sigma_{O_3} F_o \frac{1 - e^{-\Delta\tau/\mu_\ell}}{\Delta\tau/\mu_\ell} \,,$$

or

$$\sigma_{O_3} F_o \frac{1 - \exp[-\sigma_{O_2} n_{O_2} \Delta z_\ell/\mu_\ell - \sigma_{O_3} n_{O_3} \Delta z_\ell/\mu_\ell]}{\sigma_{O_2} n_{O_2} \Delta z_\ell/\mu_\ell + \sigma_{O_3} n_{O_3} \Delta z_\ell/\mu_\ell} \,.$$

Since $\sigma_{O_3}(\lambda) \cdot F_o(\lambda, t)$ is the energy absorbed by an ozone molecule at the top of the lth layer ($\tau = 0$), the factor

$$\frac{1 - \exp[-\sigma_{O_2}(\lambda) n_{O_2}(\phi, z_\ell, t) \Delta z_\ell/\mu_\ell - \sigma_{O_3}(\lambda) n_{O_3}(\phi, z_\ell, t) \Delta z_\ell/\mu_\ell]}{\sigma_{O_2}(\lambda) n_{O_2}(\phi, z_\ell, t) \Delta z_\ell/\mu_\ell + \sigma_{O_3}(\lambda) n_{O_3}(\phi, z_\ell, t) \Delta z_\ell/\mu_\ell}$$

may be considered as a correction factor for an optical thick uniform layer.

REFERENCES

Akiyoshi, H., M. Fujiwara, and M. Uryu, 1988: Radiative aspects of the Antarctic ozone hole in 1985. Geophys. Res. Lett., **15**, 919-922.

Akiyoshi, H., M. Fujiwara, and M. Uryu, 1989: Calculation of heating rate in the Antarctic stratosphere in 1985 using SAGE Ⅱ data. Proceedings of the NIPR Symposium on Upper Atmosphere Physics, **2**, 129-139.

Andrews, D. G., and M. E. McIntyre, 1976: Planetary waves in horizontal and vertical shear: The generalized Eliassen-Palm relation and the mean zonal acceleration. J. Atmos. Sci., **33**, 2031-2048.

Aoki, S., T. Yamanouchi, S. Kanamori, M. Yamato, and Y. Makide, 1990: Measurements of atmospheric minor constituents at Syowa station, Antarctica and aboard research vessel shirase. Progress report of WCRP in Japan, Japanese WCRP association, 192-197.

Austin, J., R. L. Jones, D. S. McKenna, A. T. Buckland, J. G. Anderson, D. W. Fahey, C. B. Farmer, L. E. Heidt, M. H. Proffitt, A. F. Tuck, and J. F. Vedder, 1989: Lagrangian photochemical modeling studies of the 1987 Antarctic spring vortex 2. Seasonal trends in ozone. J. Geophys. Res., **94**, 16717-16735.

Bowman, K. P., and A. J. Krueger, 1985: A global climatology of total ozone from Nimbus 7 Total Ozone Mapping Spectrometer. J. Geophys. Res., **90**, 7967-7976.

Brasseur, G., and S. Solomon, 1986: Aeronomy of the middle atmosphere, Second edition, D. Reidel Publishing Company, Dordrecht, Holland.

Brasseur, G., M. H. Hitchman, S. Walters, and M. Pirre, 1990: An interactive chemical dynamical radiative two-dimensional model of the middle atmosphere. J. Geophys. Res., **95**, 5639-5655.

Brune, W. H., J. G. Anderson, and K. R. Chan, 1989a: In situ observations of BrO over Antarctica: ER-2 aircraft results from 54°S to 72°S latitude. J. Geophys. Res., **94**, 16639-16647.

Brune, W. H., J. G. Anderson, and K. R. Chan, 1989b: In situ observations of ClO in the Antarctic: ER-2 aircraft results from 54°S to 72°S latitude. J. Geophys. Res., **94**, 16649-16663.

Callis, L. B., and M. Natarajan, 1986: The Antarctic ozone minimum: Relationship to odd oxygen, odd chlorine, the final warming, and the 11-year solar cycle. J. Geophys. Res., **91**, 10771-10796.

Chandra, S., and R. D. McPeters, 1986: Some observations on the role of planetary waves in determining the spring time ozone distribution in the Antarctic. Geophys. Res. Lett., **13**, 1224-1227.

Chipperfield, M. P., and J. A. Pyle, 1988: Two-dimensional modeling of the Antarctic lower stratosphere. Geophys. Res. Lett., **15**, 875-878.

Chubachi, S., 1984: Preliminary results of ozone observation at Syowa station from February 1982 to January 1983. Mem. Nat. Inst. Polar Res., Spec. issue, Jpn., **No. 34**, 13-19.

Cicerone, R. J., R. S. Stolarski, and S. Walters, 1974: Stratospheric ozone destruction by man-made chlorofluoromethanes. Science, **185**, 1165-1167.

Cronn, D. R., W. L. Bamesverger, F. A. Menzia, S. F. Waylett, A. S. Waylett, T. W. Ferrara, H. M. Howard, and E. Robinson, 1986: Atmospheric trace gas trends at Palmer station, Antarctica: 1982-1985. Geophys. Res. Lett., **13**, 1272-1275.

Crutzen, P. J., 1974: Estimates of possible future ozone reductions from continued use of fluoro-chloro-methanes (CF_2Cl_2, $CFCl_3$). Geophys. Res. Lett., **1**, 205-208.

Cunnold, D., F. Alyea, N. Phillips, and R. Prinn, 1975: A three-dimensional dynamical-chemical model of atmospheric ozone. J. Atmos. Sci., **32**, 170-195.

Demore, W. B., S. P. Sander, D. M. Golden, M. J. Molina, R. F. Hampson, M. J. Kurylo, C. J. Howard, and A. R. Ravishankara, 1990: Chemical kinetics and photochemical data for use in stratospheric modeling, Evaluation Number 9, **JPL Publication 90-1**, Jet Propulsion Lab., Pasadena, California.

Dickinson, R. E., 1973: Method of parameterization for infrared cooling between altitudes of 30 km and 70 km. J. Geophys. Res., **78**, 4451-4457.

Dunkerton, T., 1978: On the mean meridional mass motions of the stratosphere and mesosphere. J. Atmos. Sci., **35**, 2325-2333.

Dunkerton, T. J., 1988: Body force circulation and the Antarctic ozone minimum. J. Atmos. Sci., **45**, 427-438.

Eberstein, I. J., 1990: Photodissociation of Cl_2O_2 in the spring Antarctic lower stratosphere. Geophys. Res. Lett., **17**, 721-724.

Farman, J. C., B. G. Gardiner, and J. D. shanklin, 1985: Large losses of total ozone in Antarctica reveal seasonal ClO_x/NO_x interaction. Nature, **315**, 207-210.

Fels, S. B., J. D. Mahlman, M. D. Schwarzkopf, and R. W. Sinclair, 1980: Stratospheric sensitivity to perturbations in ozone and carbon dioxide: Radiative and dynamical response. J. Atmos. Sci., **37**, 2265-2297.

Garcia, R. R., 1987: On the mean meridional circulation on the middle atmosphere. J. Atmos. Sci., **44**, 3599-3609.

Garcia, R. R., and S. Solomon, 1987: A possible relationship between interannual variability in Antarctic ozone and quasi-biennial oscillation. Geophys. Res. Lett., **14**, 848-851.

Gardiner, B. G., and J. D. Shanklin, 1986: Recent measurements of Antarctic ozone depletion. Geophys. Res. Lett., **13**, 1199-1201.

Gray, L. J., and J. A. Pyle, 1988: A two dimensional model of the quasi-biennial oscillation of ozone. Proceedings of the Polar Ozone Workshop, **NASA Conference Publication 10014**, 240-243.

Hartmann, D. L., 1978: A note concerning the effects of varying extinction on radiative-photochemical relaxation. J. Atmos. Sci., **35**, 1125-1130.

Hasebe, F., 1983: Interannual variations of global total ozone revealed from Nimbus 4 BUV and ground-based observations. J. Geophys. Res., **88**, 6819-6834.

Hofmann, D. J., J. W. Harder, S. R. Rolf, and J. M. Rosen, 1987: Balloon-borne observations of the development and vertical structure of the Antarctic ozone hole in 1986. Nature, **326**, 59-62.

Hofmann, D. J., J. W. Harder, J. M. Rosen, J. V. Hereford, and J. R. Carpenter, 1989: Ozone profile measurements at McMurdo station, Antarctica, during the spring of 1987. J. Geophys. Res., **94**, 16527-16536.

Hou, A. Y., H. R. Schneider, and M. K. W. Ko, 1991: A dynamical explanation for the asymmetry in zonally averaged column abundances of ozone between northern and southern springs. J. Atmos. Sci., **48**, 547-556.

Jones, R. L., and J. A. Pyle, 1984: Observations of CH_4 and N_2O by the nimbus 7 SAMS: A comparison with in-situ data and two dimensional numerical model calculations. J. Geophys, Res., **89**, 5263-5279.

Kawahira, K., and T. Hirooka, 1989: Interannual temperature changes in the Antarctic lower stratosphere - A relation to the ozone hole. Geophys. Res. Lett., **16**, 41-44.

Kida, H., 1983: General circulation of air parcels and transport characteristics derived from a hemisphere GCM. Part 2: Very long term motions of air parcels in the troposphere and stratosphere. J. Meteor. Soc. Japan, **61**, 510-523.

Kiehl J. T., B. A. Boville, and B. P. Briegleb, 1988: Response of a general circulation model to a prescribed Antarctic ozone hole. Nature, **332**, 501-504.

Ko, M. K. W., J. M. Rodriguez, N. D. Sze, M. H. Proffitt, W. L. Starr, A. Krueger, E. V. Browell, and M. P. McCormick, 1989: Implications of AAOE observations for proposed chemical explanations of the seasonal and interannual behavior of Antarctic ozone. J. Geophys. Res., **94**, 16705-16715.

Komhyr, W. D., R. D. Grass, and R. K. Leonard, 1986: Total ozone decrease at south pole, Antarctica, 1964-1985. Geophys. Res. Lett., **13**, 1248-1251.

Komhyr, W. D., P. R. Franchois, B. C. Halter, and C. C. Wilson, 1987: ECC ozonesonde observations at south pole, Antarctica, during 1986, **NOAA Data Report ERL ARL-11**, Air Resources Laboratory Silver Spring, Maryland.

Komhyr, W. D., P. R. Franchois, S. E. Kuester, P. J. Reitelbach, and M. L. Fanning, 1988a: ECC ozonesonde observations at south pole, Antarctica, during 1987, **NOAA Data Report ERL ARL-15**, Air Resources Laboratory Silver Spring, Maryland.

Komhyr, W. D., S. J. Oltmans, and R. D. Grass, 1988b: Atmospheric ozone at South Pole, Antarctica, in 1986. J. Geophys. Res., **93**, 5167-5184.

Komhyr, W. D., J. A. Lathrop, R. W. Poston, and T. O. Mullen, 1989a: ECC ozonesonde observations at south pole, Antarctica, during 1988, **NOAA Data Report ERL ARL-18**, Air Resources Laboratory Silver Spring, Maryland.

Komhyr, W. D., R. D. Grass, P. J. Reitelbach, S. E. Kuester, P. R. Franchois, and M. L. Fanning, 1989b: Total ozone, ozone vertical distributions, and the stratospheric temperatures at South Pole, Antarctica, in 1986, and 1987. J. Geophys. Res., **94**, 11429-11436.

Krueger, A. J., P. E. Ardanuy, F. S. Sechrist, L. M. Penn, D. E. Larko, S. D. Doiron, and R. N. Galimore, 1988: The 1987 Airborne Antarctic Ozone Experiment, **NASA Reference Publication 1201.**

Lait, L. R., M. R. Schoeberl, P. A. Newman, and R. S. Stolarski, 1988: The QBO and interannual variation in total ozone. Proceedings of the Polar Ozone Workshop, **NASA Conference Publication 10014**, 211-213.

Leu, M. T., 1988: Heterogeneous reactions of N_2O_5 with H_2O and HCl on ice surfaces: Implications for Antarctic ozone depletion. Geophys. Res. Lett., **15**, 851-854.

Lindzen, R. S., and S. Chapman, 1969: Atmospheric tides. Space Science Reviews, **10**, 3-188.

Mahlman, J. D., and S. B. Fels, 1986: Antarctic ozone decreases: A dynamical cause? Geophys. Res. Lett., **13**, 1316-1319.

Matsuno, T., 1980: Lagrangian motion of air parcels in the stratosphere in the presence of planetary waves. Pure Appl. Geophys., **118**, 189-216.

Matsuno, T., 1982: A quasi one-dimensional model of the middle atmosphere circulation interacting with internal gravity waves. J. Meteor. Soc. Japan, **60**, 215-226.

McCormick, M. P., and C. P. Trepte, 1987: Polar stratospheric optical depth observed between 1978 and 1985. J. Geophys. Res., **92**, 4297-4306.

McElroy, M. B., R. J. Salawitch, S. C. Wofsy, and J. A. Logan, 1986: Reductions of Antarctic ozone due to synergistic interactions of chlorine and bromine. Nature, **321**, 759-762.

McGrath, M. P., K. C. Clemitshaw, F. S. Rowland, and W. J. Hehre, 1988: Thermochemical stabilities and vibrational spectra of isomers of the chlorine oxide dimer. Geophys. Res. Lett., **15**, 883-886.

McPeters, R. D., D. F. Hearth, and P. K. Bhartia, 1984: Average ozone profiles for 1979 from the NIMBUS 7 SBUV instrument. J. Geophys. Res., **89**, 5199-5214.

Meador, W. E., and W. R. Weaver, 1980: Two-stream approximations to radiative transfer in planetary atmospheres; A unified description of existing methods and a new improvement. J. Atmos. Sci., **37**, 630-643.

Miller, C., D. L. Filkin, A. J. Owens, J. M. Steed, and J. P. Jesson, 1981: A two-dimensional model of stratospheric chemistry and transport. J. Geophys. Res., **86**, 12039-12065.

Molina, L. T., and M. J. Molina, 1987: Production of Cl_2O_2 from the self reaction of the ClO radical. J. Phys. Chem., **91**, 433-436.

Molina, M. J., and F. S. Rowland, 1974: Stratospheric sink for chlorofluoromethanes: Chlorine atom-catalyzed destruction of ozone. Nature, **249**, 810-812.

Nagatani, R. M., and A. J. Miller, 1987: The influence of lower stratospheric forcing on the October Antarctic ozone decrease. Geophys. Res. Lett., **14**, 202-205.

Parrish, A., R. L. deZafra, M. Jaramillo, B. Connor, P. M. Solomon, and J. W. Barret, 1988: Extremely low N_2O concentrations in the springtime stratosphere at Mcmurdo Station, Antarctica. Nature, **332**, 53-55.

Plumb, R. A., 1982: Zonally symmetric Hough modes and meridional circulations in the middle atmosphere. J. Atmos. Sci., **39**, 983-991.

Plumb, R. A., and J. D. Mahlman, 1987: the zonally averaged transport characteristics of the GFDL general circulation/transport model. J. Atmos. Sci., **44**, 298-327.

Rodriguez, J. M., M. K. W. Ko, and N. D. Sze, 1986: Chlorine chemistry in the Antarctic stratosphere: Impact of OClO and Cl_2O_2 and implications for observations. Geophys. Res. Lett., **13**, 1292-1295.

Rodriguez, J. M., M. K. W. Ko, N. D. Sze, S. D. Pierce, J. G. Anderson, D. W. Fahey, K. Kelly, C. B. Farmer, G. C. Toon, M. T. Coffey, L. E. Heidt, W. G. Mankin, K. R. Chan, W. L. Starr, J. F. Vedder, and M. P. McCormick, 1989: Nitrogen and chlorine species in the spring Antarctic stratosphere: Comparison of models with Airborne Antarctic Ozone Experiment observations. J. Geophys. Res., **94**, 16683-16703.

Rodriguez, J. M., M. K. W. Ko, and N. D. Sze, 1990: The role of chlorine chemistry in Antarctic ozone loss: Implications of new kinetic data. Geophys. Res. Lett., **17**, 255-258.

Salawitch, R. J., S. C. Wofsy, and M. B. McElroy, 1988: Influence of polar stratospheric clouds on the depletion of Antarctic ozone. Geophys. Res. Lett., **15**, 871-874.

Sawada, R., and A. Matsushima, 1964: Thermally driven annual atmospheric oscillations as a cause of dynamic heating of the winter polar upper mesosphere. J. Meteor. Soc. Japan, **42**, 97-108.

Schneider, H. R., M. K. W. Ko, N. D. Sze, G. Y. Shi, and W. C. Wang, 1989: An evaluation of the role of eddy diffusion in stratospheric interactive two-dimensional model. J. Atmos. Sci, **46**, 2079-2093.

Schoeberl, M. R., and A. J. Krueger, 1986: The morphology of Antarctic total ozone as seen by TOMS. Geophys. Res. Lett., **13**, 1217-1220.

Shi, G. Y., W. C. Wang, and M. K. W. Ko, 1986: Radiative heating due to stratospheric aerosols over Antarctica. Geophys. Res. Lett., **13**, 1335-1338.

Solomon, S., R. R. Garcia, and F. Stordal, 1985: Transport processes and ozone perturbations. J. Geophys. Res., **90**, 12981-12989.

Solomon, S., R. R. Garcia, F. S. Rowland, and D. J. Wuebbles, 1986: On the depletion of Antarctic ozone. Nature, **321**, 755-758.

Stolarski, R. S., A. J. Krueger, M. R. Schoeberl, R. D. McPeters, P. A. Newman, and J. C. Alpert, 1986: Nimbus 7 SBUV/TOMS measurements of the spring time Antarctic ozone hole. Nature, **322**, 808-811.

Strobel, D. F., 1978: Parameterization of the Atmospheric heating rate from 15 to 120 km due to O_2 and O_3 absorption of solar radiation. J. Geophys. Res., **83**, 6225-6230.

Tolbert, M. A., M. J. Rossi, R. Malhotra, and D. M. Goldeu, 1987: Radiation of chlorine nitrate with hydrogen chloride and water at Antarctic stratospheric temperatures. Science, **238**, 1258-1260.

Tolbert, M. A., M. J. Rossi, and D. M. Golden, 1988: Heterogeneous interactions of chlorine nitrate, hydrogen chloride, and nitric acid with sulfuric acid surfaces at stratospheric temperatures. Geophys. Res. Lett., **15**, 847-850.

Toon, G. C., C. B. Farmer, L. L. Lowes, P. W. Schaper, J. F. Blavier, and R. H. Norton, 1989: Infrared aircraft measurements of stratospheric composition over Antarctica during September 1987. J. Geophys. Res., **94**, 16571-16594.

Trenberth, K. E., 1973: Global model of the general circulation of the atmosphere below 75 kilometers with an annual heating cycle. Mon. Weather Rev., **101**, 287-305.

Tung, K. K., M. K. W. Ko, J. M. Rodriguez, and N. D. Sze, 1986: Are Antarctic ozone variations a manifestation of dynamics or chemistry? Nature, **322**, 811-814.

Tung, K. K., 1987: A coupled model of zonally averaged dynamics, radiation and chemistry. Transport Process in the Middle Atmosphere, Visconti, G., and R. R. Garcia, Eds., Reidel.

Tung, K. K., and H. Yang, 1988: Dynamical component of seasonal and year-to-year changes in Antarctic and global ozone. J. Geophys. Res., **93**, 12537-12559.

Turco, R., A. Plumb, and E. Condon, 1990: The Airborne Arctic Stratospheric Expedition: Prologue. Geophys. Res. Lett., **17**, 313-316.

Wofsy, S. C., M. B. McElroy, and M. D. Sze, 1975: Freon consumption: Implications for atmospheric ozone. Science, **187**, 535-537.

Yamamoto, G., 1962: Direct absorption of solar radiation by atmospheric water vapor, carbon dioxide and molecular oxygen. J. Atmos. Sci., **19**, 182-188.

Yang, H., K. K. Tung, and E. Olaguer, 1990: Nongeostrophic theory of zonally averaged circulation, PartⅡ : Eliassen-Palm flux divergence and isentropic mixing coefficient. J. Atmos. Sci., **47**, 215-241.

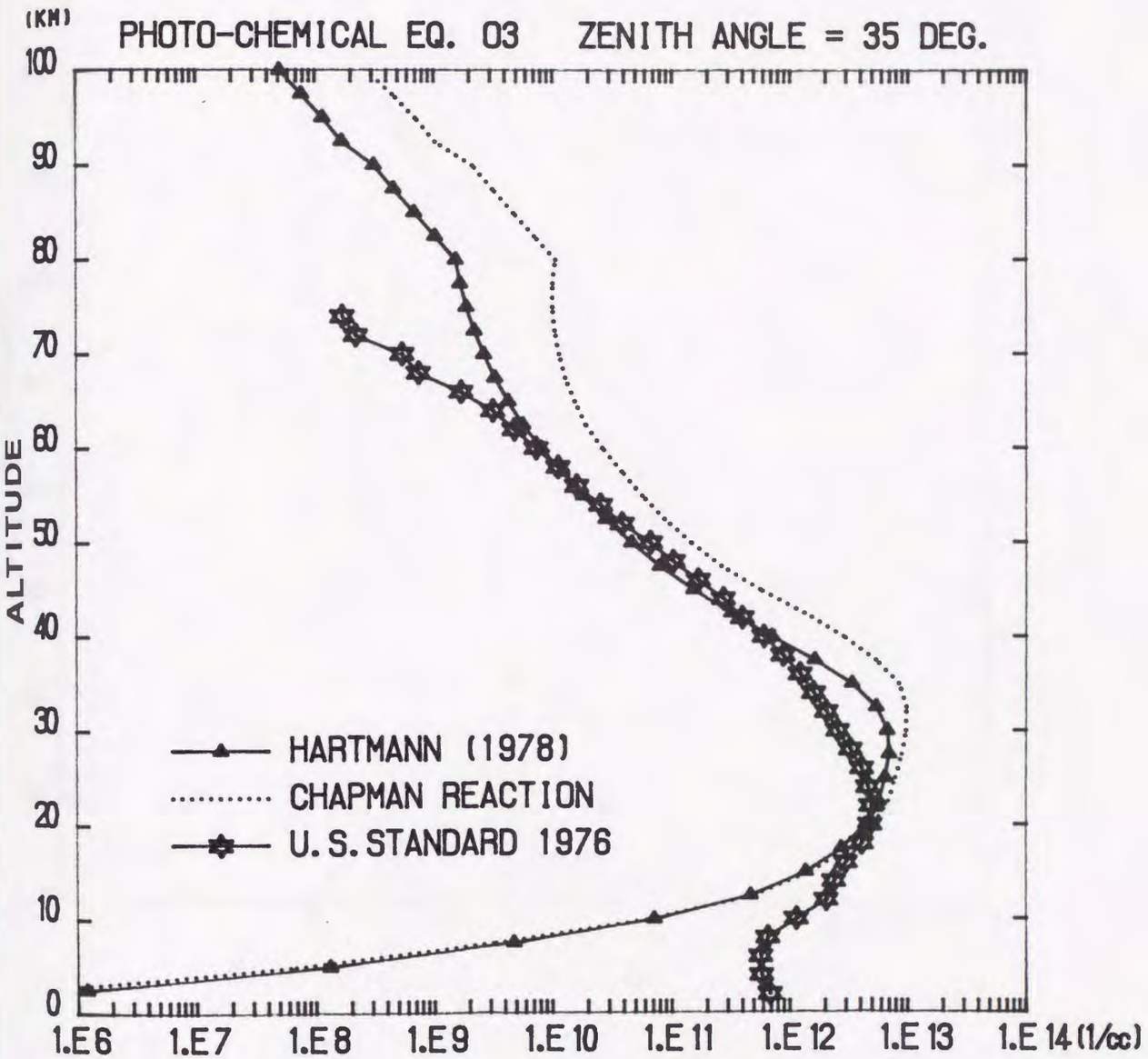

Figure 3.1. Vertical distributions of photochemical equilibrium ozone concentration calculated by assuming the normal Chapman cycle and the Chapman cycle parameterized by Hartmann (1978). Ozone profile from U. S. Standard Atmosphere (1976) is also shown.

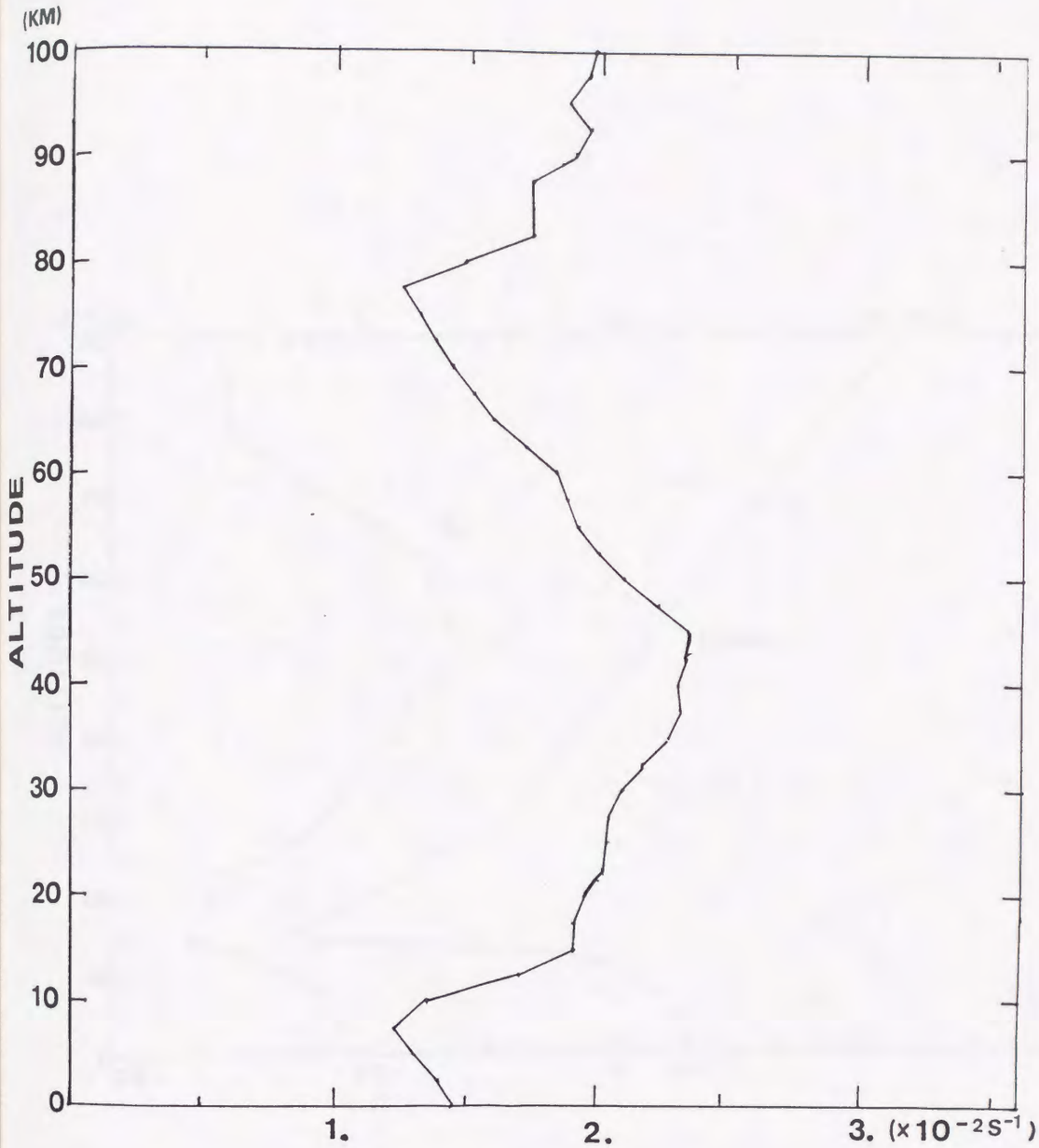

Figure 3.2a. Vertical profile of Brunt-Väisälä frequency N(z) used in the model.

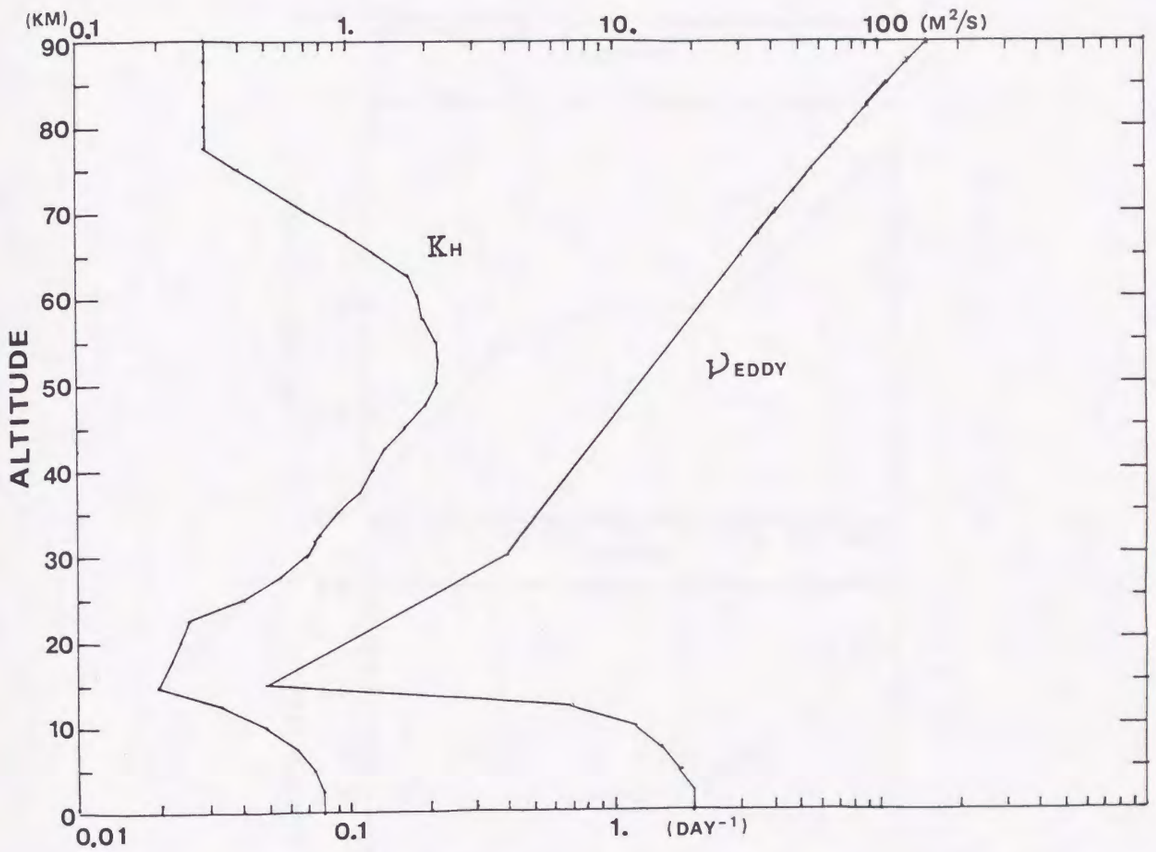

Figure 3.2b. Vertical profiles of eddy viscosity coefficient ν (z) and Newtonian cooling coefficient $k_H(z)$. The upper abscissa shows the scale for ν (z) and the lower abscissa shows the scale for $k_H(z)$.

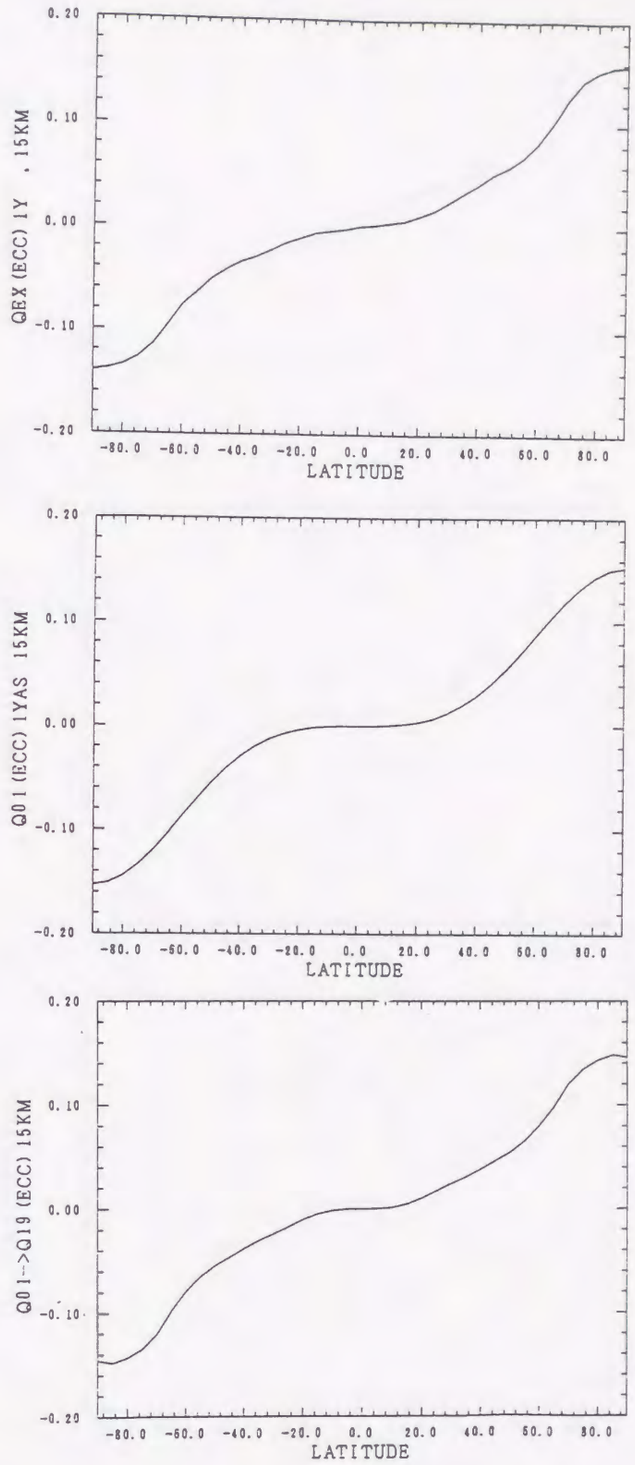

Figure 3.3a. Latitudinal distribution of the external heating function at 15 km high estimated by using observational ozone distribution data, the absorption cross section data of ozone and oxygen, and a radiative transfer scheme (the top), the one represented by the gravest anti-symmetric Hough mode alone (the middle), and the one represented by the sum of the 10 anti-symmetric Hough modes (the bottom). Note that water vapor heating is not included. (See Figure 3.5.)

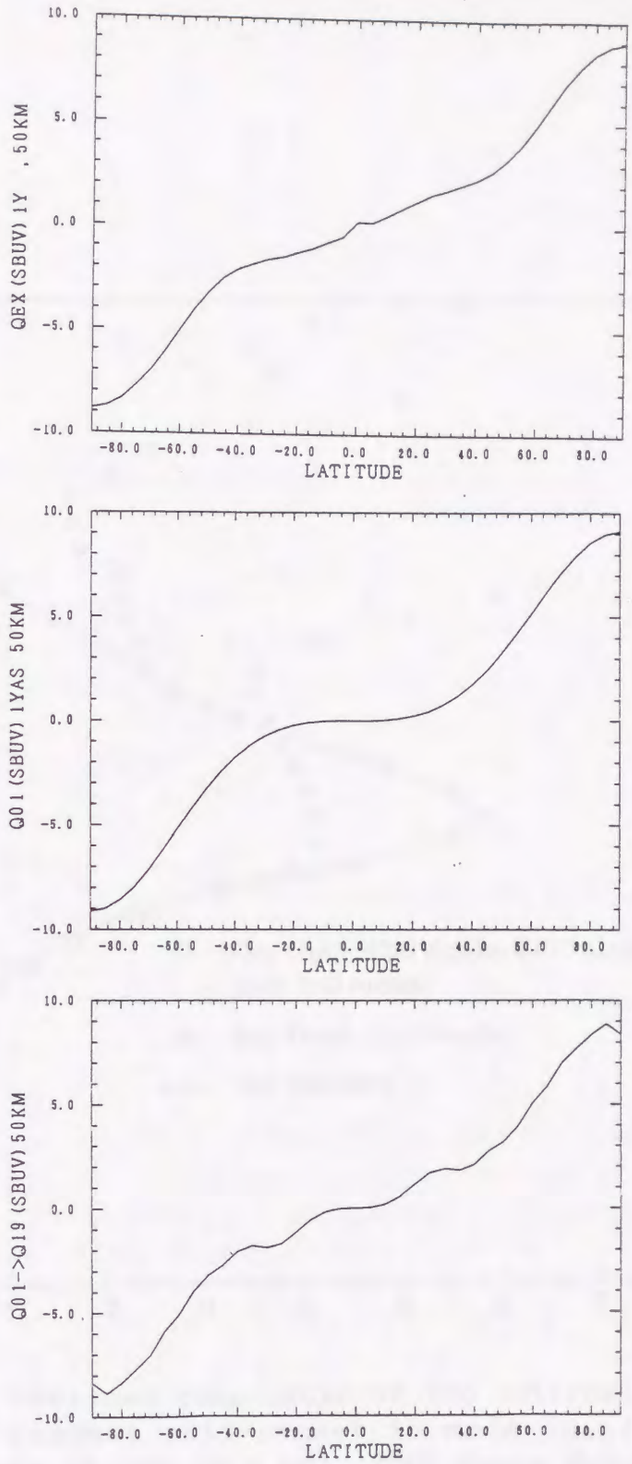

Figure 3.3b. Same as Figure 3.3a, but at 50 km high.

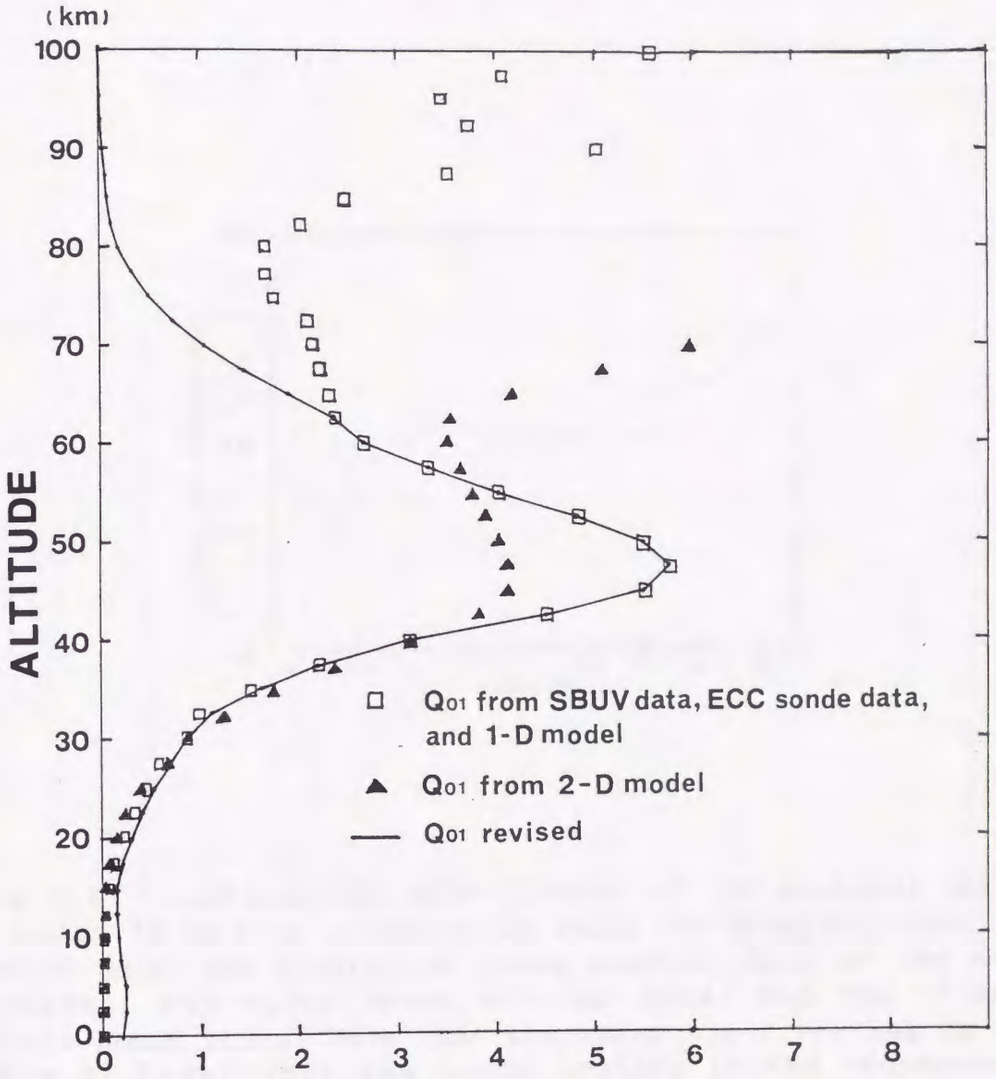

Figure 3.4. Vertical components of the external heating functions for the gravest anti-symmetric mode ($Q_{o1}(z)$): (□) ECC ozone sonde data (below 15.0 km), SBUV ozone data (between 17.5 km and 70 km), ozone distribution of 1-D radiative-chemical model (above 72.5 km) are used; (▲) Ozone distribution in the 2-D model is used; (—) The profile (□) is revised below 37.5 km (by including water vapor heating) and above 65 km (in order to avoid unusual amplitude of the seasonal variation of temperature).

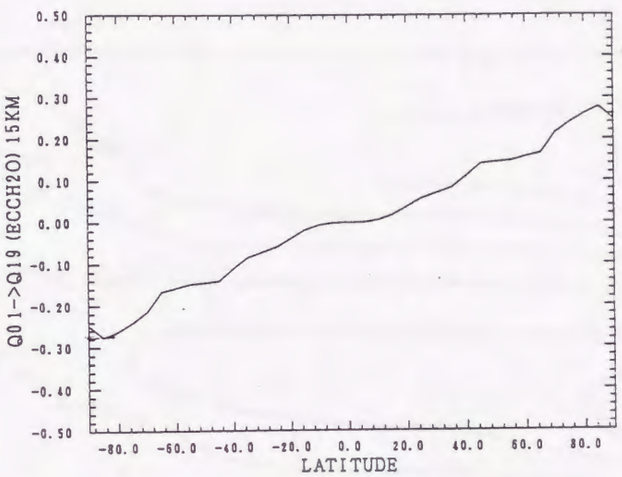

Figure 3.5. Latitudinal distribution of the external heating function at 15 km high estimated by using the observed ozone distribution data, the absorption cross section data of the ozone and oxygen, the water vapor heating data, and the 10 antisymmetric Hough modes. Note that the water vapor heating is comparable or lager than the ozone heating in the troposphere. (Compare to Figure 3.3a.)

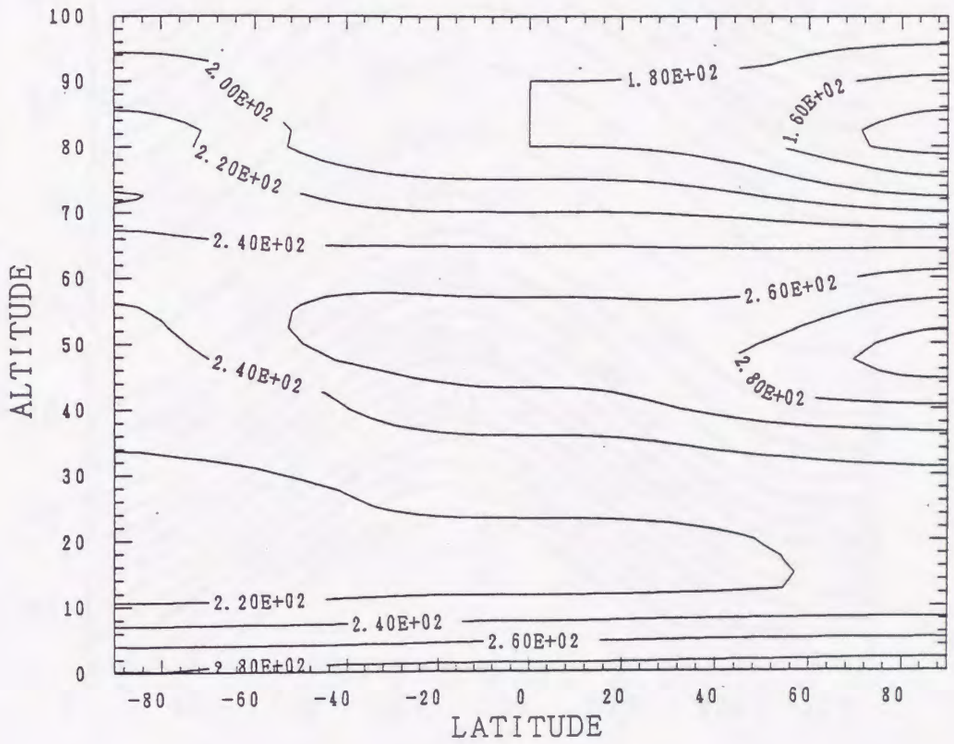

Figure 3.6. Temperature distribution calculated from equation (3a.4)-(3a.7) on the condition of the summer solstice in the northern hemisphere.

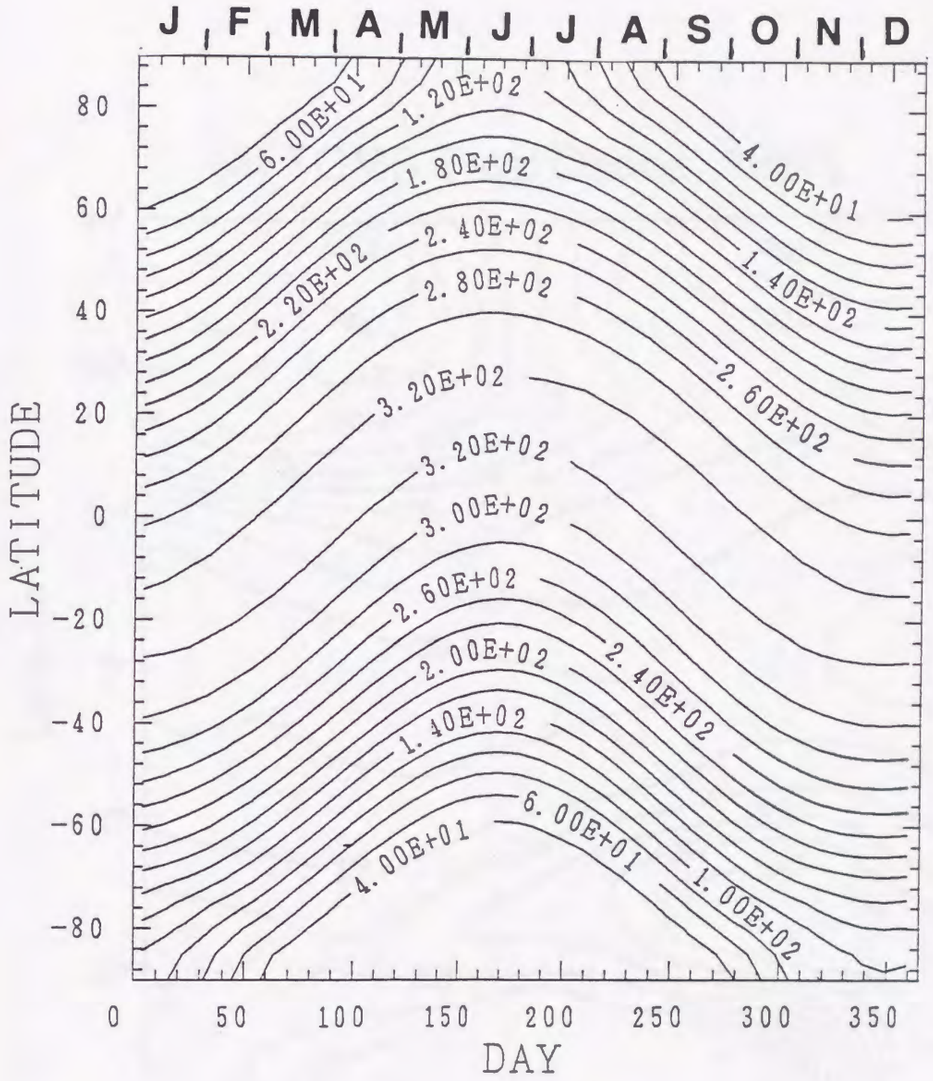

Figure 3.7. Time-latitude cross section of the total ozone amount calculated under the condition of photochemical equilibrium. The unit of the value in the figure is Dobson unit. Day number 1 and Day number 365 correspond to January 1 and December 31, respectively. The months are also indicated on the upper abscissa.

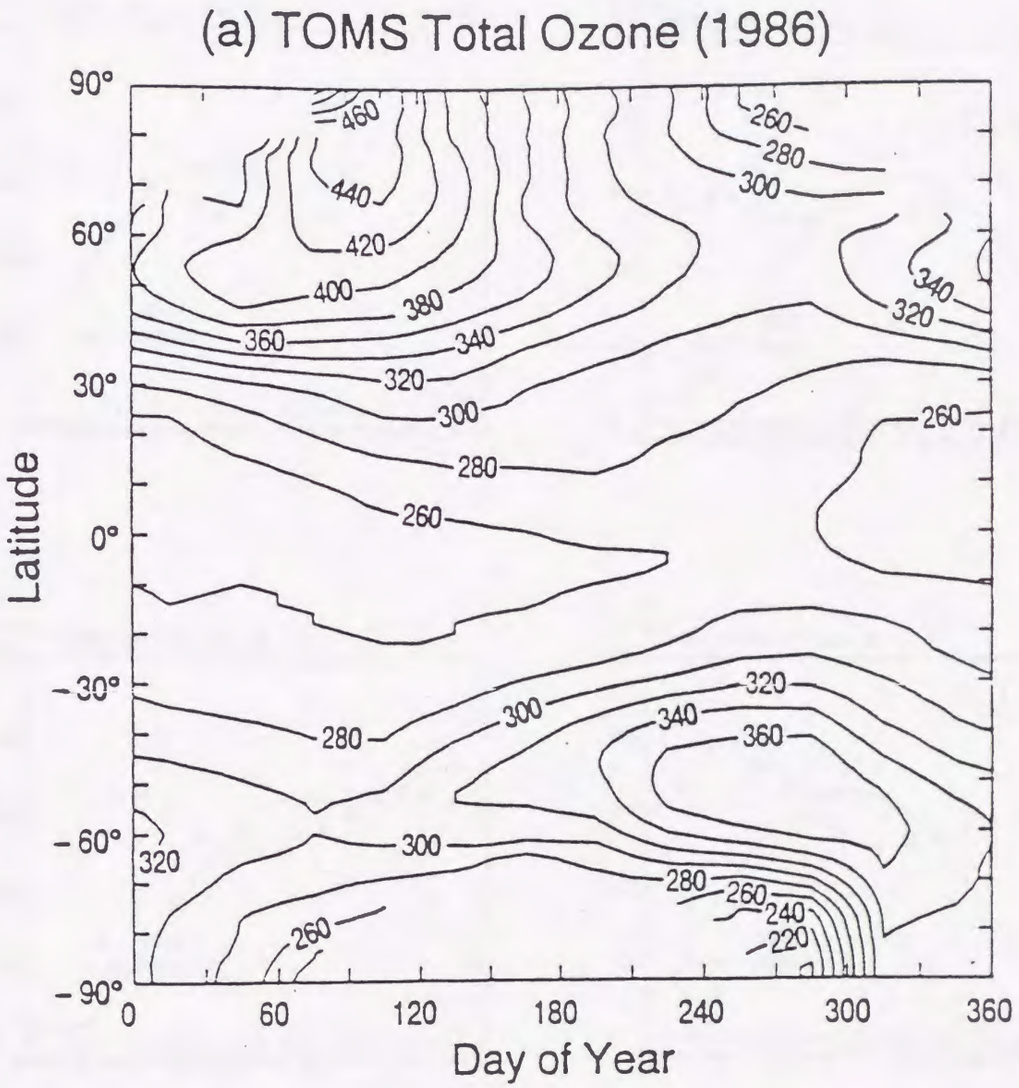

Figure 3.8. Total ozone amount for 1986 in Dobson units from TOMS.

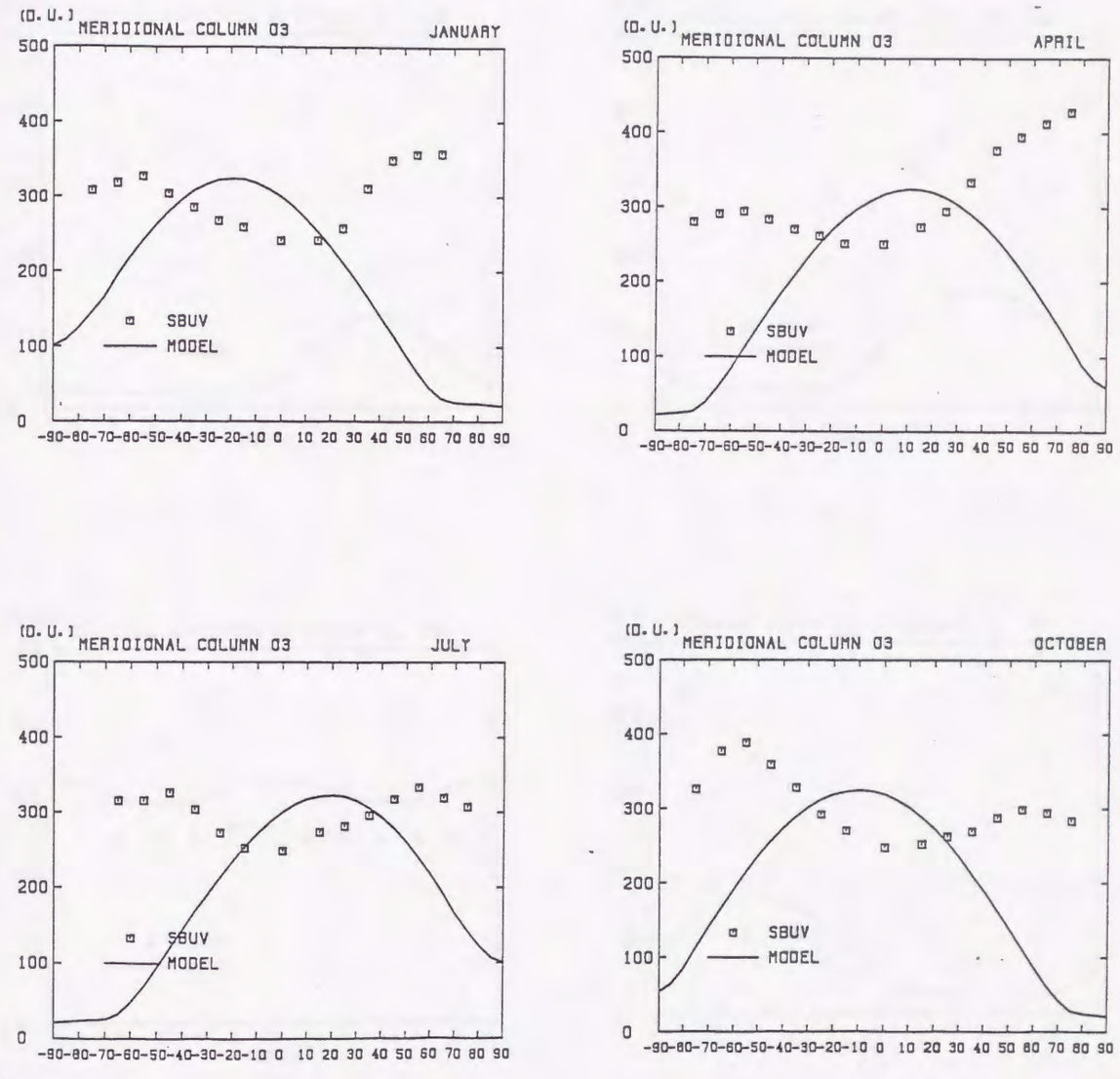

Figure 3.9. Latitudinal distributions of the observed total ozone amount (SBUV, 1979) and the calculated one (same as Figure 3.7) in January, April, July, and October.

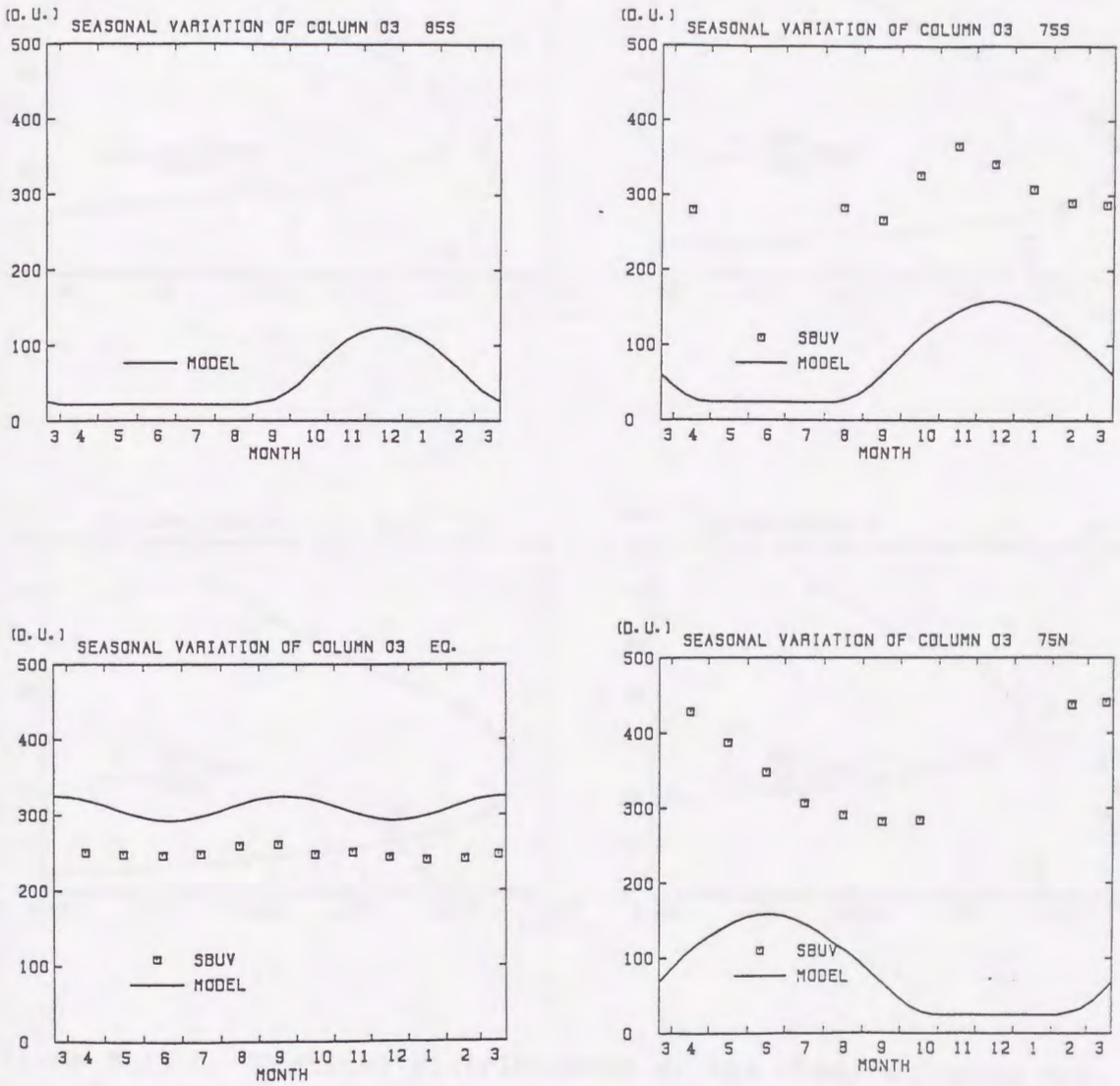

Figure 3.10. Seasonal variations of the observed total ozone amount (SBUV, 1979) and the calculated one (same as Figure 3.7) at 85°S, 75°S, the equator, and 75°N. Note that there is no SBUV data at 85°S and in the winter period at 75°S and 75°N.

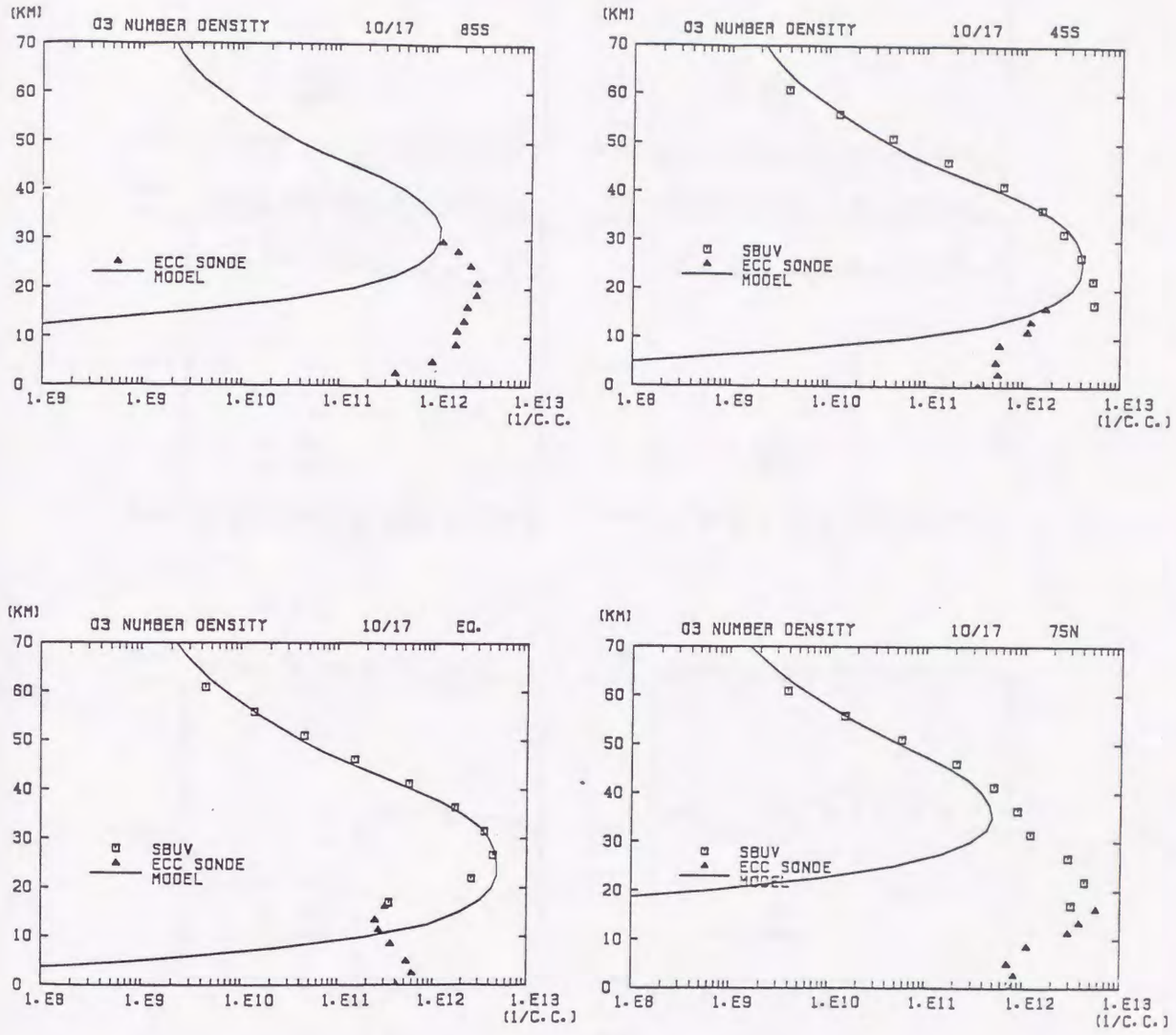

Figure 3.11. Vertical distributions of the observed ozone concentration and the calculated one at 85°S, 45°S, the equator, and 75°N in October. SBUV ozone data (1979) are plotted above 100 mb, and ECC ozone sonde data (1985-1987) are plotted below 100 mb where the accuracy of SBUV data is questionable.

50km

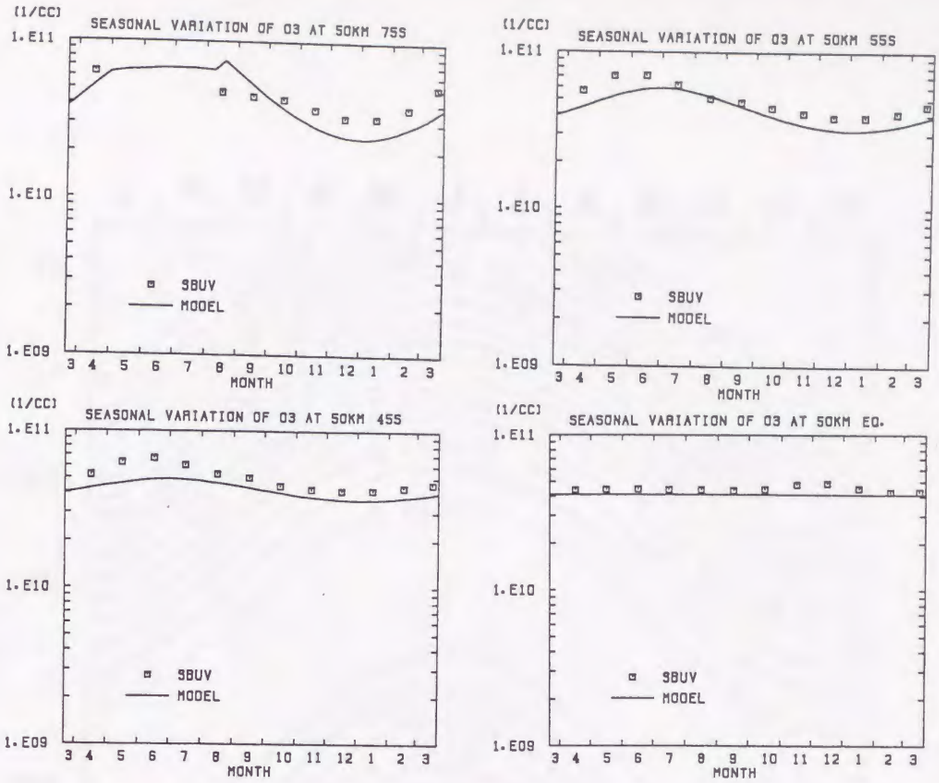

35km

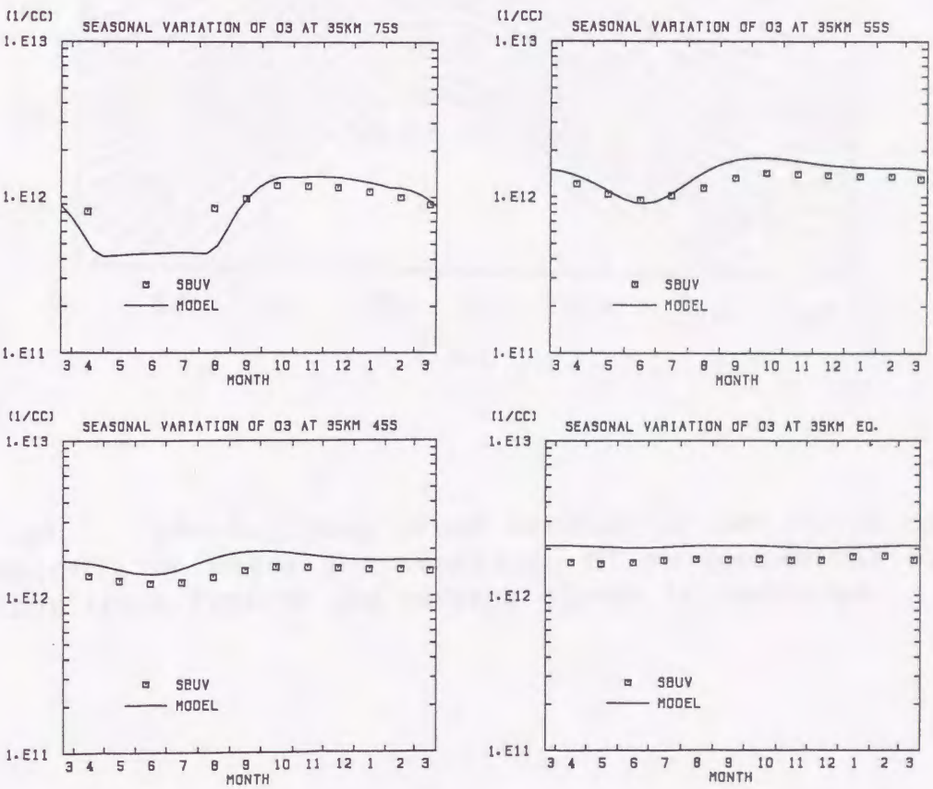

Figure 3.12. Seasonal variations of observed and calculated ozone concentration at 50 km and 35 km.

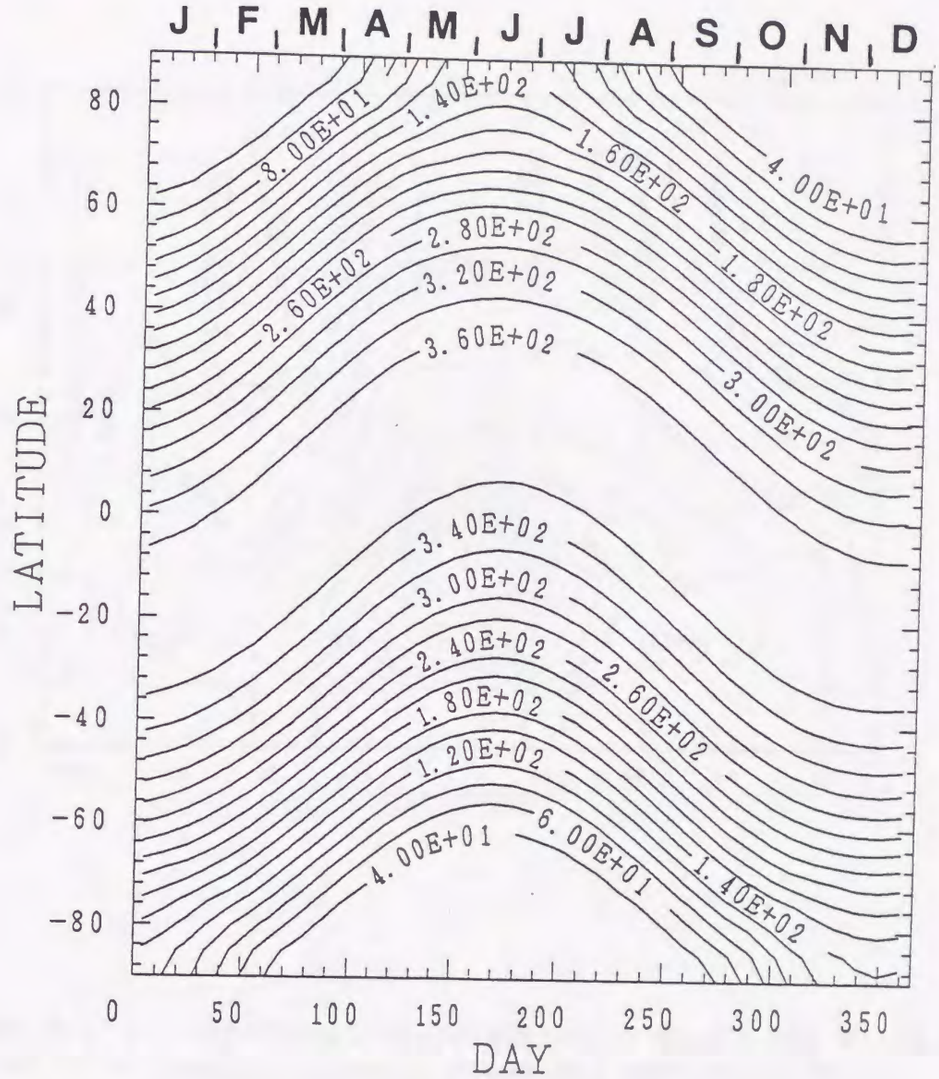

Figure 3.13. Time-latitude cross section of the total ozone amount calculated under the condition of photochemical equilibrium, but the effect of the surface albedo is neglected.

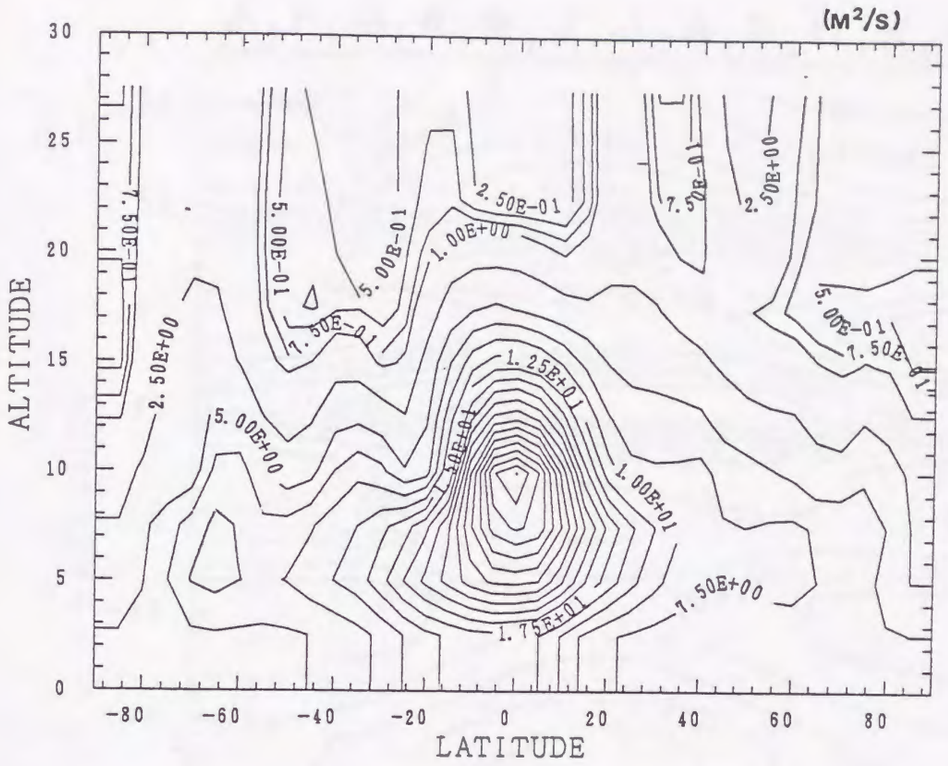

Figure 3.14. Meridional distribution of $K_{zz}(\phi, z)$ which is calculated by averaging annually Plumb and Mahlman (1987)'s $K_{zz}(\phi, z, t)$.

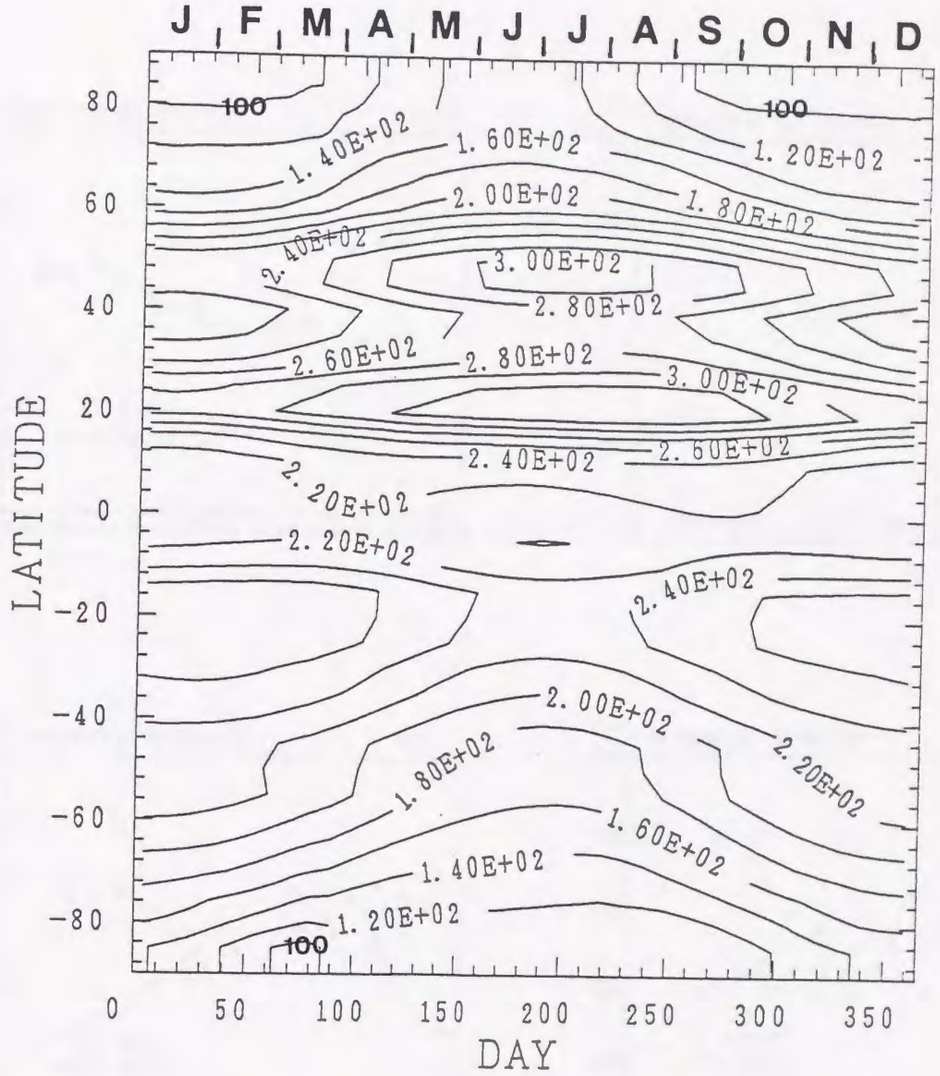

Figure 3.15. Time-latitude cross section of the total ozone amount obtained by numerical integration of equation (3b.1) for three years. The vertical eddy transport of ozone and an ozone dissipation process at the surface are considered. The seasonal variation of the third year is shown.

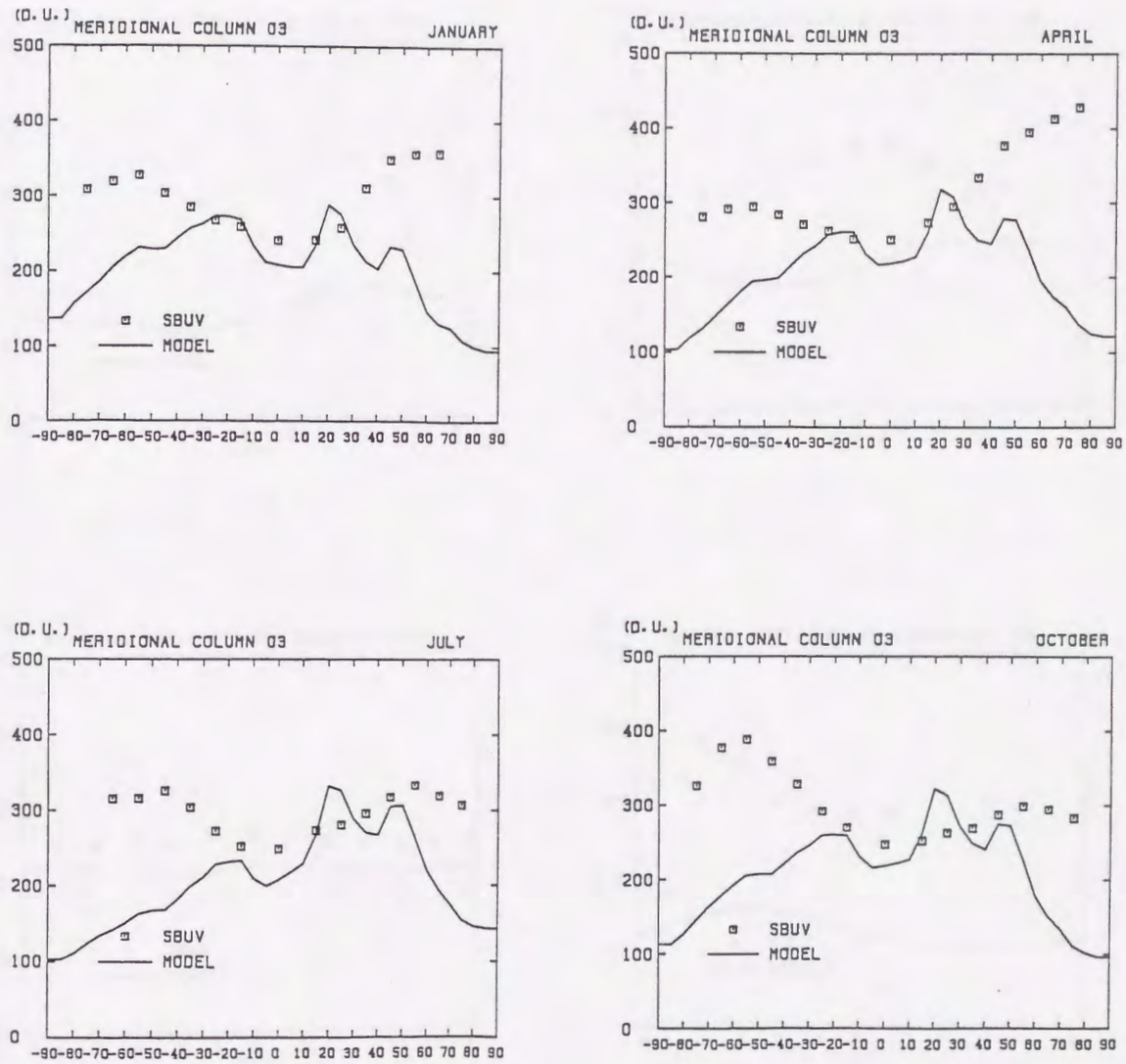

Figure 3.16. Latitudinal distributions of the observed total ozone (SBUV, 1979) and the calculated one (same as Figure 3.15) in January, April, July, and October.

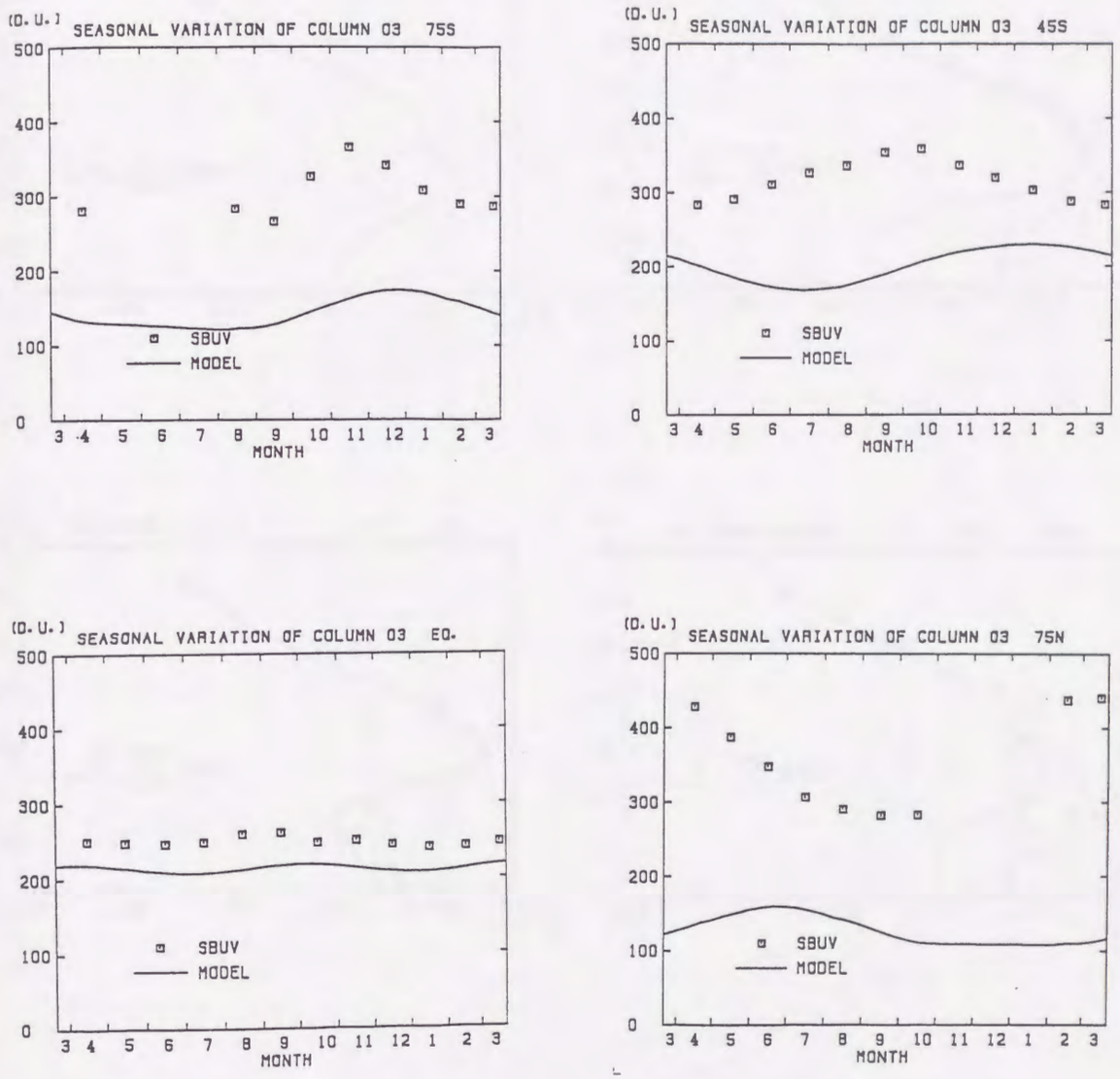

Figure 3.17. Seasonal variations of the observed total ozone (SBUV, 1979) and the calculated one (same as Figure 3.15) at 75°S, 45°S, the equator, and 75°N.

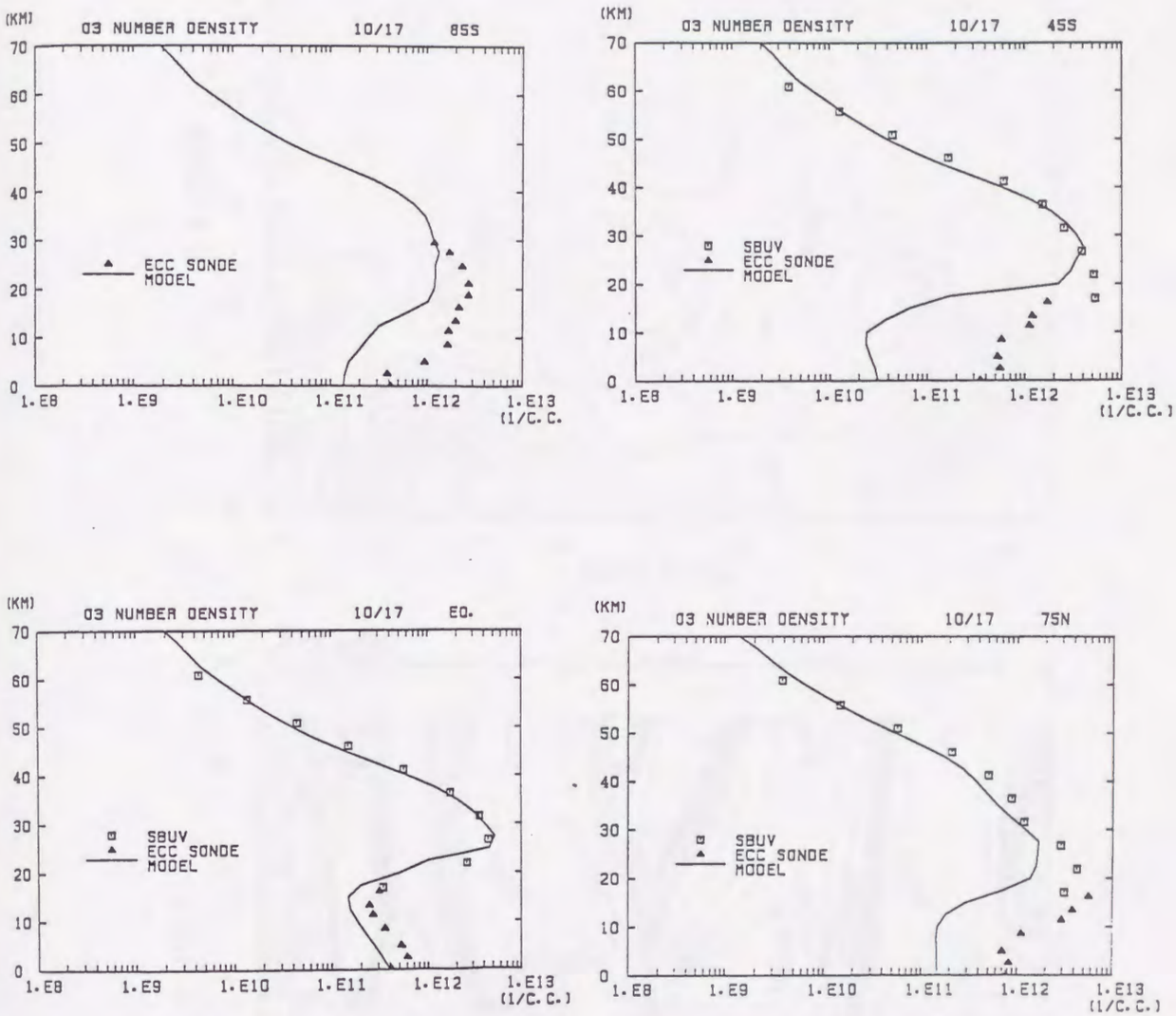

Figure 3.18. Vertical distributions of the observed ozone concentration and the calculated one at 85°S, 45°S, the equator, and 75°N in October.

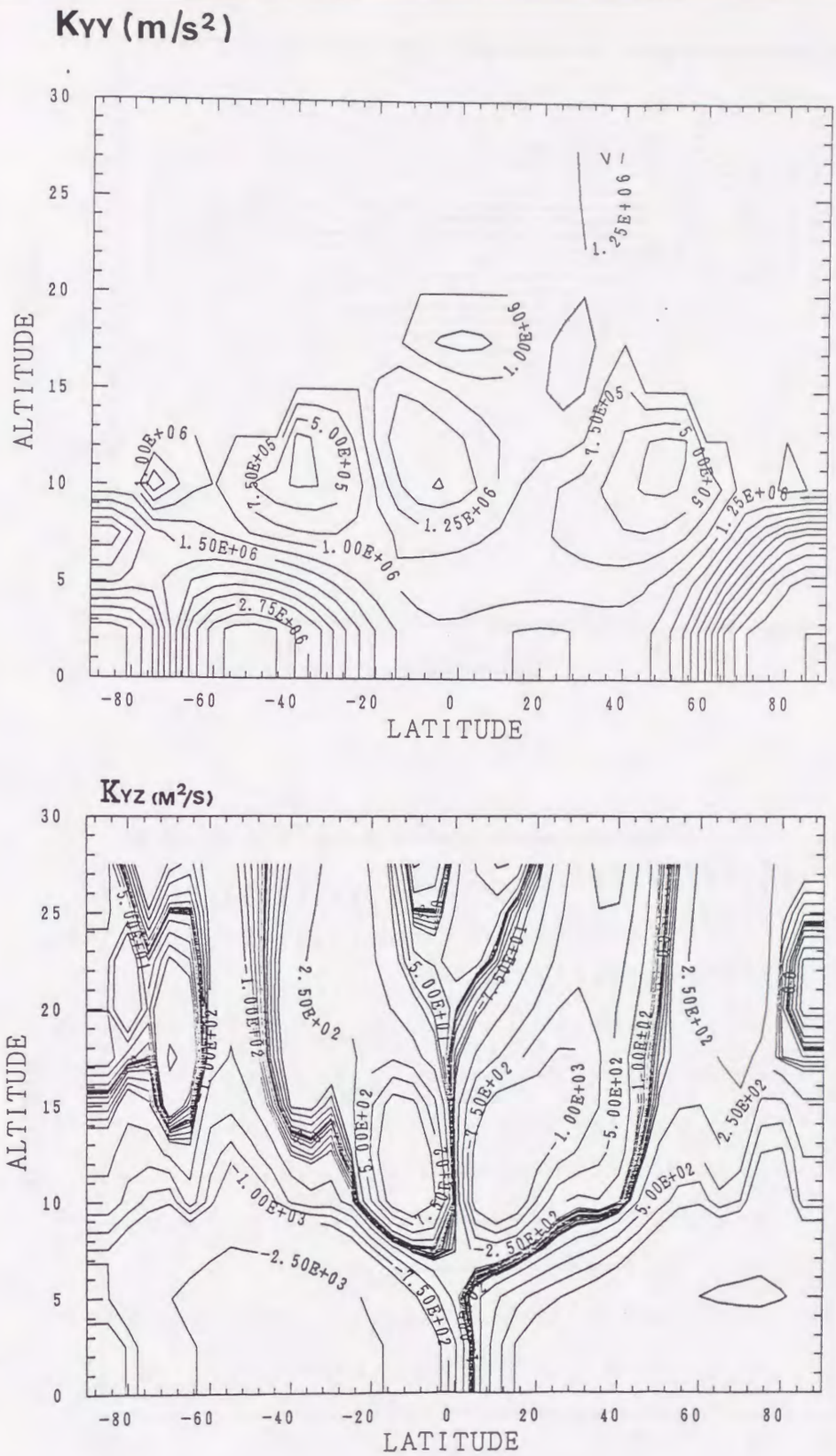

Figure 3.19. Meridional cross sections of K_{yy} and K_{yz} used in the model.

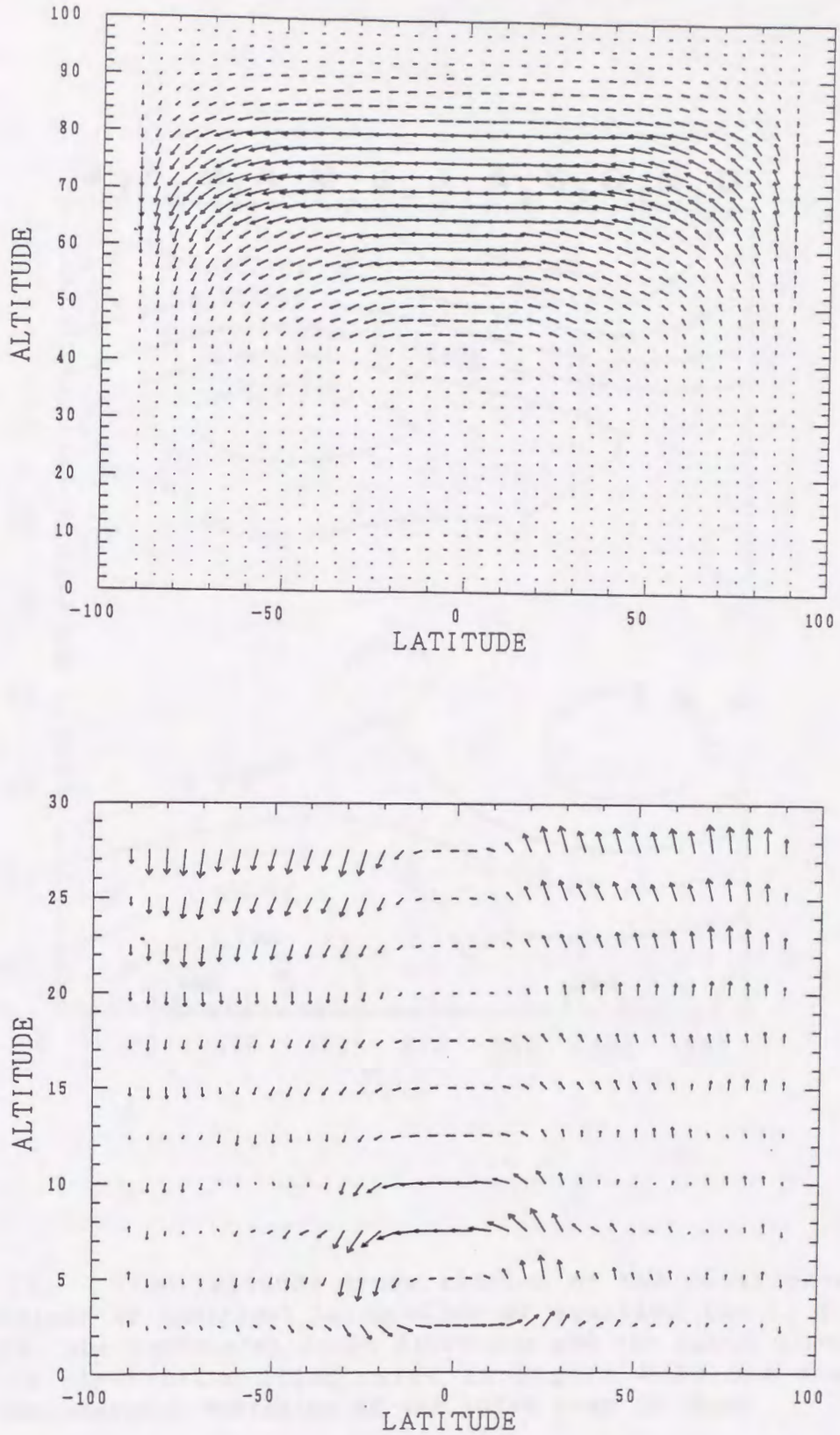

Figure 3.20. Anti-symmetric circulation at the summer solstice due to the atmospheric heating by ozone, oxygen, and water vapor. The lower panel is the magnification of the lower part of the circulation.

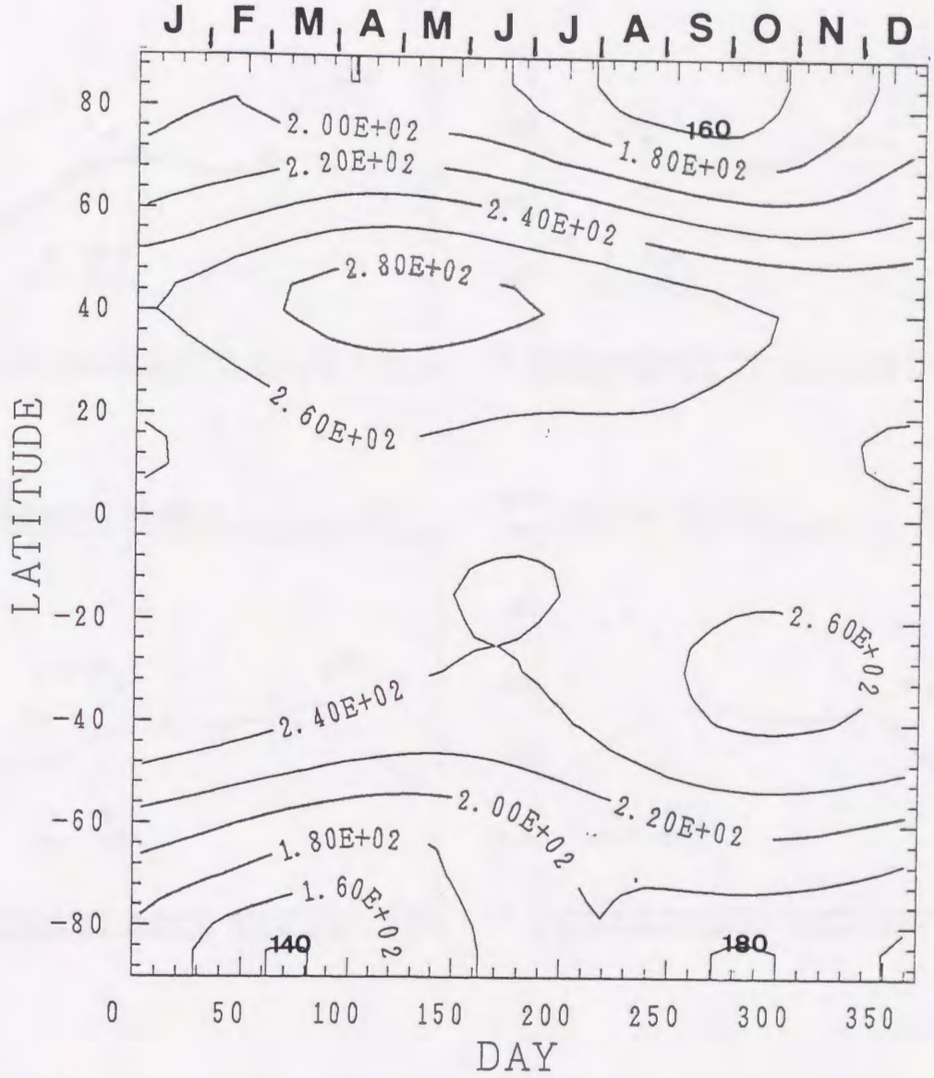

Figure 3.21. Time-latitude cross section of the total ozone amount obtained by numerical integration of equation (3c.1) for three years. The horizontal ozone diffusion and the ozone advection by the circulation illustrated in Figure 3.20 are considered. The seasonal variation of the third year is shown.

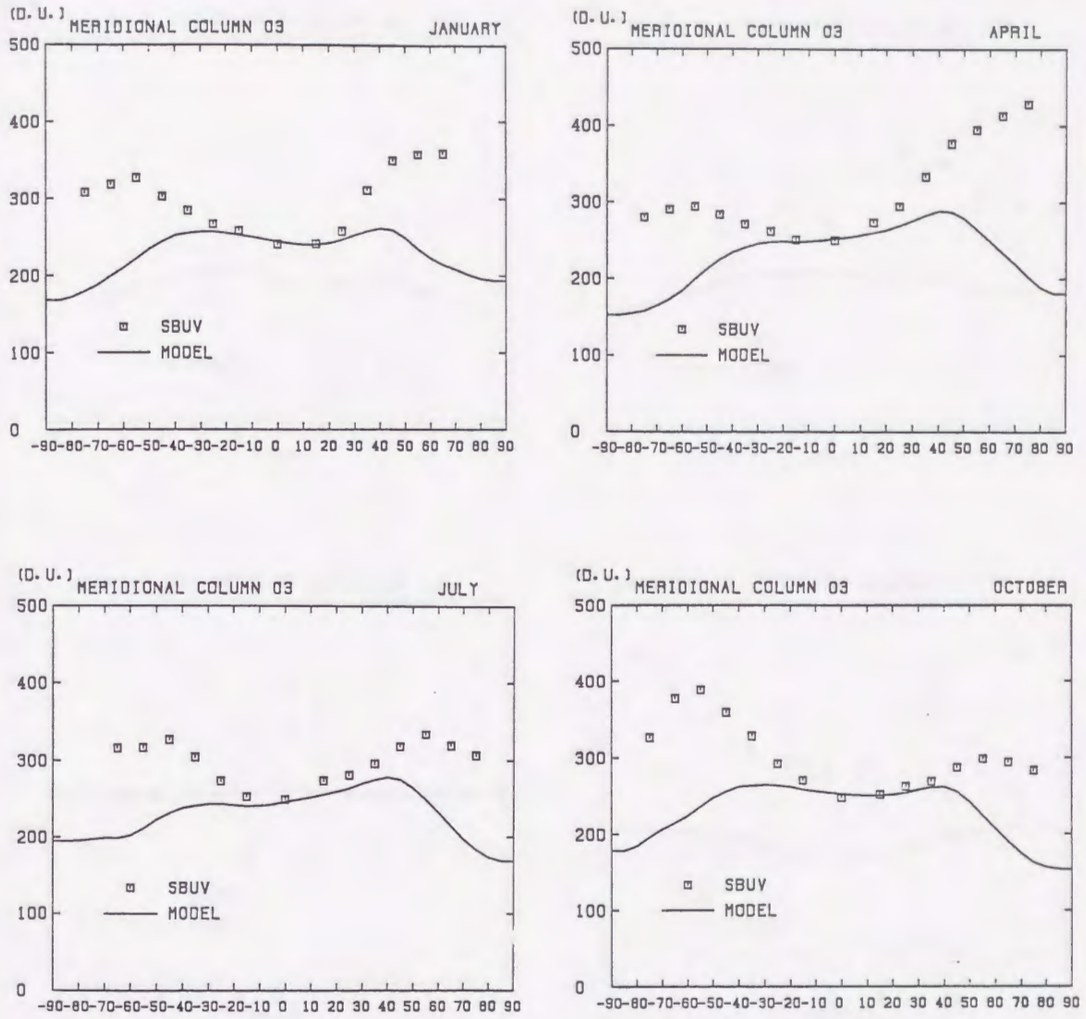

Figure 3.22. Latitudinal distributions of the observed total ozone amount (SBUV, 1979) and the calculated one (same as Figure 3.21) in January, April, July, and October.

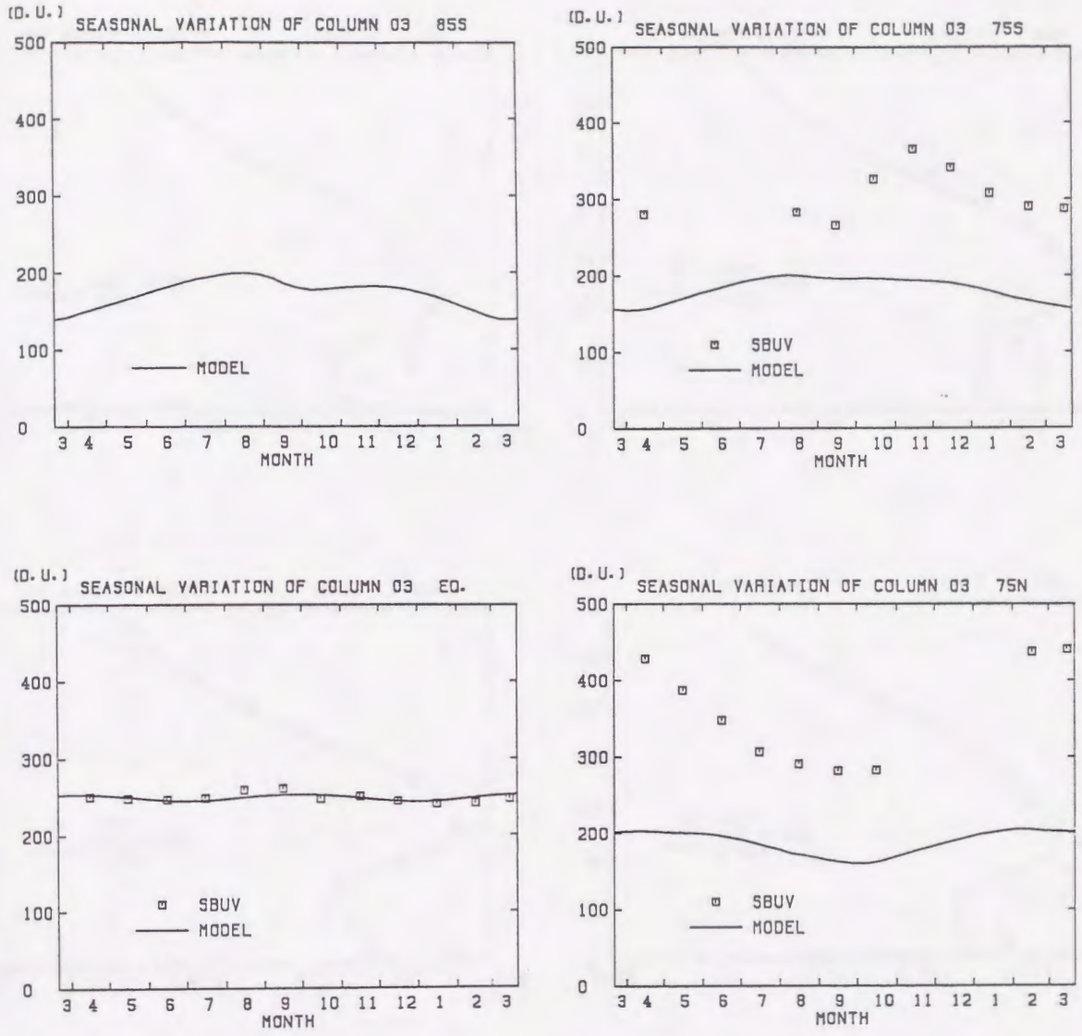

Figure 3.23. Seasonal variations of the observed total ozone amount (SBUV, 1979) and the calculated one (same as Figure 3.21) at 85°S, 75°S, the equator, and 75°N.

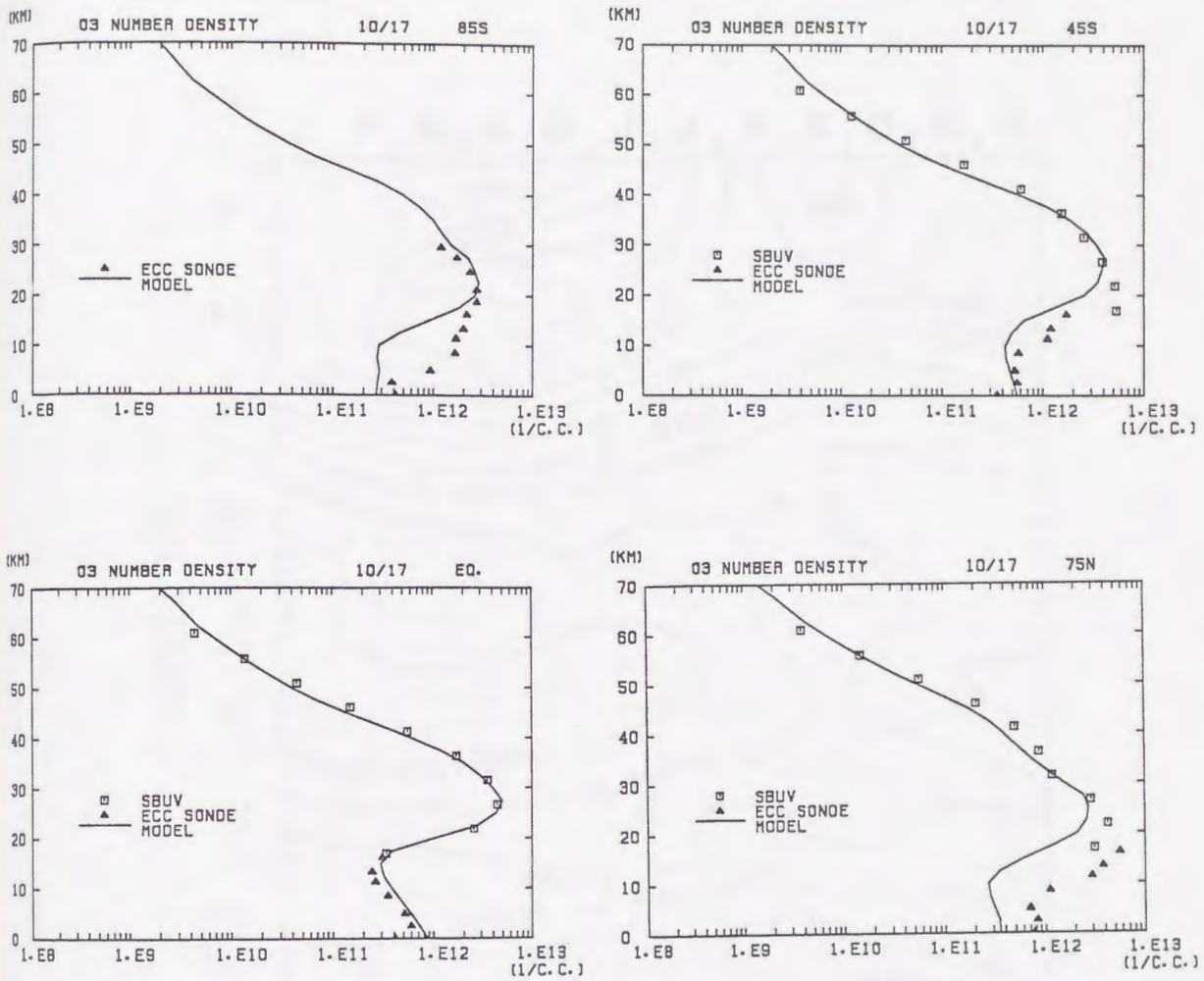

Figure 3.24. Vertical distributions of the observed ozone concentration and the calculated one at 85°S, 45°S, the equator, and 75°N in October.

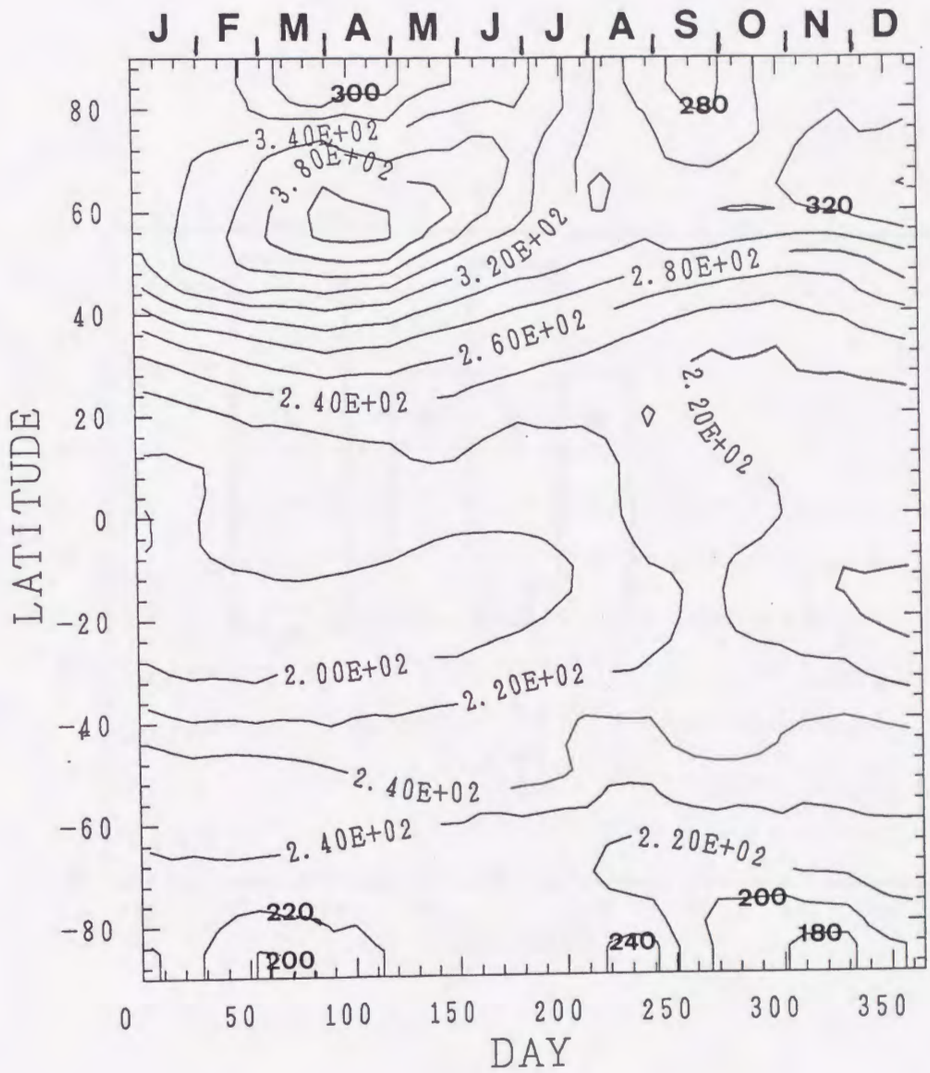

Figure 3.25. Time-latitude cross section of the total ozone amount which is calculated by using Plumb and Mahlman's monthly global transport velocity and diffusion coefficients.

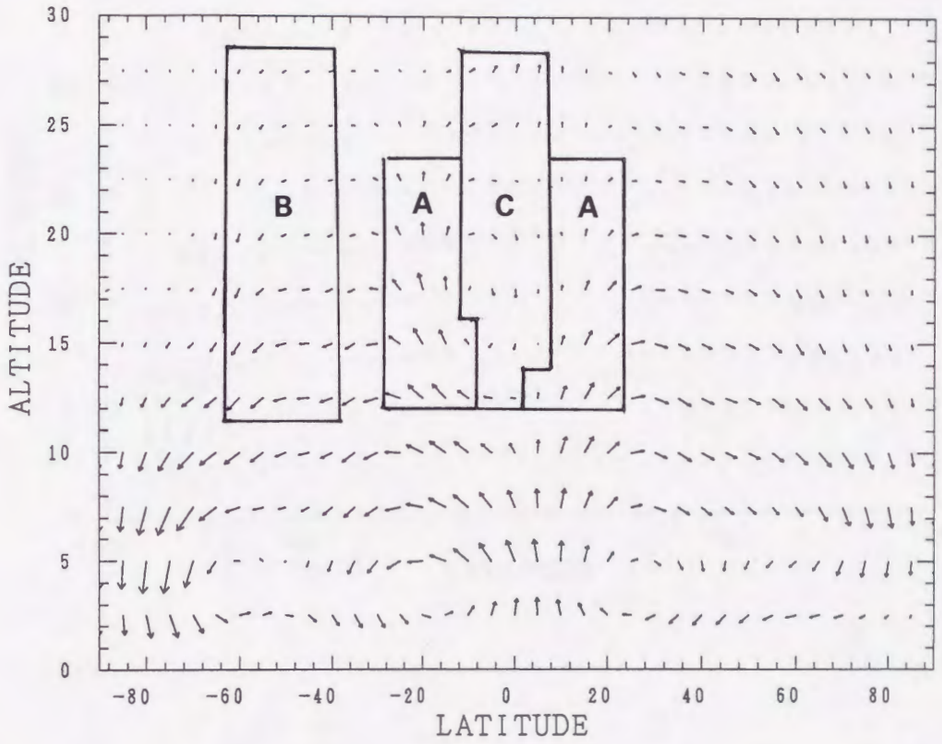

Figure 3.26. The result of the annual average of the transport velocity which was calculated by Plumb and Mahlman (1987). W_T in the regions of A, B, and C are modified in the ozone calculation. (See text and Figure 3.27.)

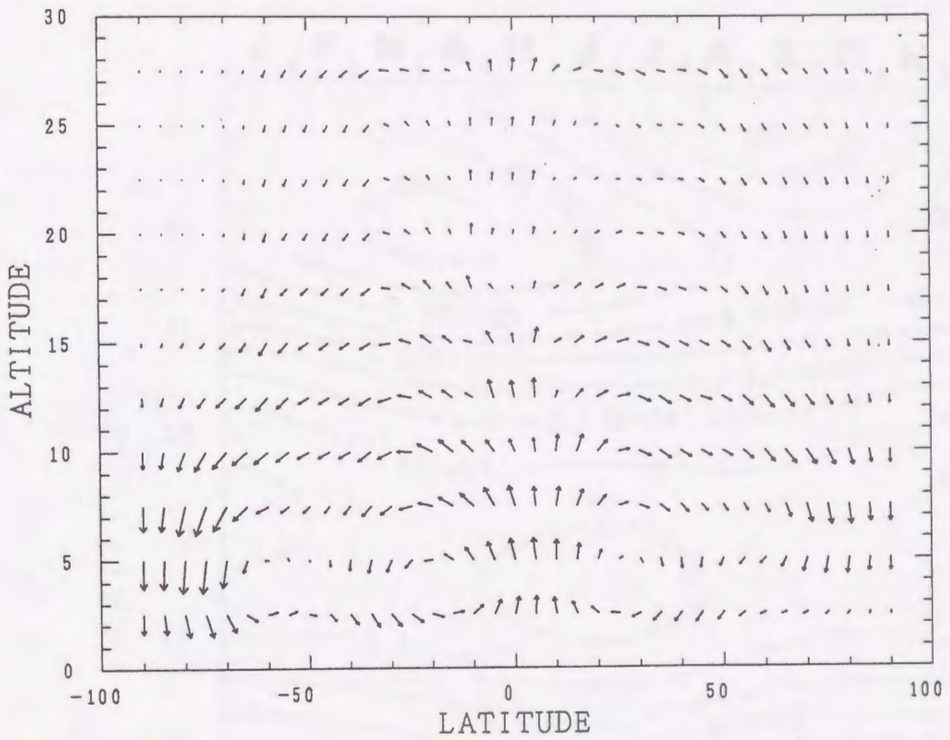

Figure 3.27. Modified annually averaged transport velocity.

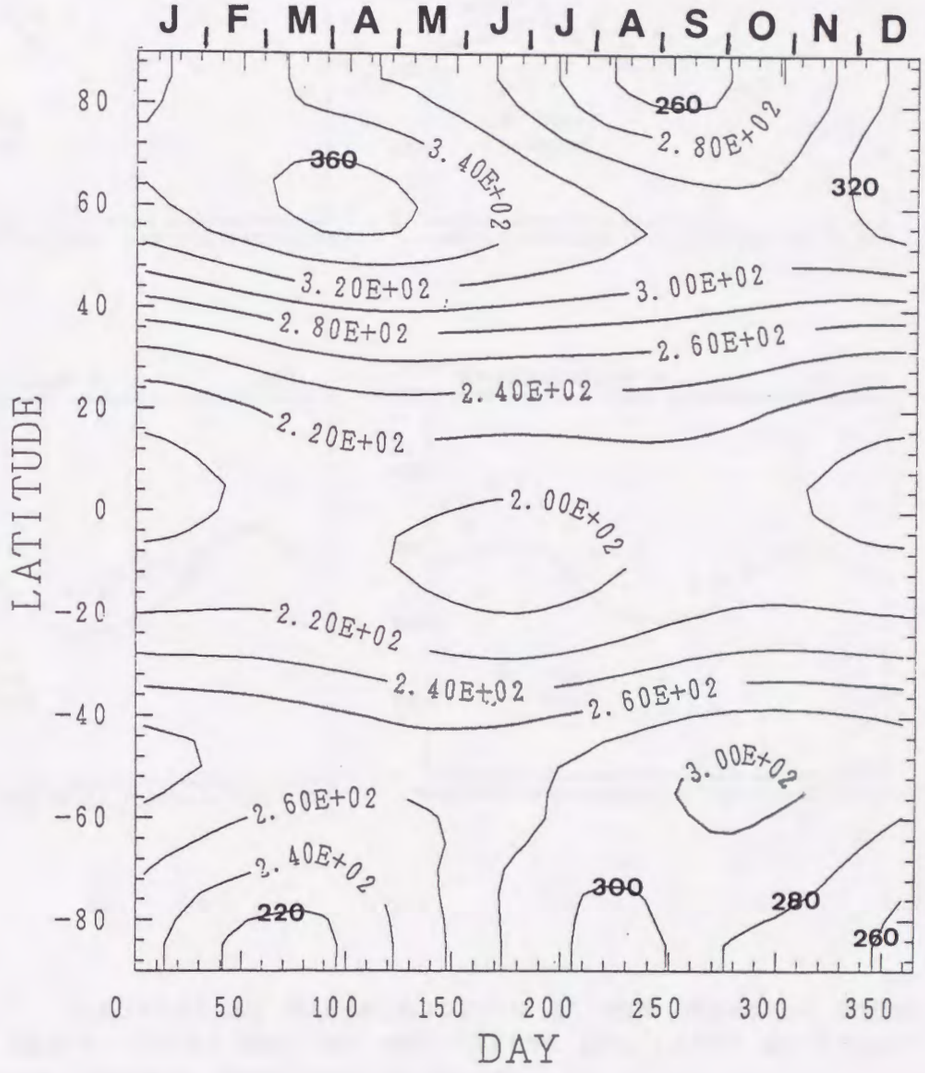

Figure 3.28. Same as Figure 3.21, but the modified annually averaged transport velocity in Figure 3.27 is added to the advection terms in equation (3c.1).

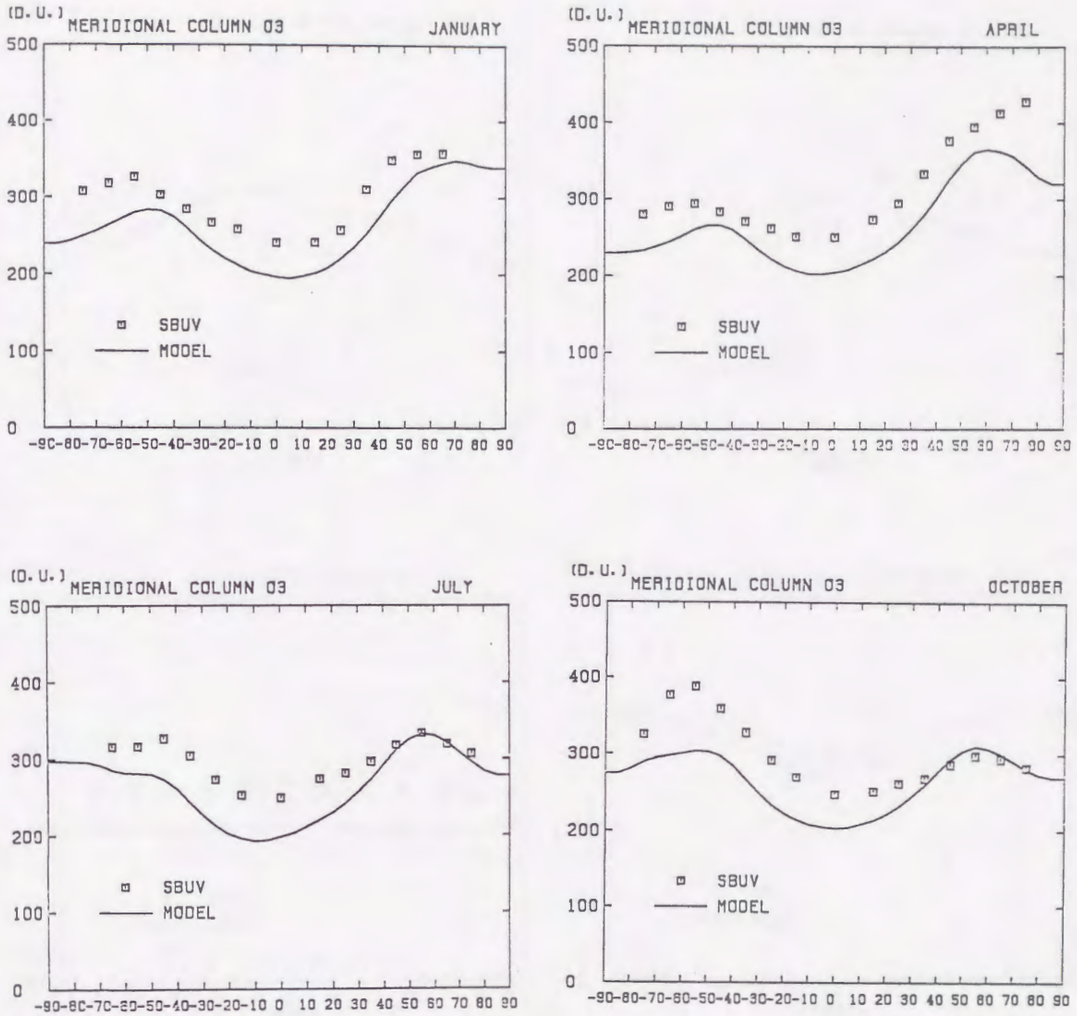

Figure 3.29. Latitudinal distributions of the observed total ozone amount (SBUV, 1979) and the calculated one (same as Figure 3.28) in January, April, July, and October.

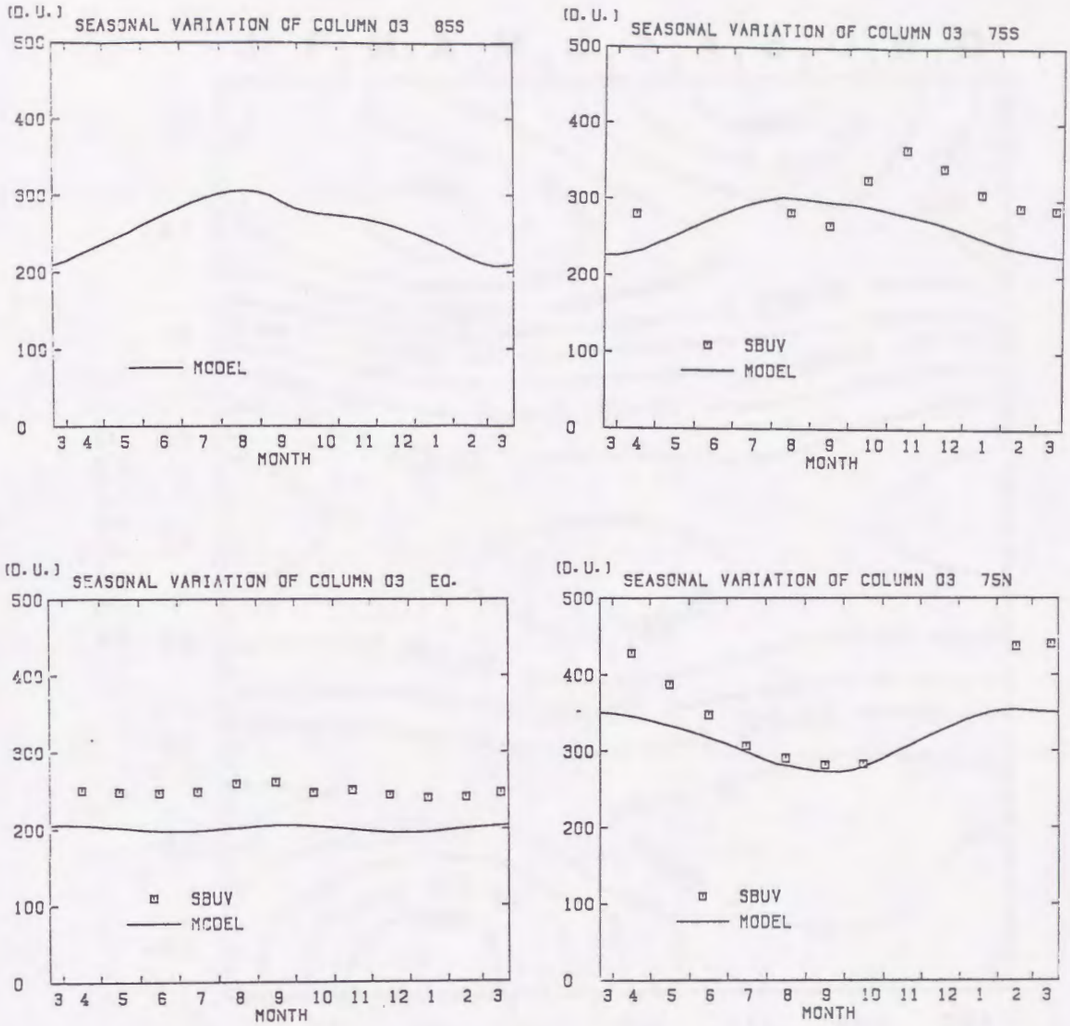

Figure 3.30. Seasonal variations of the observed total ozone amount (SBUV, 1979) and the calculated one (same as Figure 3.28) at 85°S, 75°S, the equator, and 75°N.

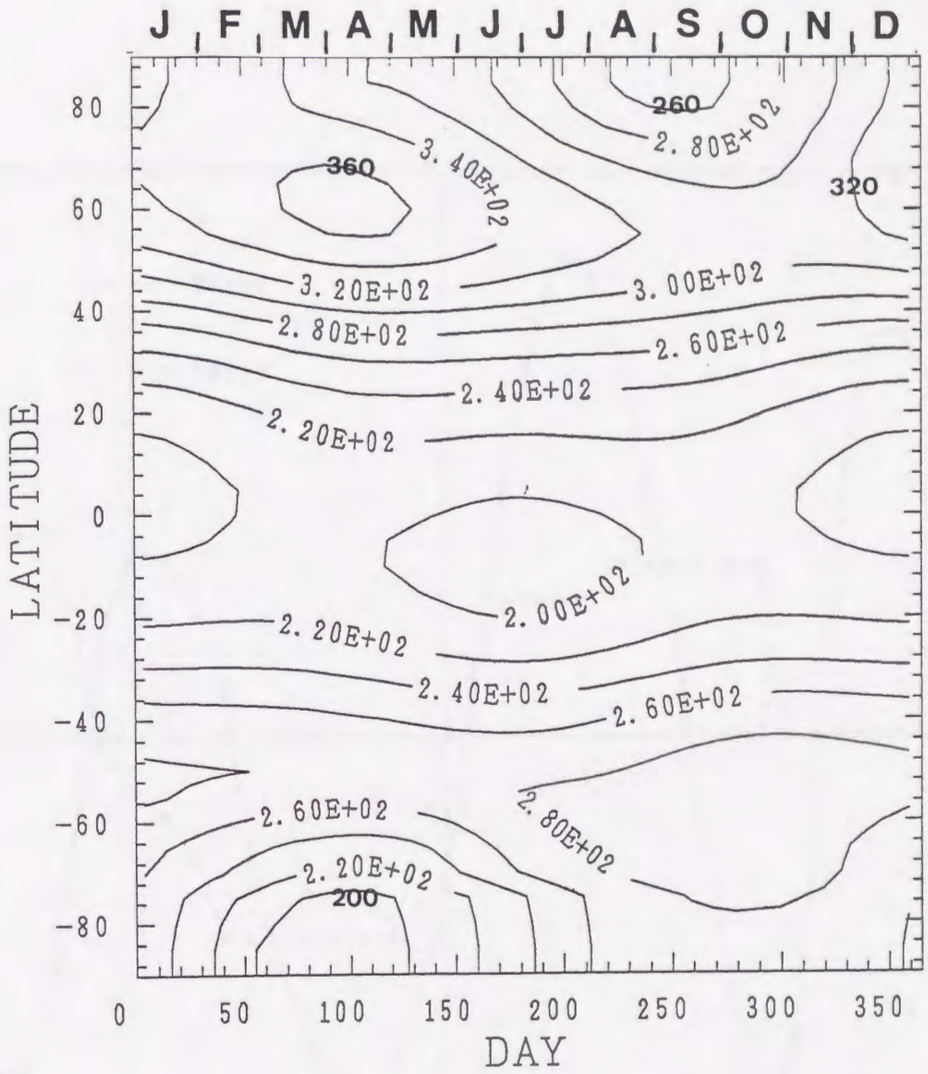

Figure 3.31. Same as Figure 3.28, but K_{yy} in the stratosphere at the latitudes between 50°S and 75°S is reduced to 2×10^5 $m^2\ s^{-1}$ all the year.

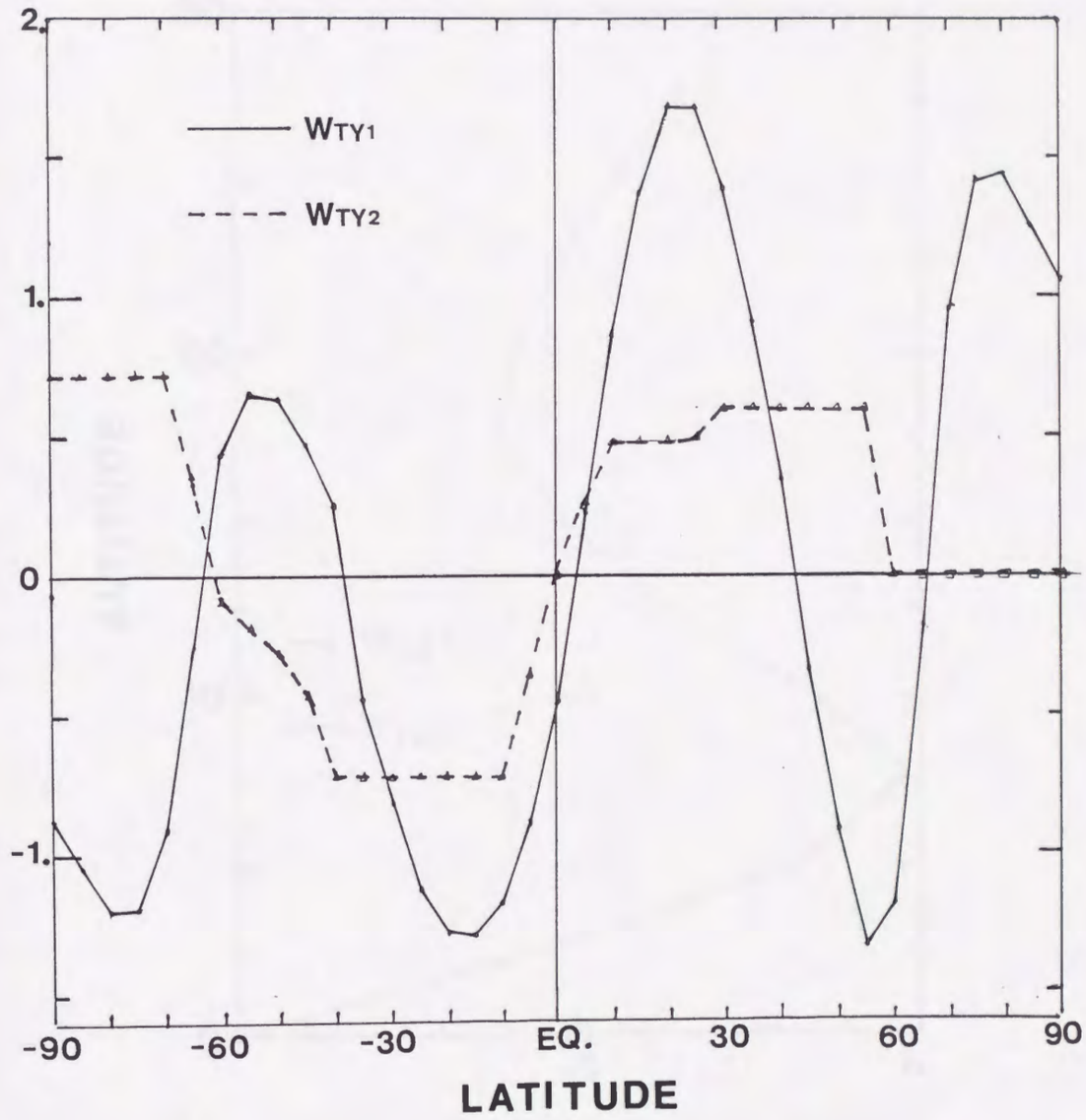

Figure 3.32. Assumed latitudinal structures of the seasonal variation component of the transport velocity, $W_{TY1}'(\phi)$ and $W_{TY2}'(\phi)$.

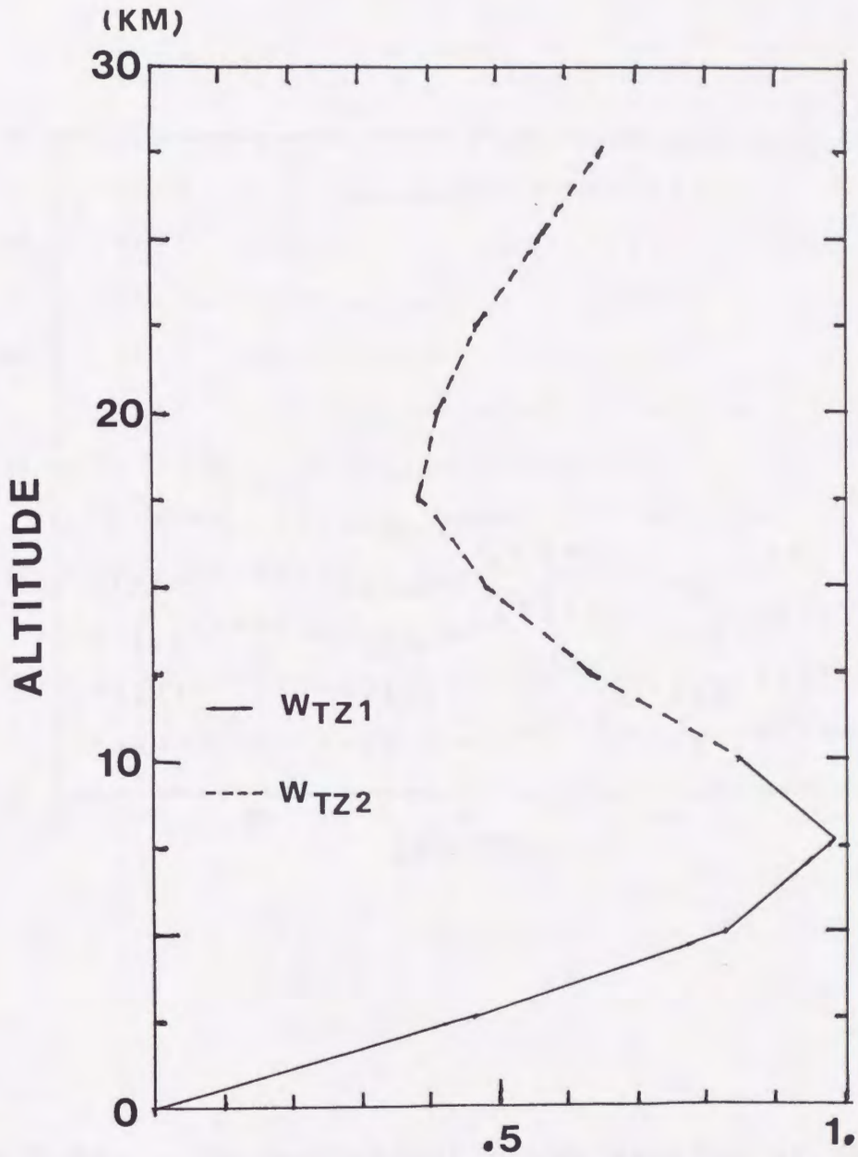

Figure 3.33. Assumed vertical structures of the seasonal variation component of the transport velocity, $W_{Tz1}'(z)$ and $W_{Tz2}'(z)$.

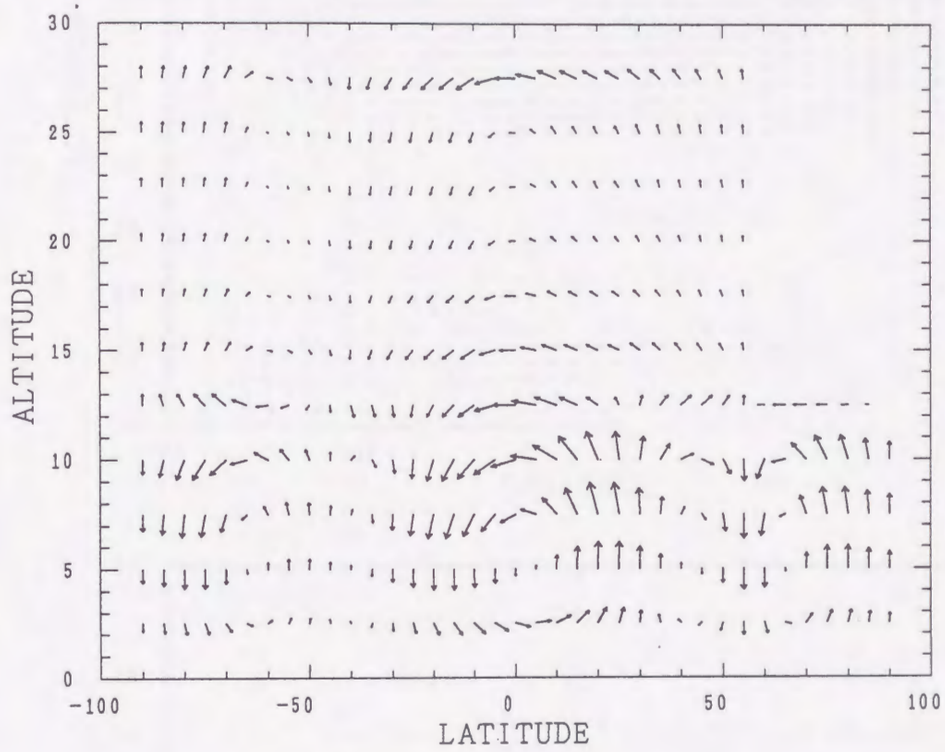

Figure 3.34. The meridional cross section of the assumed seasonal variation component of the transport velocity ($V_T'(\phi, z, t)$, $W_T'(\phi, z, t)$) on June 20.

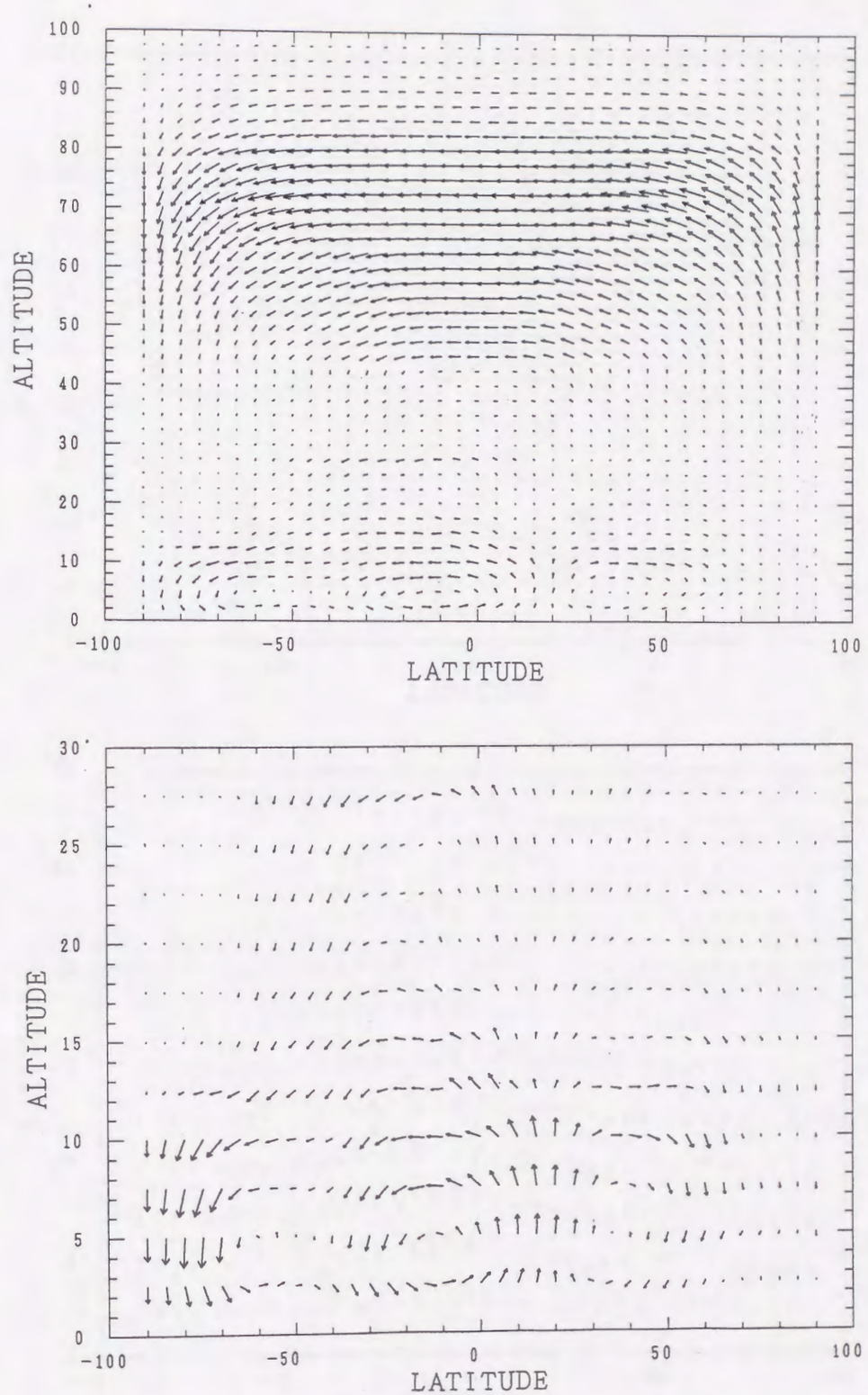

Figure 3.35a. The composite circulation ($v(\phi,z,t)+V_T(\phi,z)+V_T'(\phi,z,t)$, $w(\phi,z,t)+W_T(\phi,z)+W_T'(\phi,z,t)$) on June 20. The lower panel is the magnification of the lower part of the circulation.

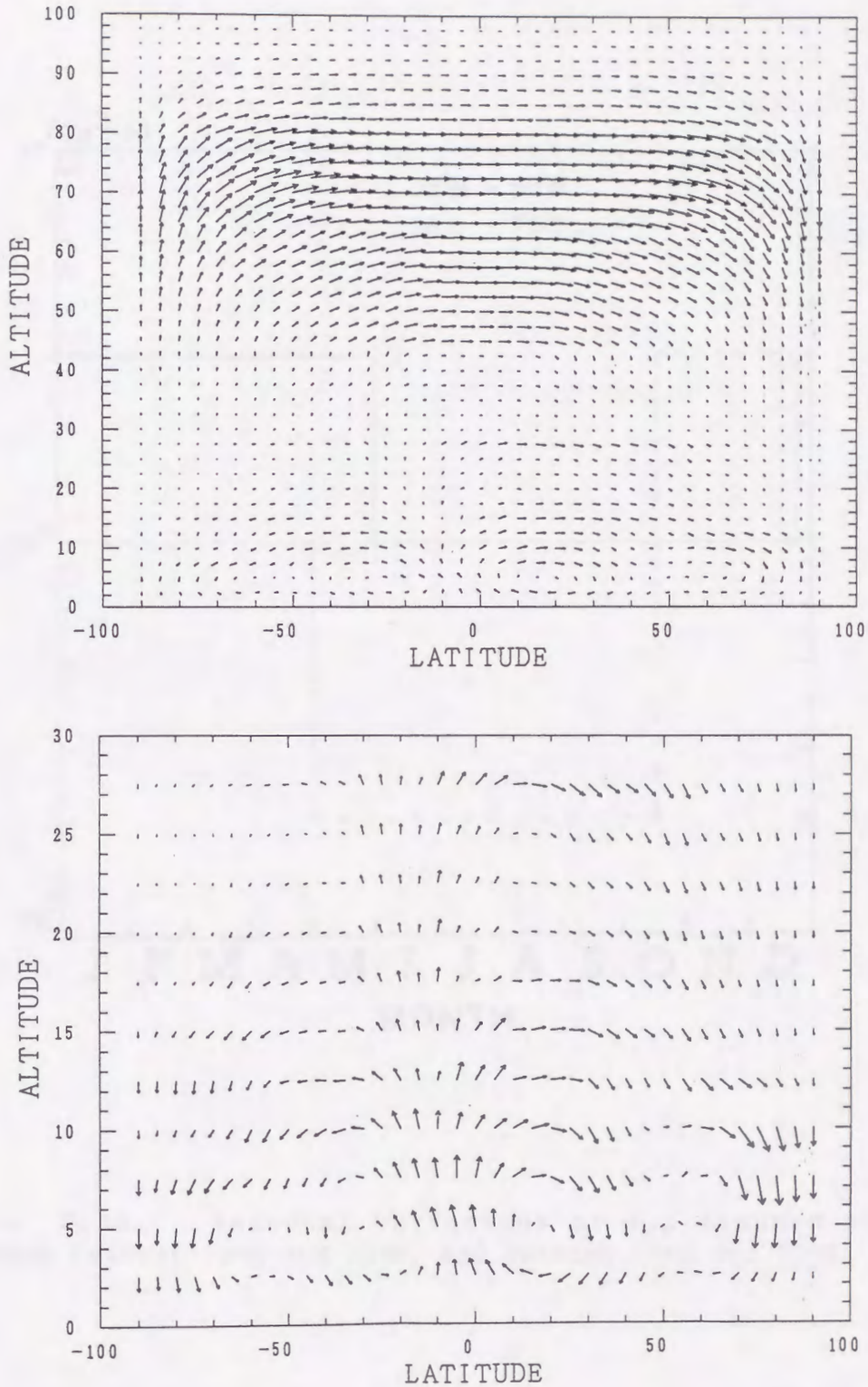

Figure 3.35b. Same as Figure 3.35a, but on December 19.

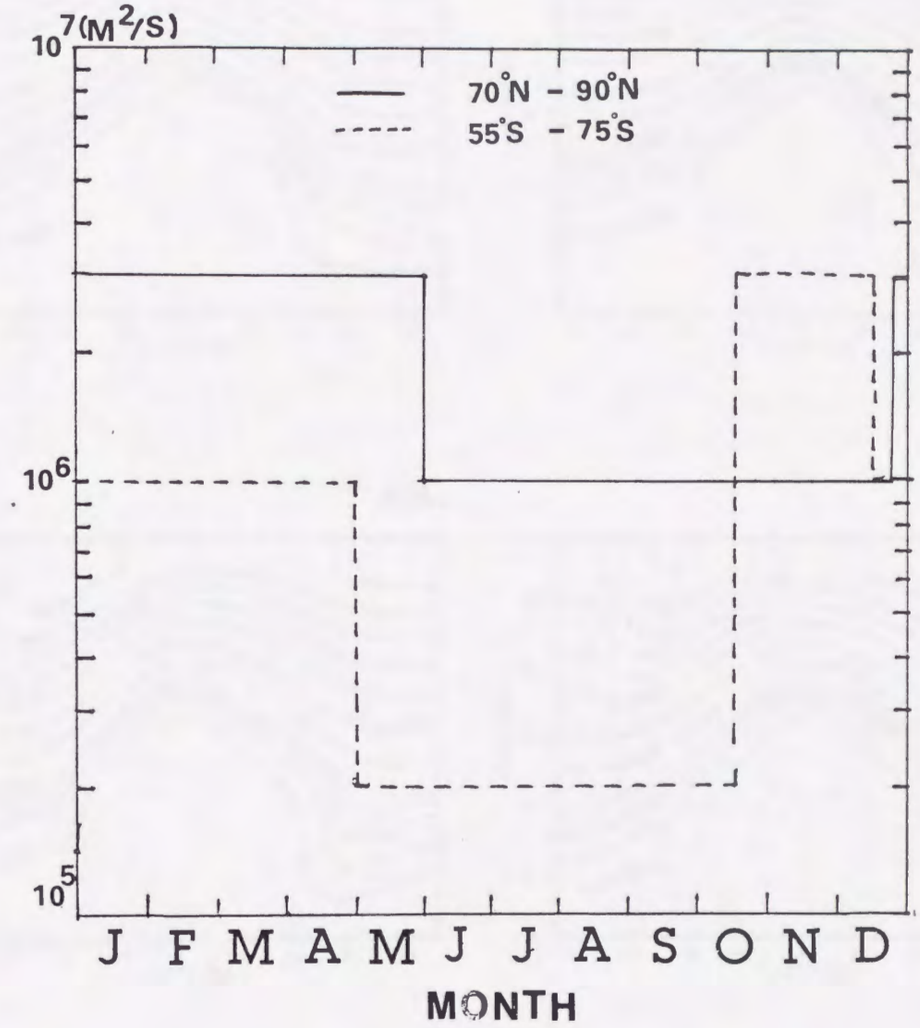

Figure 3.36. Seasonal variations of K_{yy} assumed at the latitudes between 70°N and 90°N, and between 55°S and 75°S.

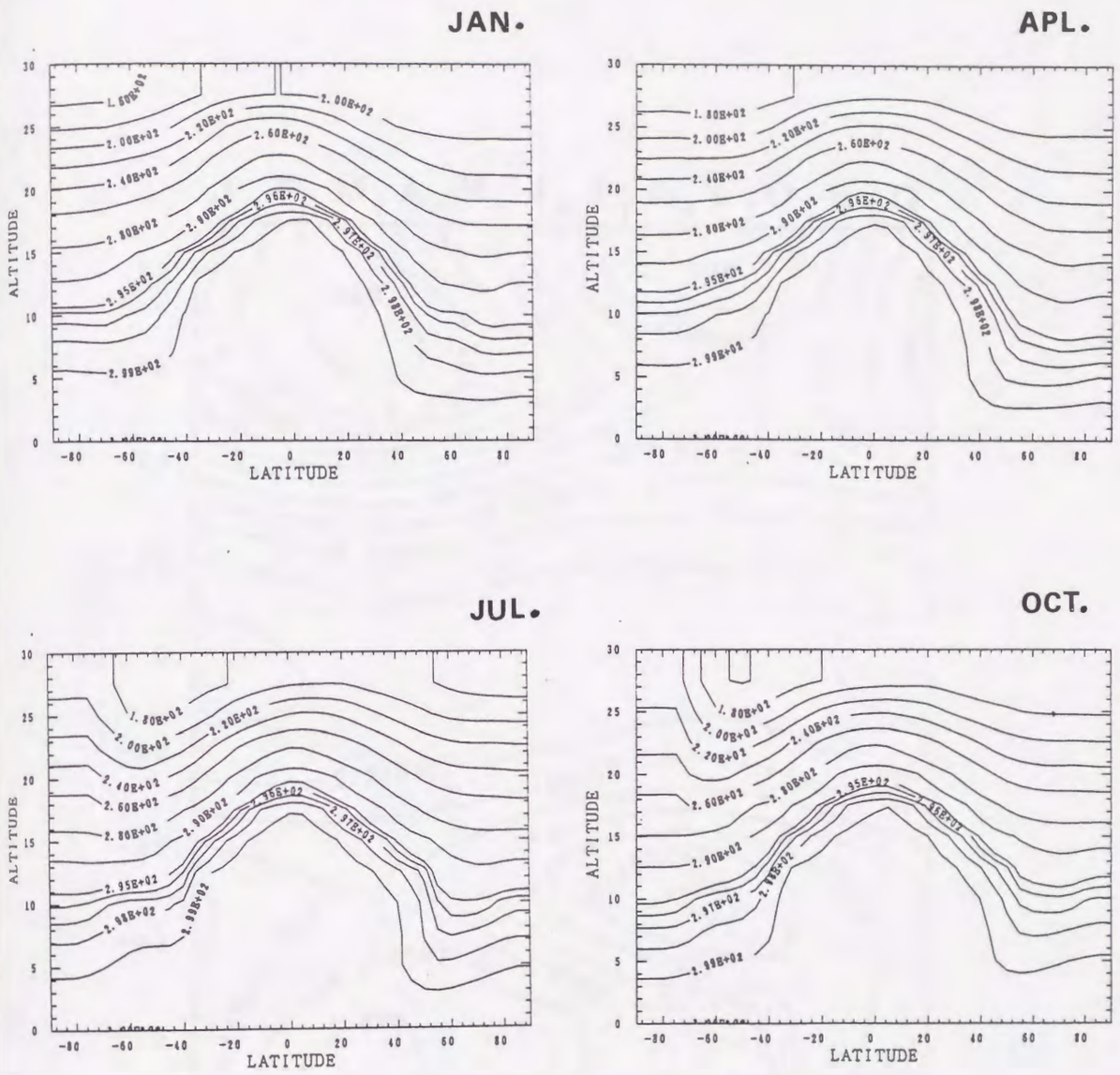

Figure 3.37. Calculated latitude-altitude section of N_2O mixing ratio in January, April, July, and October. Unit is ppbv.

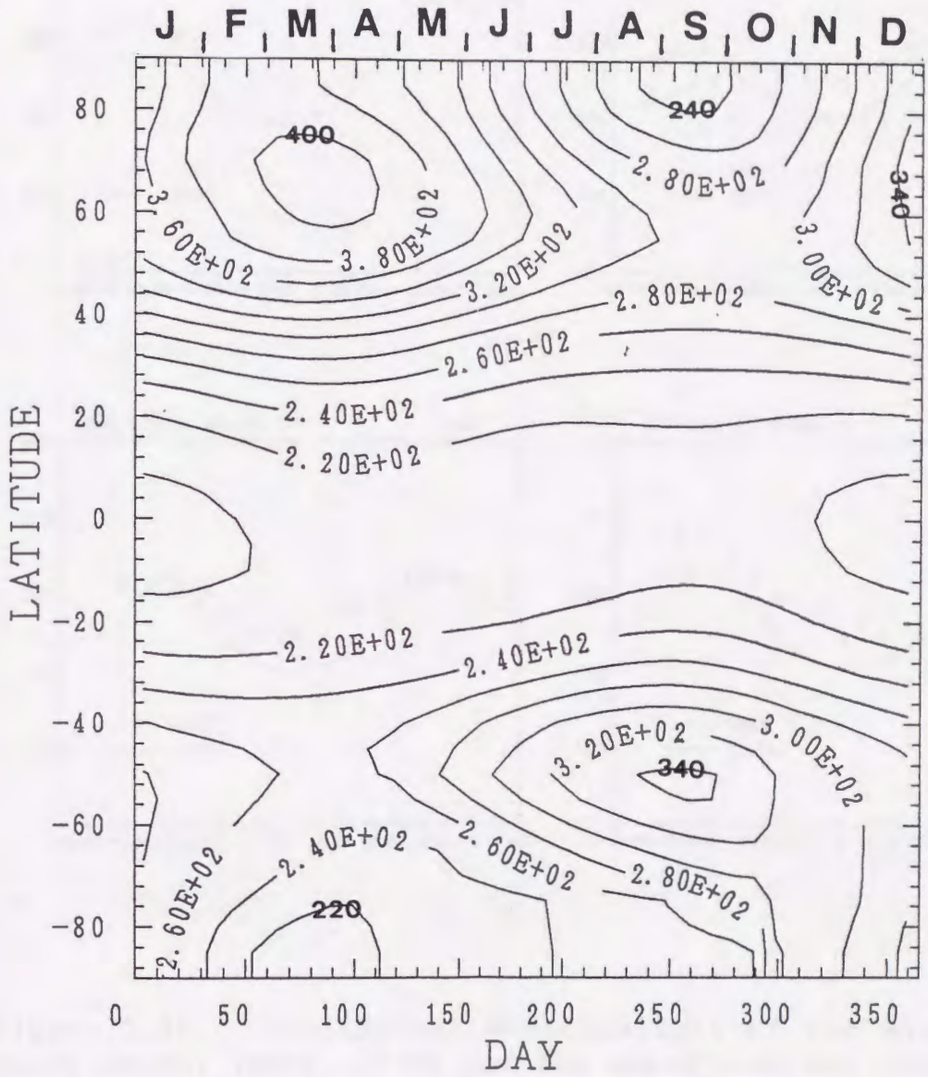

Figure 3.38. Same as Figure 3.21, but the steady component and the assumed seasonal variation component of the transport velocity are added to the advection terms in equation (3c.1). The time-dependence of K_{yy} in the stratosphere at the latitudes between 70°N and 90°N, and between 55°S and 75°S is also considered.

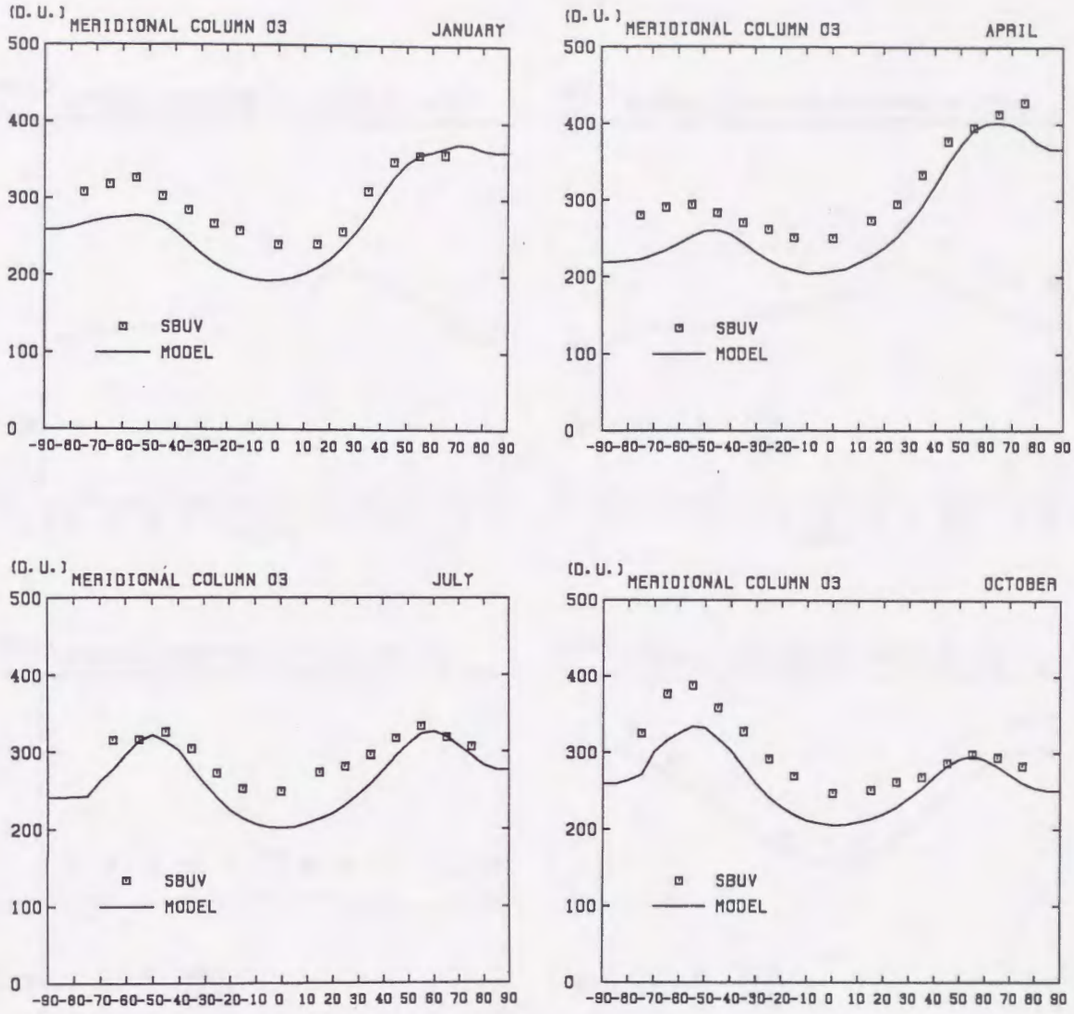

Figure 3.39. Latitudinal distributions of the observed total ozone amount (SBUV, 1979) and the calculated one (same as Figure 3.38) in January, April, July, and October.

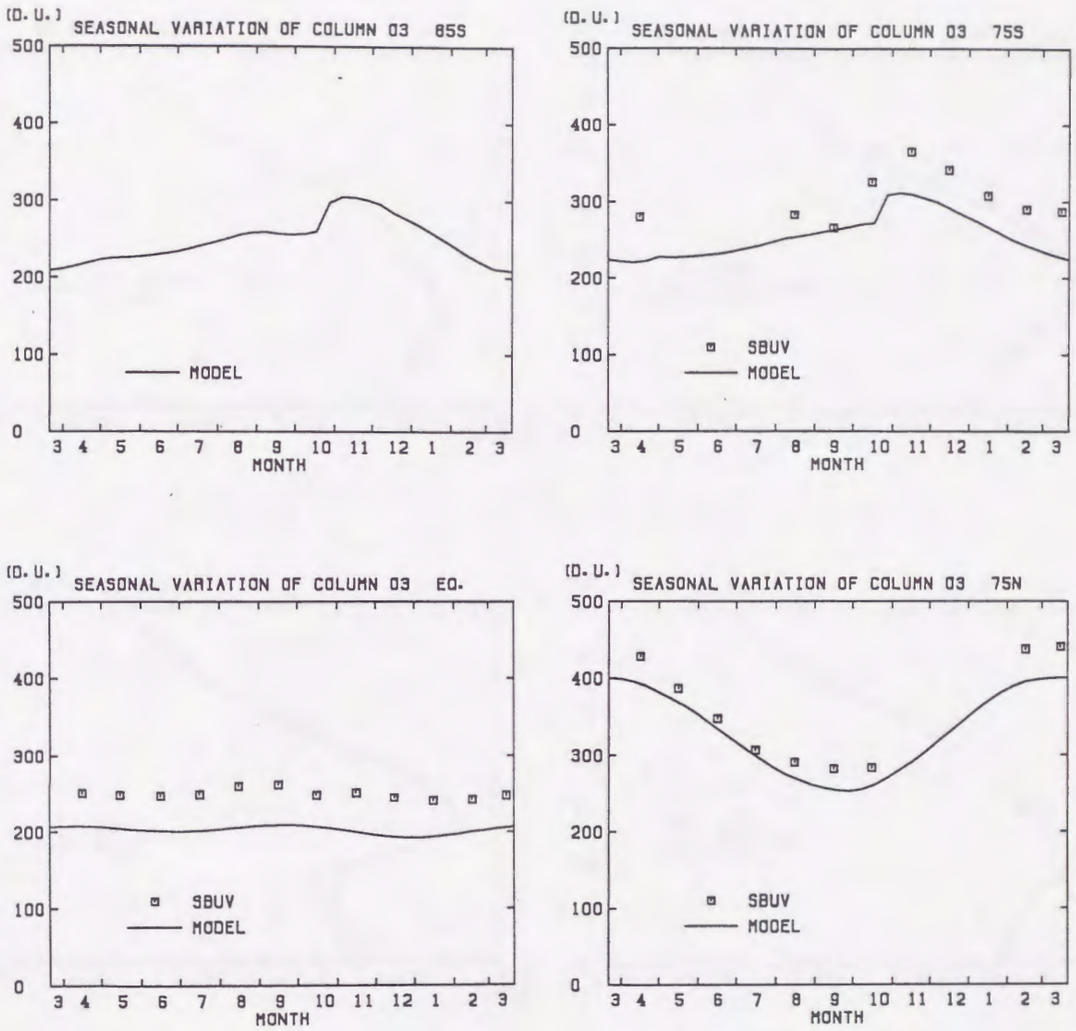

Figure 3.40. Seasonal variations of the observed total ozone amount (SBUV, 1979) and the calculated one (same as Figure 3.38) at 85°S, 75°S, the equator, and 75°N.

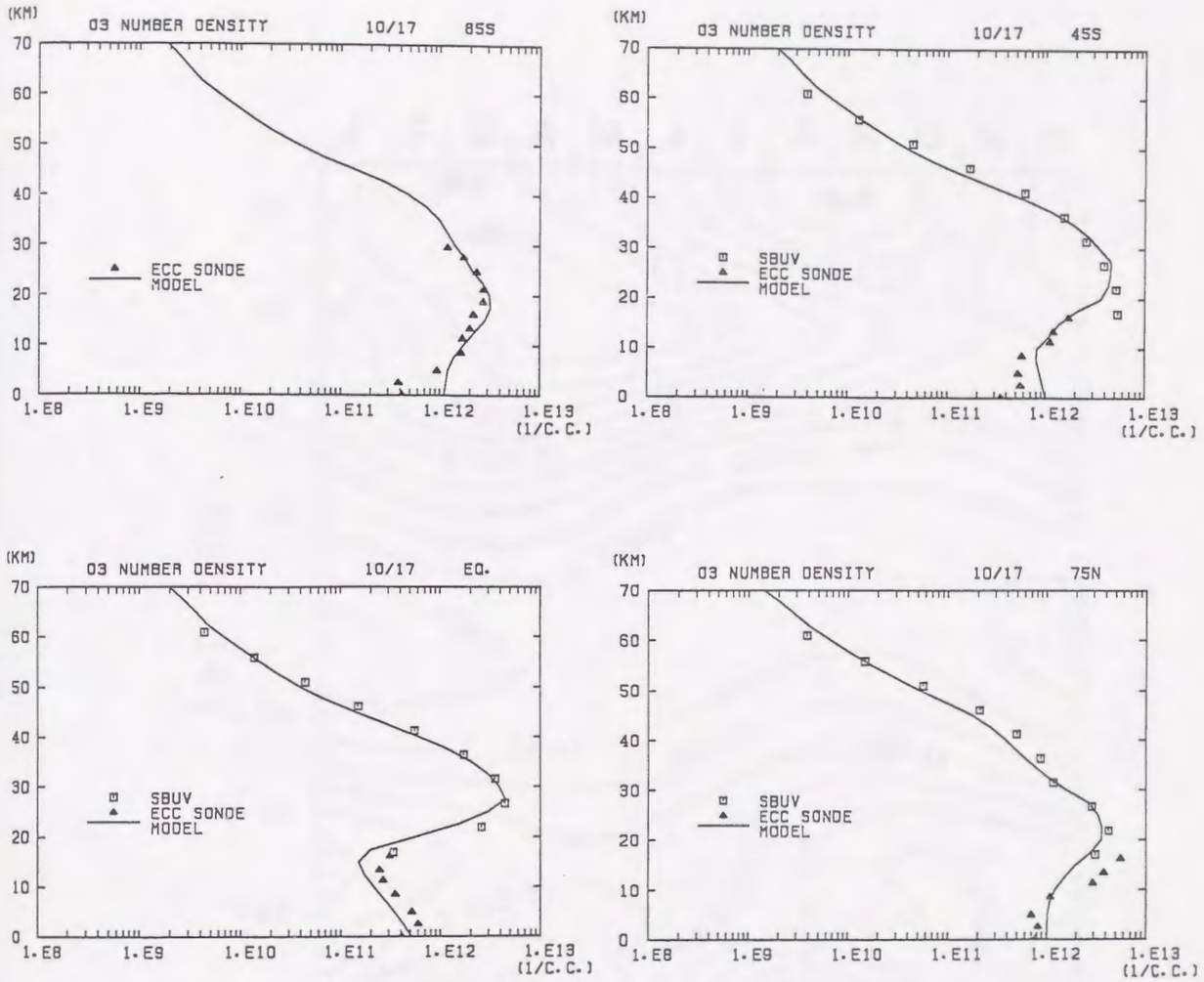

Figure 3.41. Vertical distributions of the observed ozone concentration and the calculated one at 85°S, 45°S, the equator, and 75°S in October.

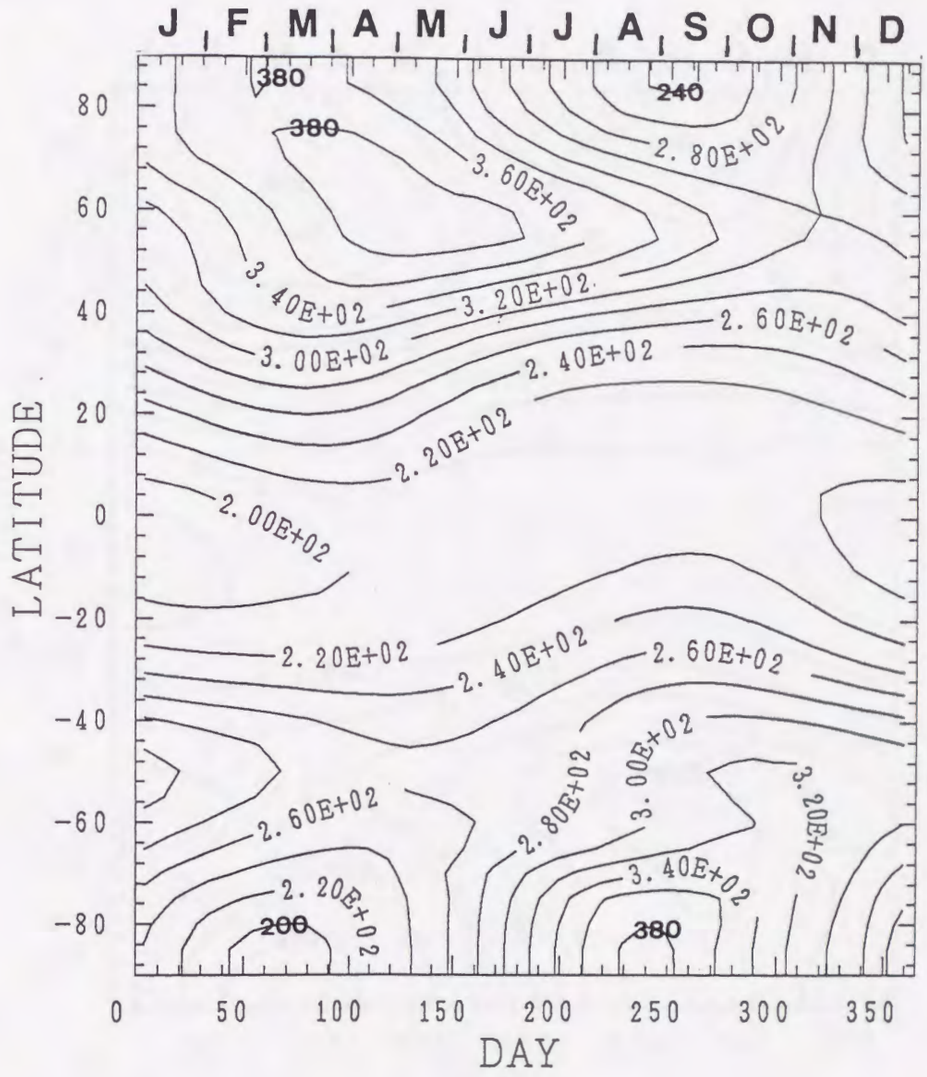

Figure 3.42. Same as Figure 3.38, but $W_T'(\phi, z, t)$ which only consists of the product of $W_{TY1}'(\phi)$ and $W_{TZ1}'(z)$ is used. (The component of $W_{TY2}'(\phi) \cdot W_{TZ2}'(z)$ is ignored.)

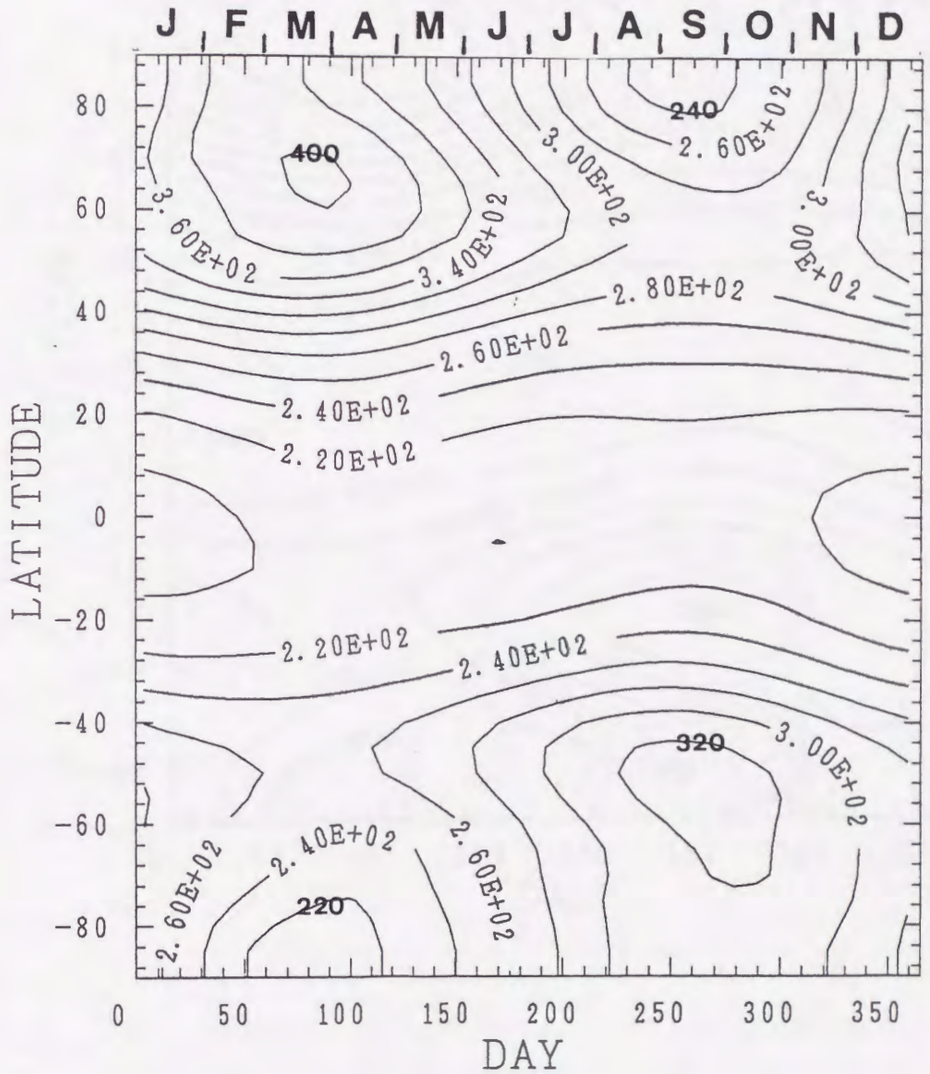

Figure 3.43. Same as Figure 3.38, but the time-dependence of K_{yy} is ignored and K_{yy} is set at a constant value of 1×10^6 $m^2\ s^{-1}$ in the stratosphere.

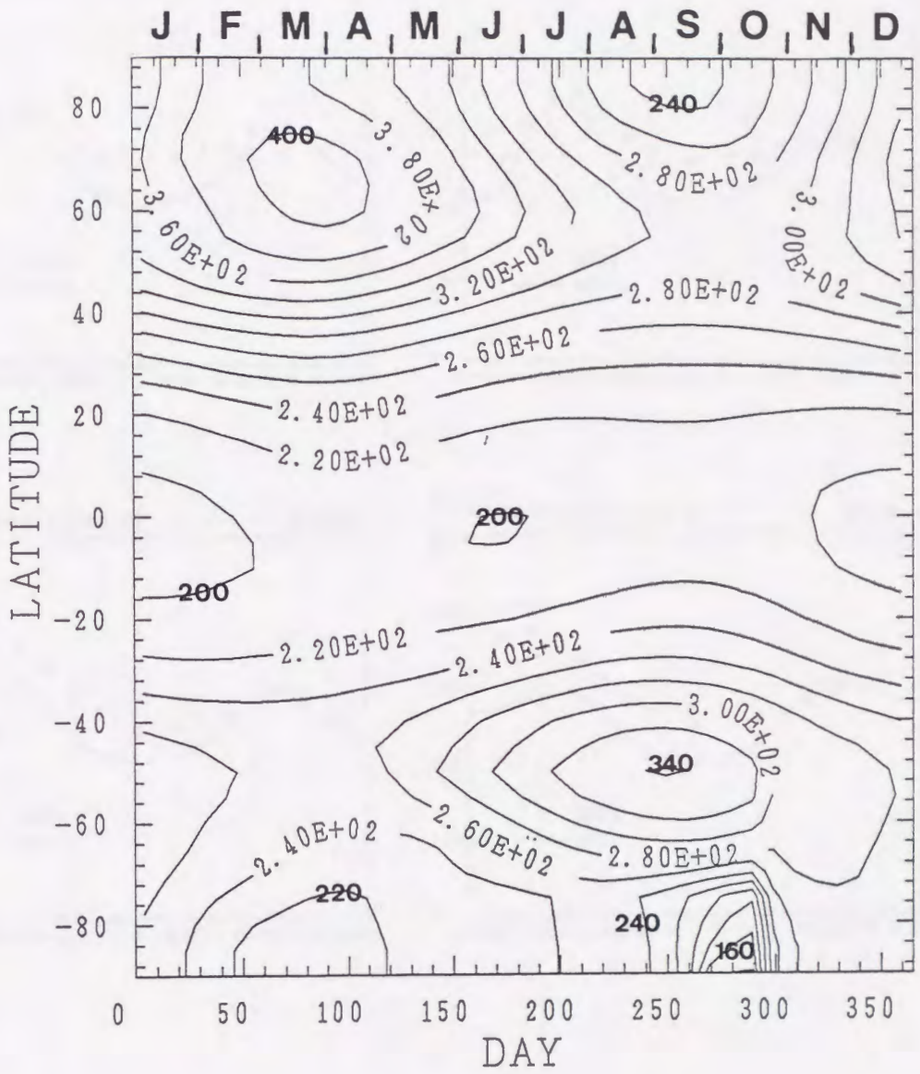

Figure 4.1. Same as Figure 3.38, but the chlorine catalytic cycle is included at the altitudes between 11.25 km and 21.25 km in the south of 70°S.

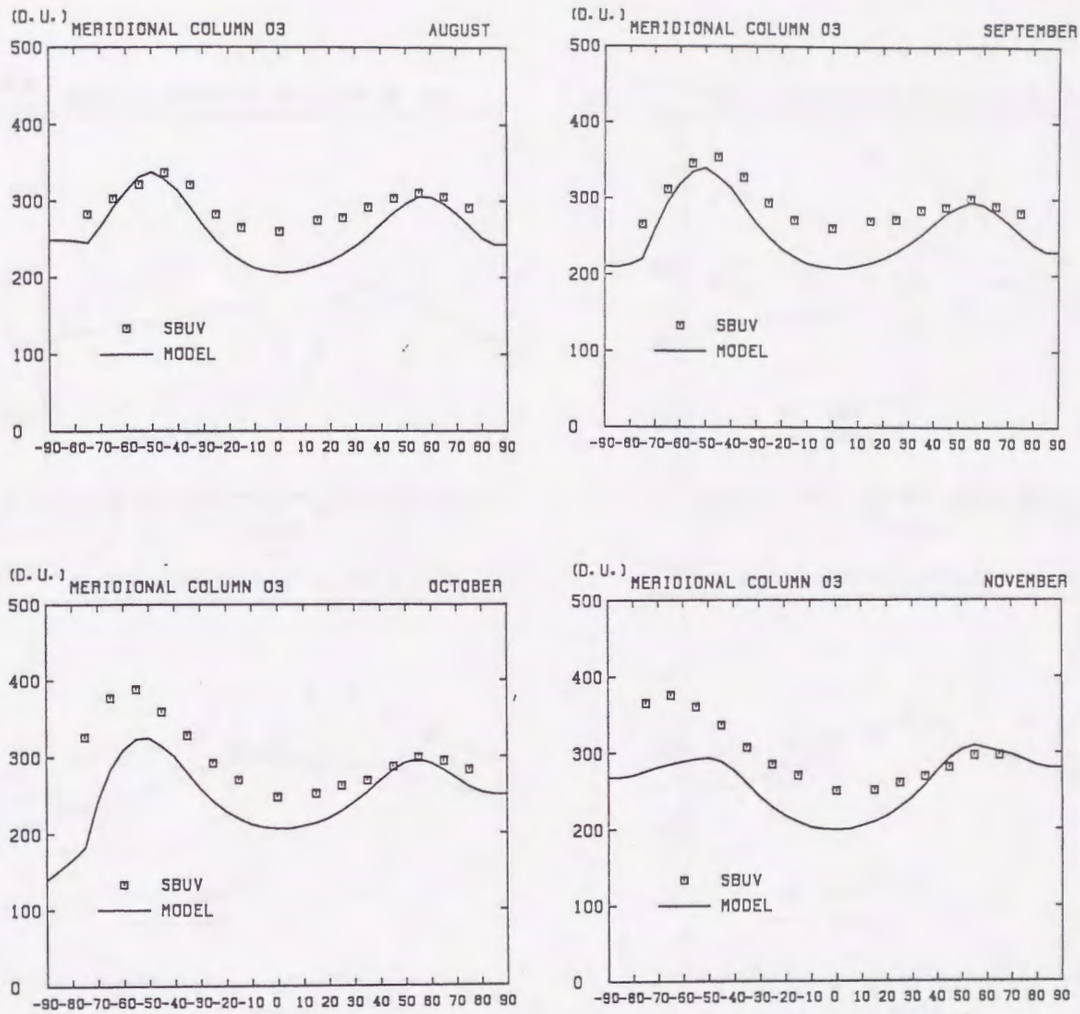

Figure 4.2. Latitudinal distributions of the observed total ozone amount (SBUV, 1979) and the calculated one (same as Figure 4.1) in August, September, October, and November.

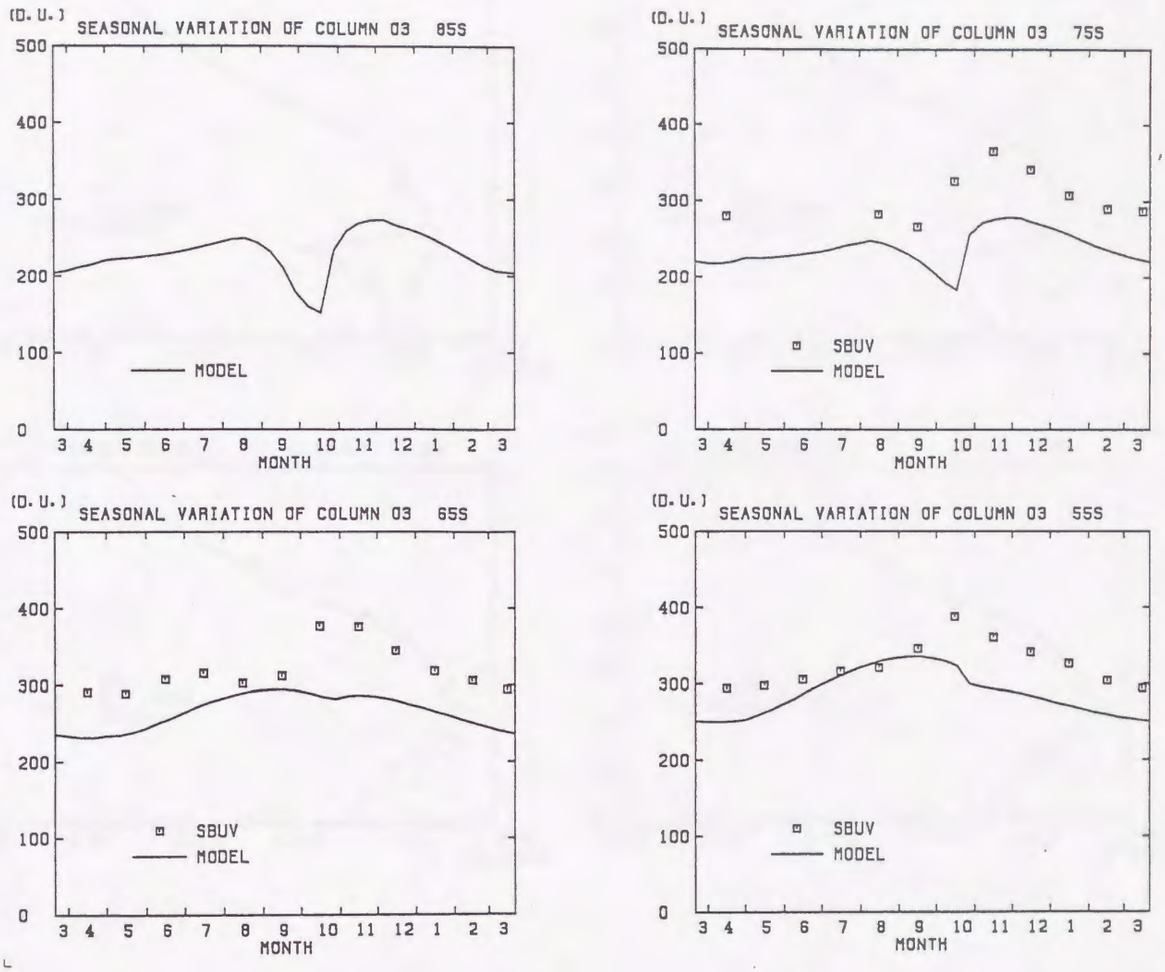

Figure 4.3. Seasonal variations of the observed total ozone amount (SBUV, 1979) and the calculated one (same as Figure 4.1) at 85°S, 75°S, 65°S, and 55°S.

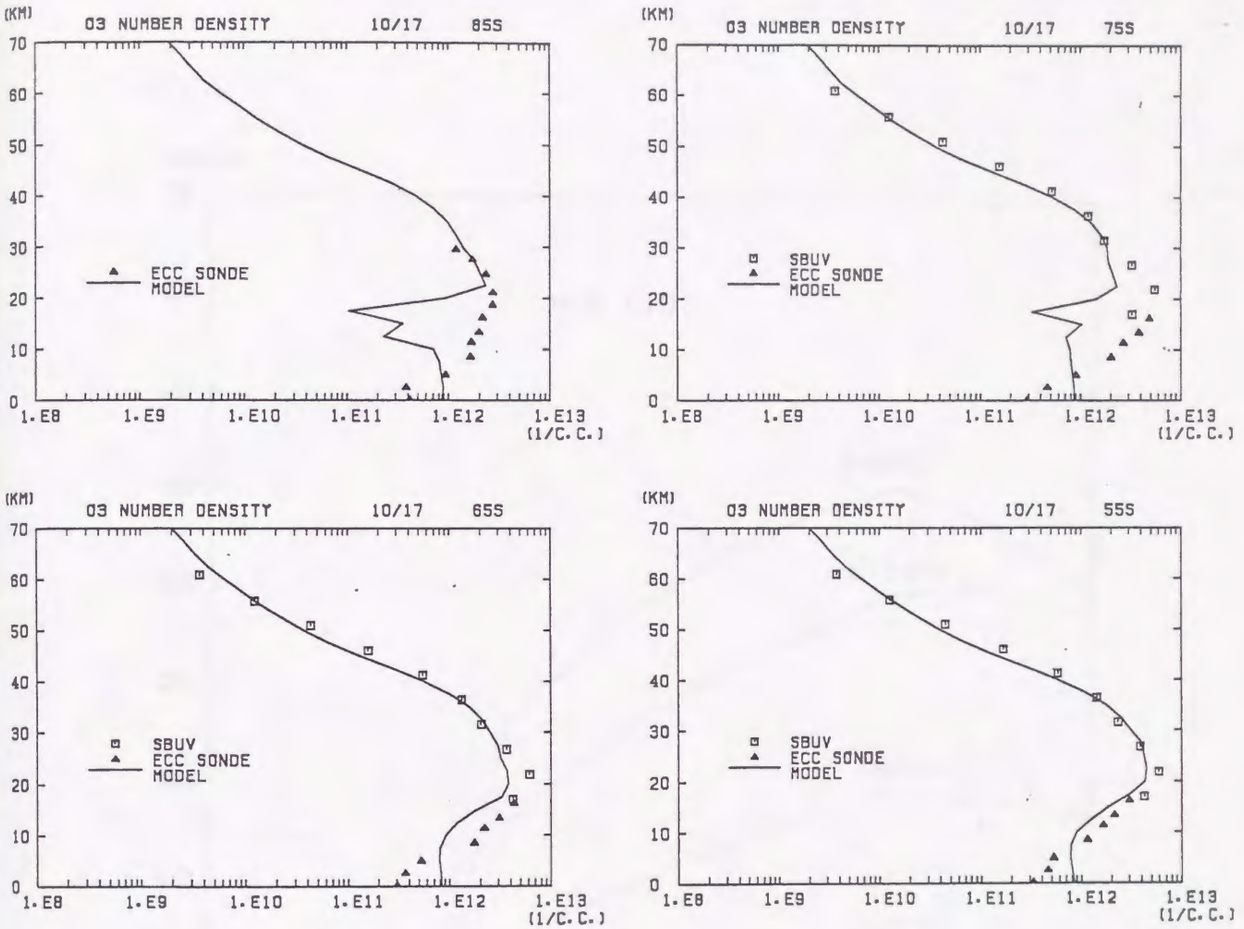

Figure 4.4. Vertical distributions of the observed ozone concentration and the calculated one at 85°S, 75°S, 65°S, and 55°S in October.

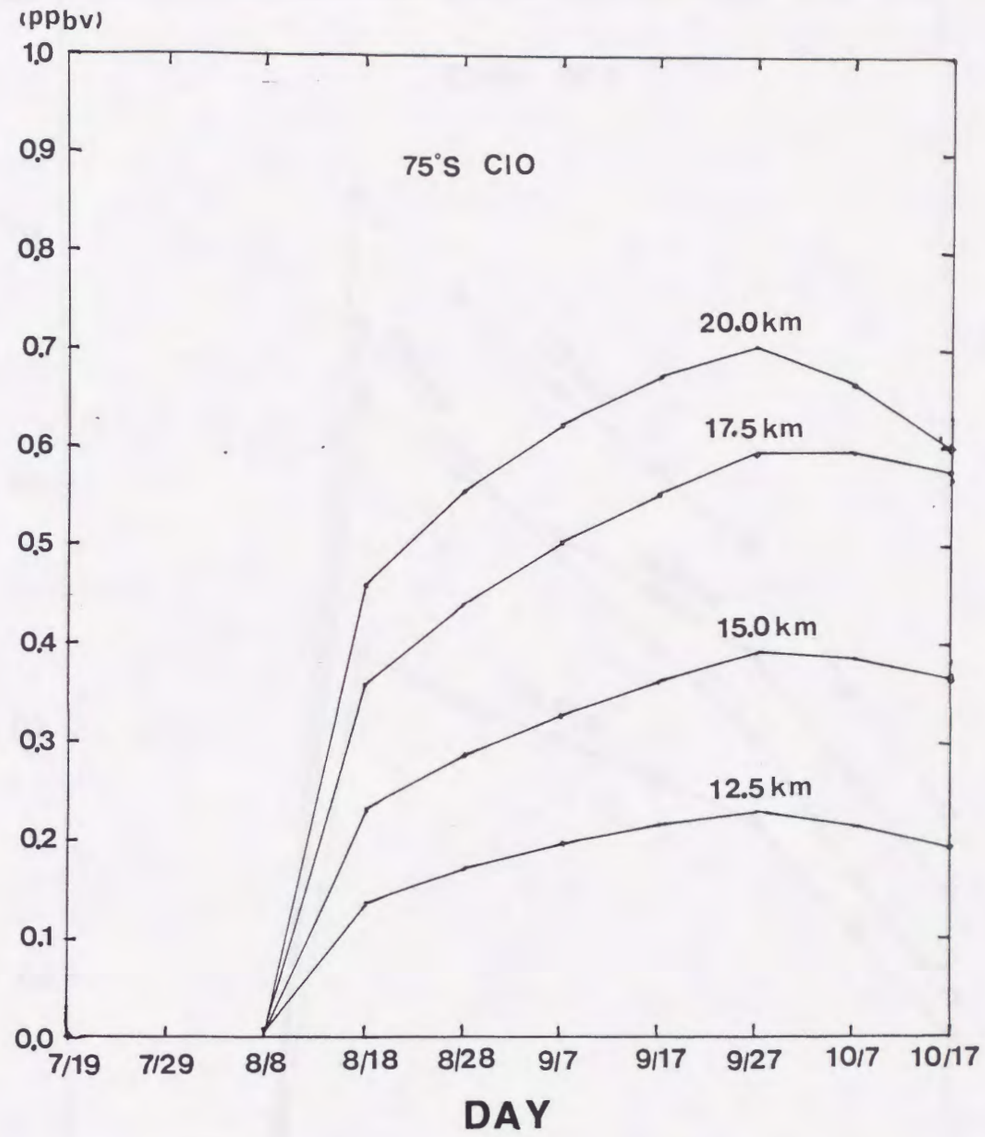

Figure 4.5a. Time evolution of mixing ratio of ClO at 75°S.

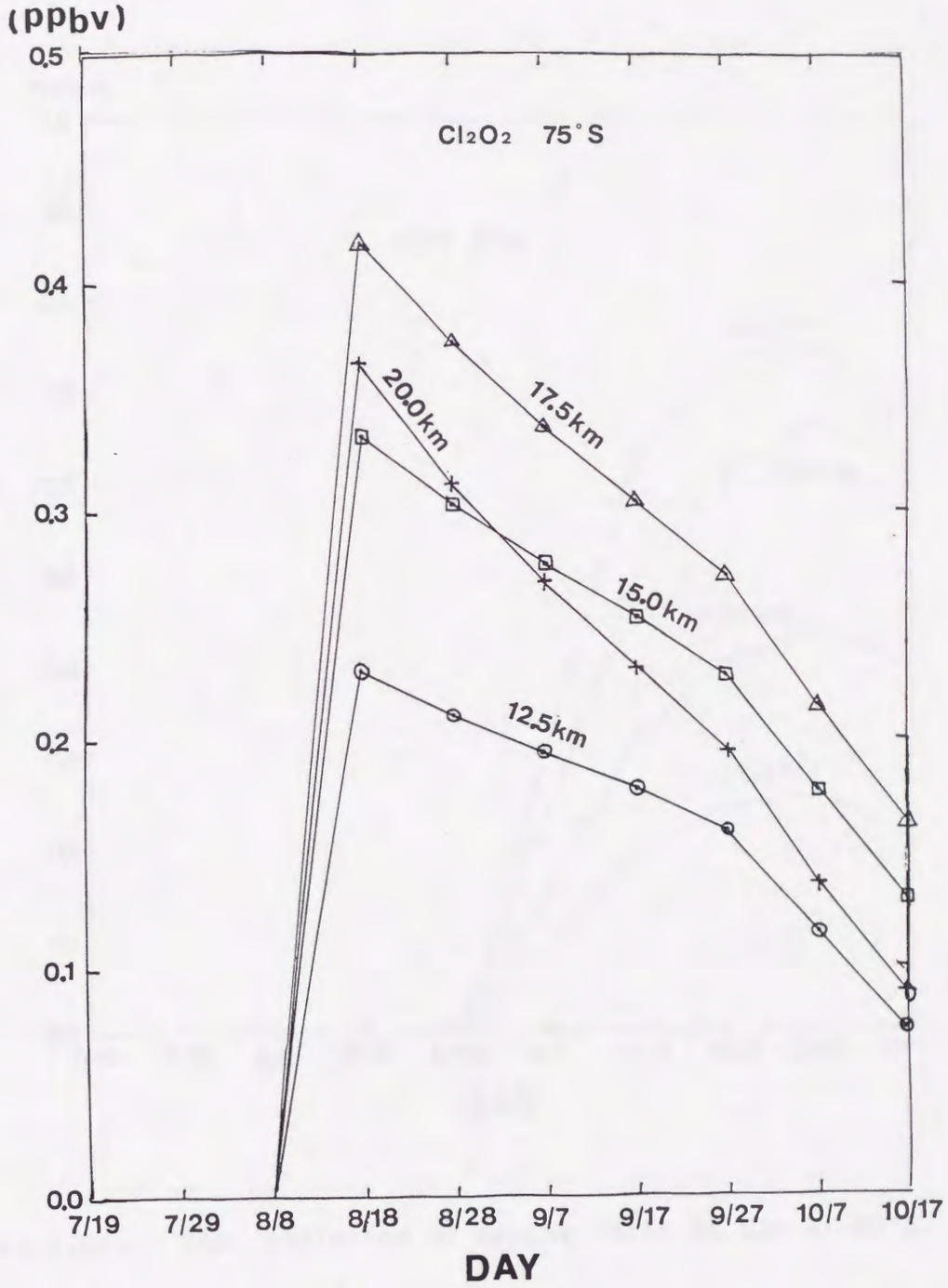

Figure 4.5b. Time evolution of mixing ratio of Cl_2O_2 at 75°S.

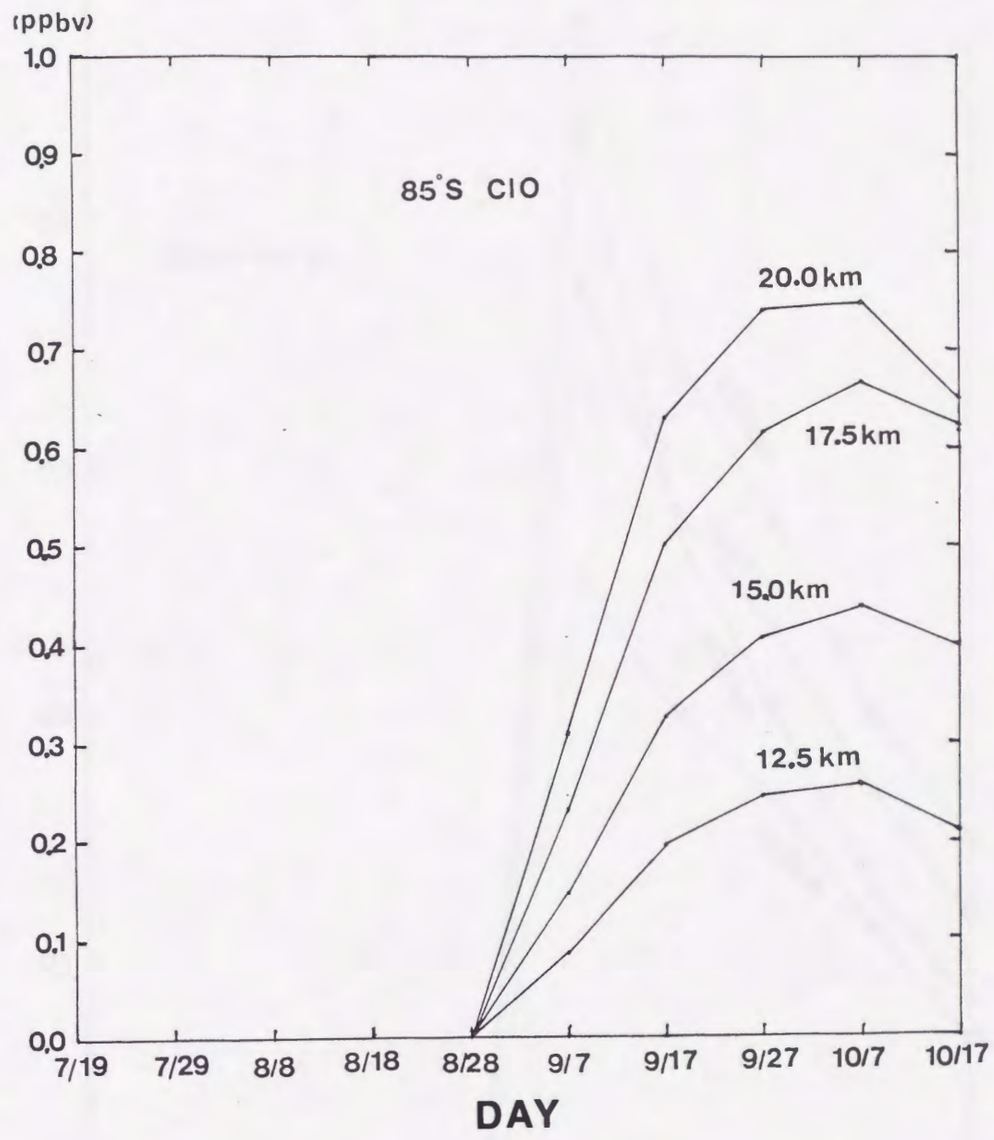

Figure 4.5c. Time evolution of mixing ratio of ClO at 85°S.

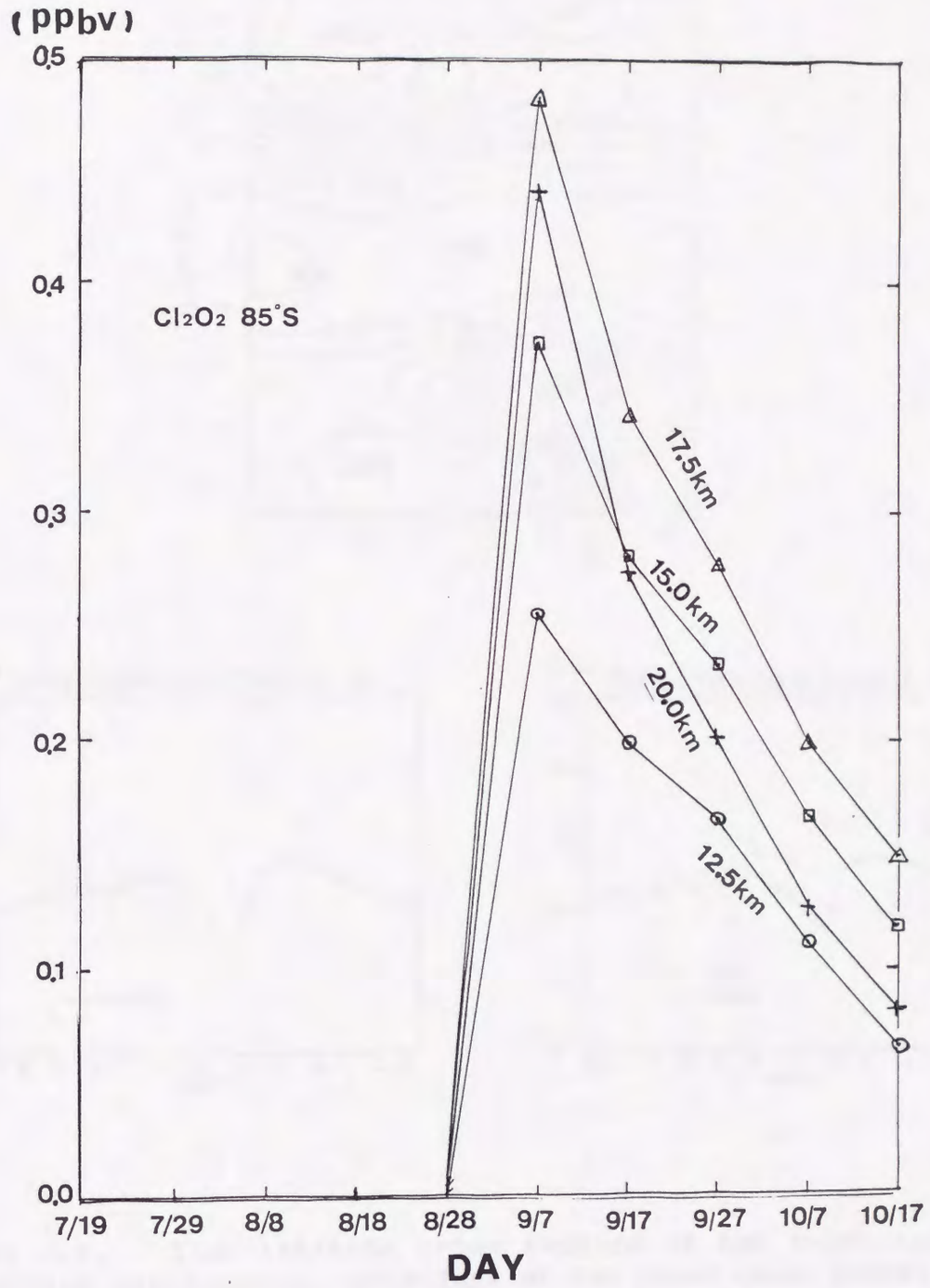

Figure 4.5d. Time evolution of mixing ratio of Cl_2O_2 at 85°S.

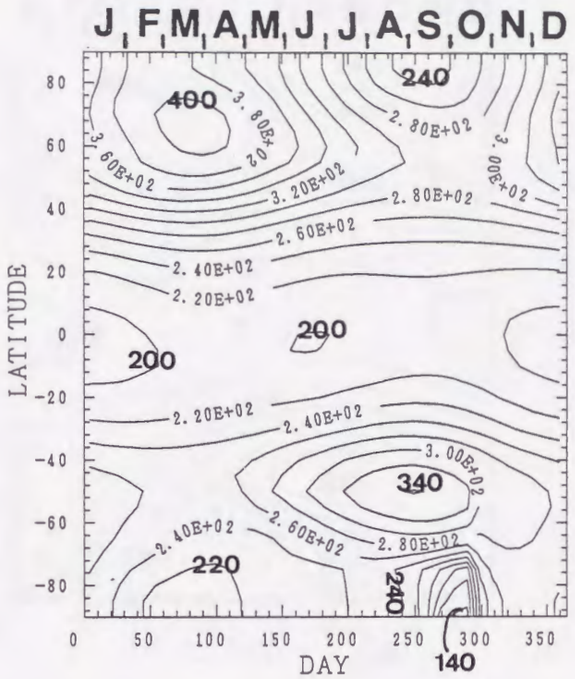

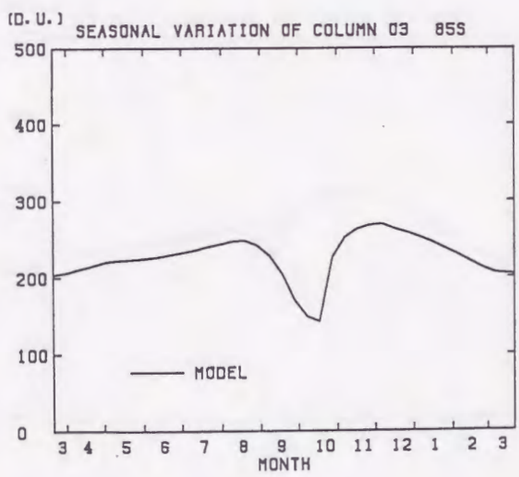

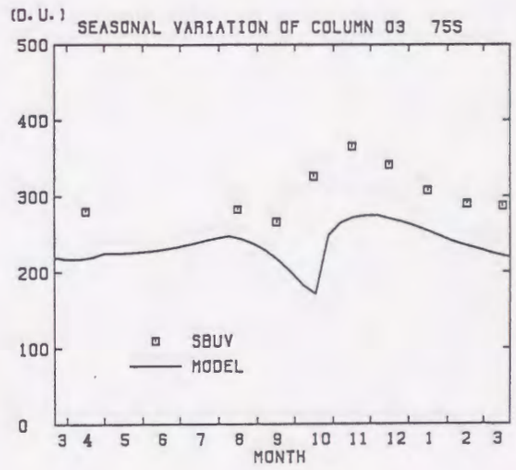

Figure 4.6. Time-latitude cross section of the total ozone amount and the seasonal variations of the total ozone amount at 85°S and 75°S. Temperature at 12.5 km, 15.0 km, 17.5 km, and 20.0 km between 70°S and 90°S is fixed at 192 K from June 19 to October 18. The other conditions are the same as Figure 4.1.

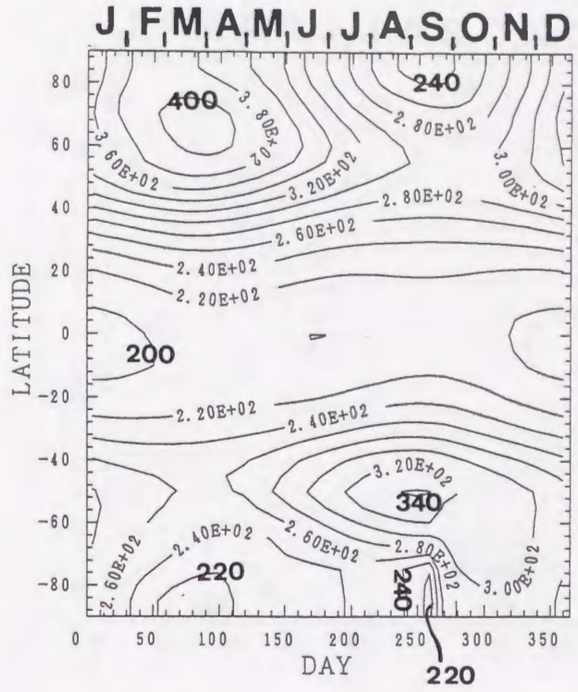

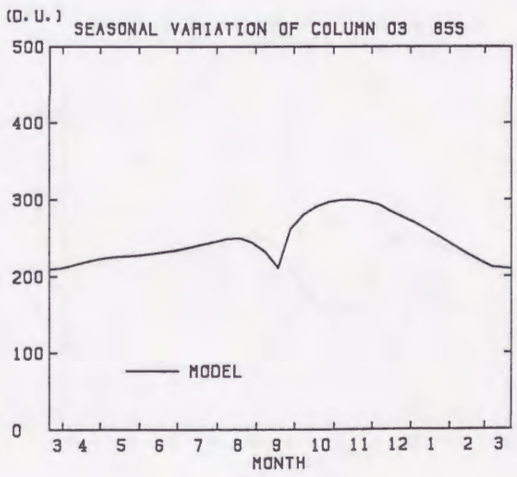

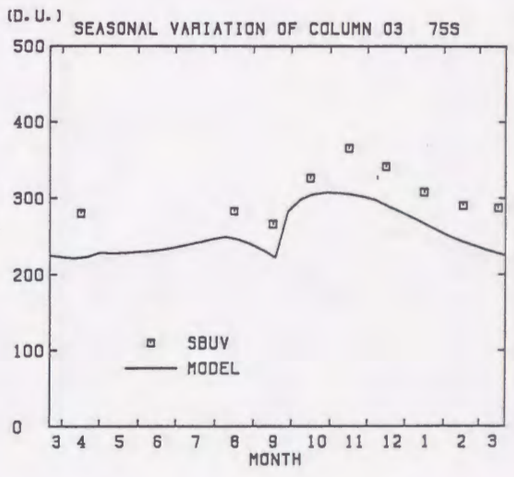

Figure 4.7. Time-latitude cross section of the total ozone amount and the seasonal variations of the total ozone amount at 85°S and 75°S. K_{yy} between 55°S and 75°S is increased on September 18, and at the same time, the chlorine chemistry is stopped. The other conditions are the same as Figure 4.1.

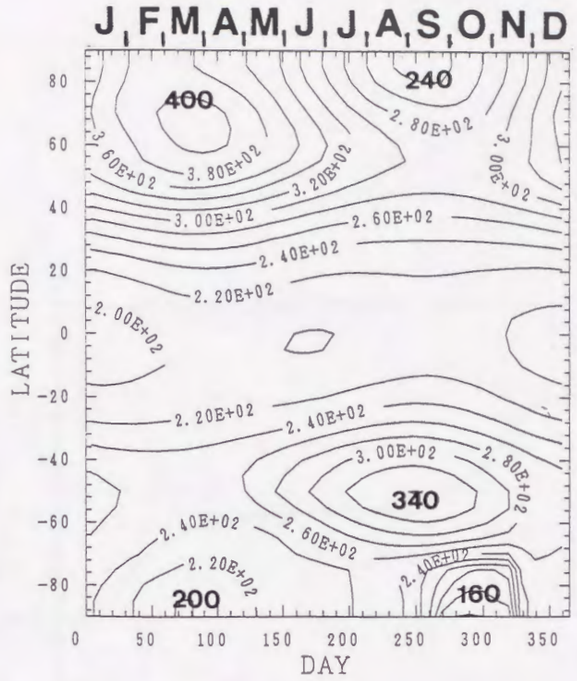

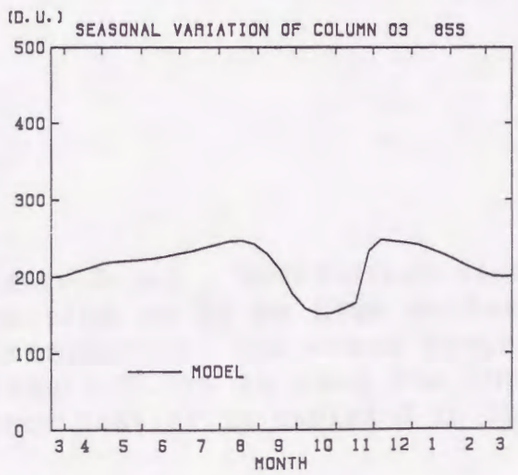

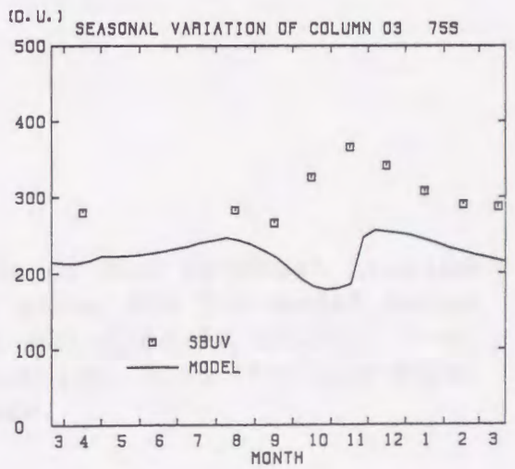

Figure 4.8. Same as Figure 4.7, but K_{yy} is increased on November 17, and at the same time, the chlorine chemistry is stopped.

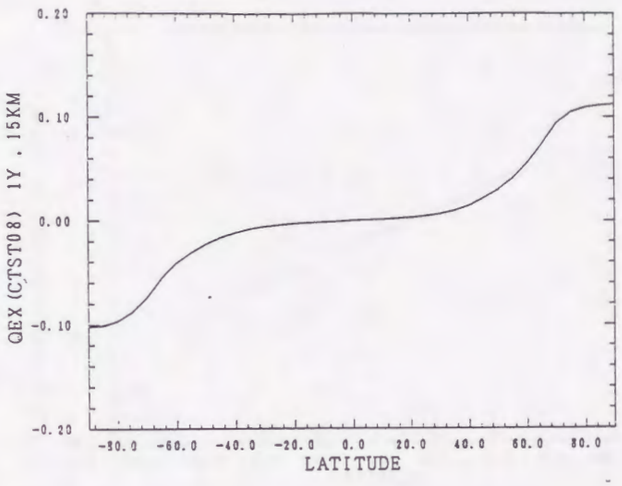

Figure 5.1a. Latitudinal distribution of the external heating function at 15 km high estimated by using the 2-D model ozone distribution. The ozone distribution obtained in Chapter 3-e) (Figure 3.38) is used for the calculation. Note that the water vapor heating is excluded in this figure.

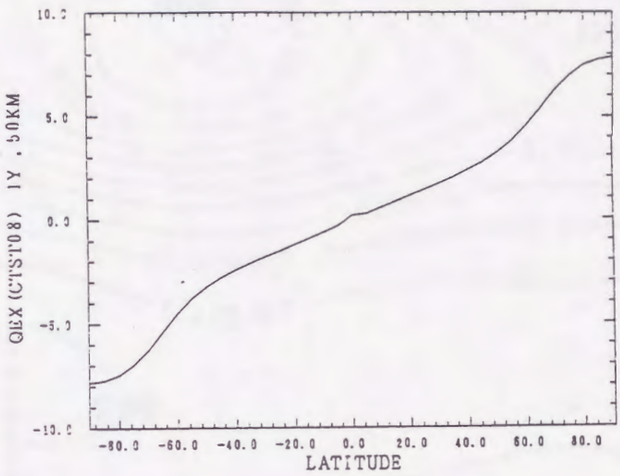

Figure 5.1b. Same as Figure 5.1a, but at 50 km high.

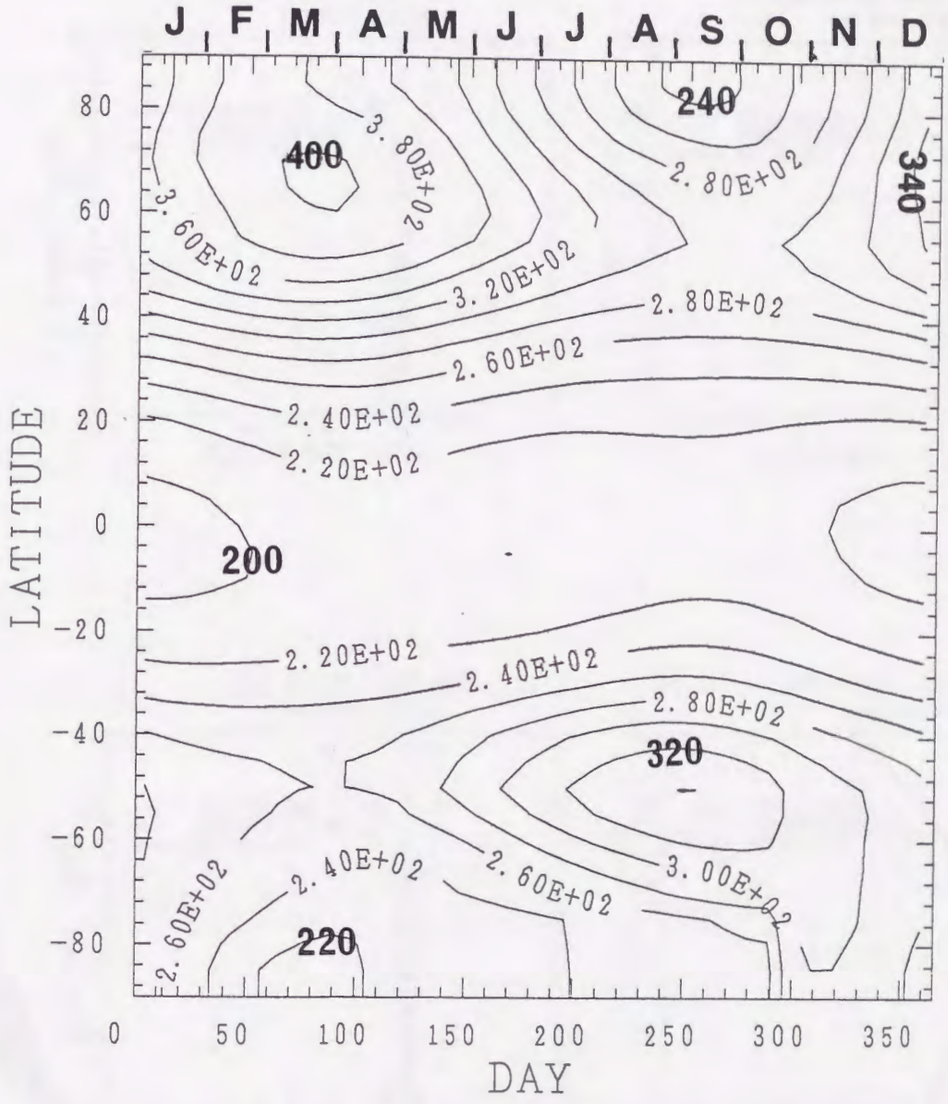

Figure 5.2. Same as Figure 3.38, but the external heating function consistent with the ozone distribution in the model (see Figure 5.1a and 5.1b) is used between the surface and 62.5 km. The effect of the water vapor heating on the external heating function is also added between the surface and 37.5 km.

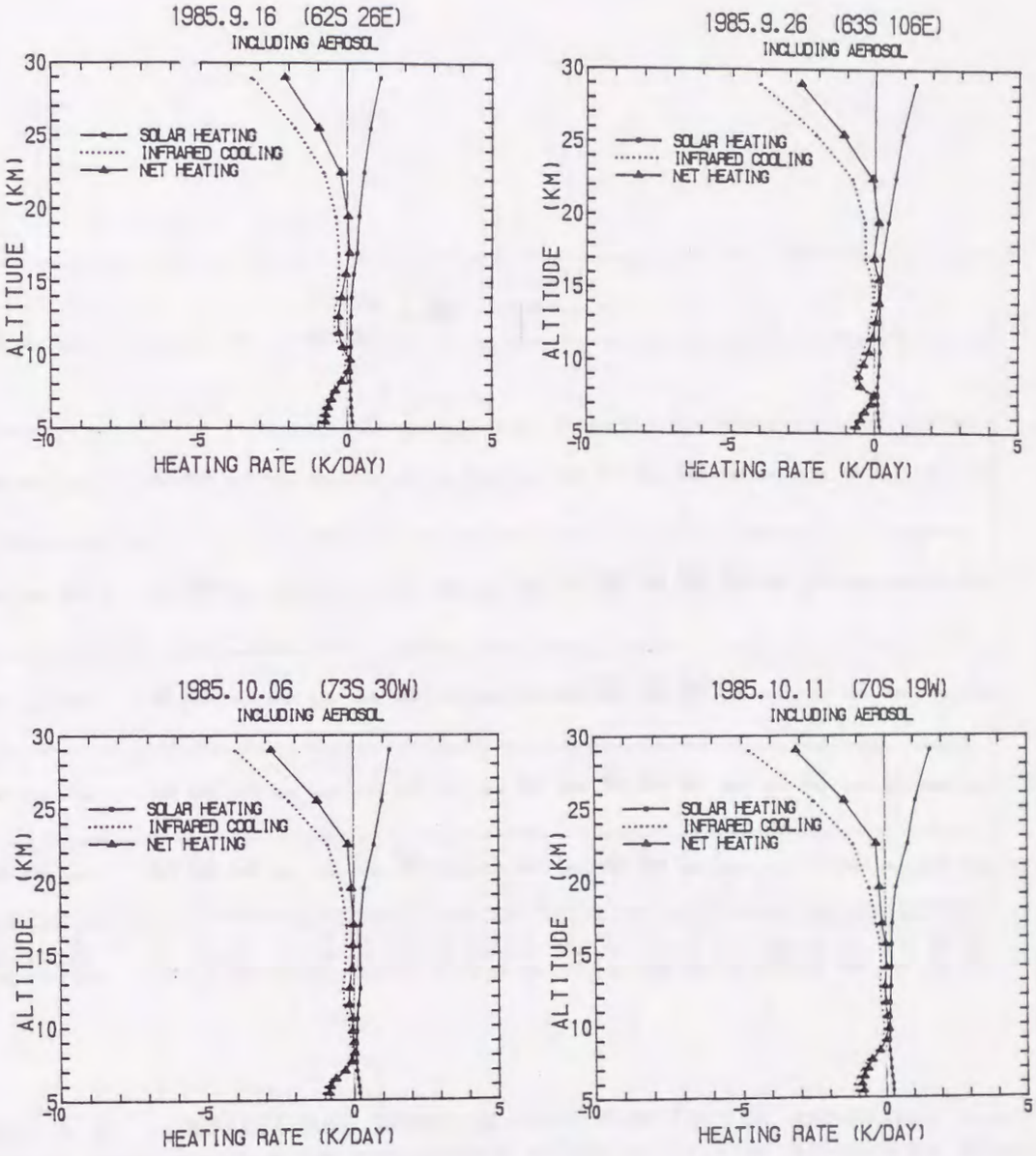

Figure A.1. Diurnally averaged atmospheric heating rates including the aerosol heating effect on September 16, September 26, October 6, and October 11 in 1985. Solid line, dotted line, and the line with triangles denote solar heating, thermal cooling, and net heating, respectively. These calculations are based on SAGEII data.

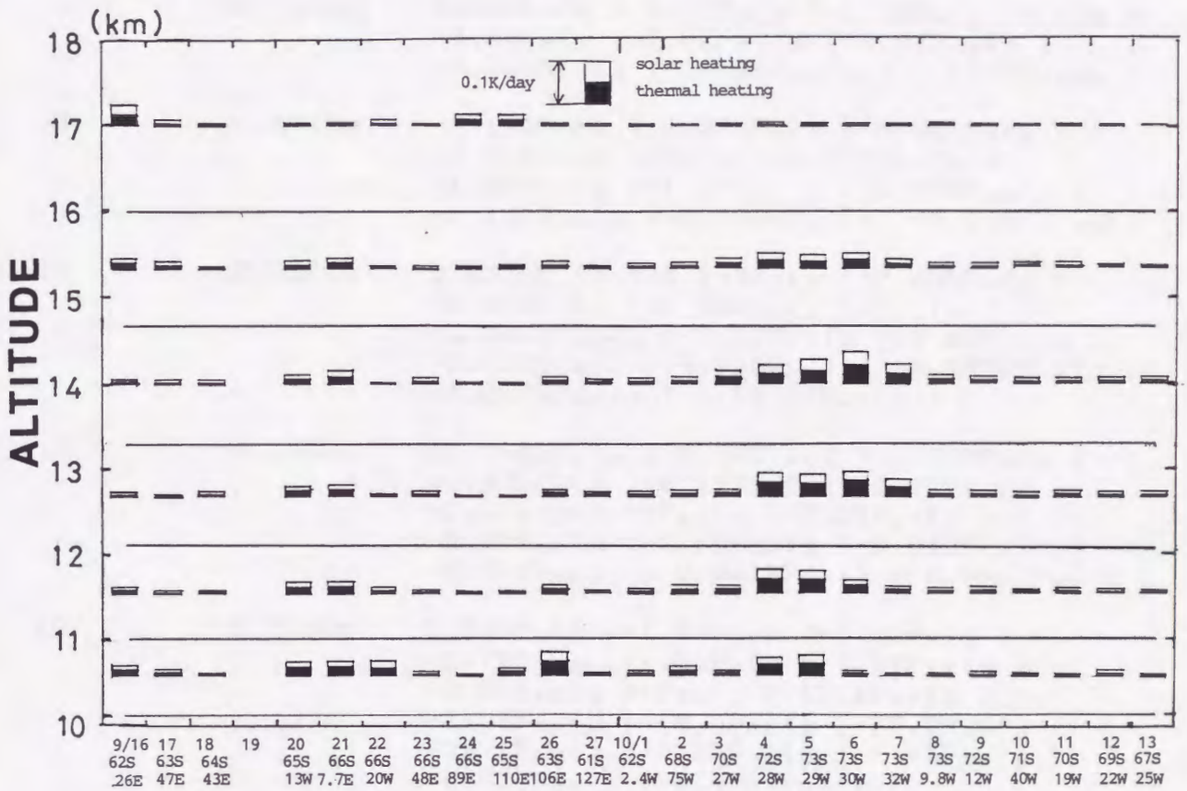

Figure A.2. Additional heating rate due to the aerosols, i.e., [heating rate including radiative effects of the aerosols] minus [heating rate without them]. The white part indicates the solar heating, and the black part indicates the thermal heating. Dates, latitudes, and longitudes of the data used in this calculation are indicated in abscissa. The heating rate scale to 0.1 K d^{-1} is also indicated in the figure.

Mode	Equivalent depth	Eigenfunction
1	-10.82km	$P_1(\mu)+0.807P_3(\mu)+0.120P_5(\mu)+0.00727P_7(\mu)$
3	-2.484km	$-0.398P_1(\mu)+P_3(\mu)+1.57P_5(\mu)+0.582P_7(\mu)$ $+0.101P_9(\mu)+0.0101P_{11}(\mu)$
5	-1.067km	$0.648P_1(\mu)-1.99P_3(\mu)+P_5(\mu)+5.37P_7(\mu)$ $+3.51P_9(\mu)+1.09P_{11}(\mu)+0.204P_{13}(\mu)$ $+0.0230P_{15}(\mu)$
7	-0.590km	$0.329P_1(\mu)-1.07P_3(\mu)+1.25P_5(\mu)+P_7(\mu)$ $-3.50P_9(\mu)-3.92P_{11}(\mu)-1.87P_{13}(\mu)$ $-0.535P_{15}(\mu)-0.105P_{17}(\mu)-0.0142P_{19}(\mu)$
9	-0.374km	$-0.106P_1(\mu)+0.354P_3(\mu)-0.516P_5(\mu)$ $+0.113P_7(\mu)+P_9(\mu)-0.823P_{11}(\mu)$ $-1.96P_{13}(\mu)-1.37P_{15}(\mu)-0.553P_{17}(\mu)$ $-0.151P_{19}(\mu)-0.0305P_{21}(\mu)-0.00367P_{23}(\mu)$
11	-0.258km	$0.0730P_1(\mu)-0.248P_3(\mu)+0.401P_5(\mu)$ $-0.274P_7(\mu)-0.386P_9(\mu)+P_{11}(\mu)$ $+0.0872P_{13}(\mu)-1.55P_{15}(\mu)-1.65P_{17}(\mu)$ $-0.905P_{19}(\mu)-0.329P_{21}(\mu)-0.0875P_{23}(\mu)$ $-0.0179P_{25}(\mu)-0.00198P_{27}(\mu)$
13	-0.188km	$-0.0862P_1(\mu)+0.295P_3(\mu)-0.505P_5(\mu)$ $+0.475P_7(\mu)+0.117P_9(\mu)-1.09P_{11}(\mu)$ $+P_{13}(\mu)+1.17P_{15}(\mu)-1.39P_{17}(\mu)$ $-2.67P_{19}(\mu)-2.00P_{21}(\mu)-0.940P_{23}(\mu)$ $-0.318P_{25}(\mu)-0.0828P_{27}(\mu)-0.0157P_{29}(\mu)$
15	-0.143km	$0.563P_1(\mu)-1.94P_3(\mu)+3.43P_5(\mu)$ $-3.78P_7(\mu)+1.01P_9(\mu)+5.27P_{11}(\mu)$ $-9.31P_{13}(\mu)+P_{15}(\mu)+13.2P_{17}(\mu)$ $-1.39P_{19}(\mu)-18.8P_{21}(\mu)-20.0P_{23}(\mu)$ $-12.1P_{25}(\mu)-5.12P_{27}(\mu)-1.65P_{29}(\mu)$ $-0.423P_{31}(\mu)-0.0807P_{33}(\mu)$
17	-0.113km	$0.0780P_1(\mu)-0.270P_3(\mu)+0.489P_5(\mu)$ $-0.590P_7(\mu)+0.331P_9(\mu)+0.443P_{11}(\mu)$ $-1.30P_{13}(\mu)+1.01P_{15}(\mu)+P_{17}(\mu)$ $-1.92P_{19}(\mu)-1.26P_{21}(\mu)+1.99P_{23}(\mu)$ $+3.52P_{25}(\mu)+2.79P_{27}(\mu)+1.46P_{29}(\mu)$ $+0.571P_{31}(\mu)+0.177P_{33}(\mu)+0.0433P_{35}(\mu)$ $+0.00145P_{37}(\mu)$
19	-0.0913km	$-0.0392P_1(\mu)+0.136P_3(\mu)-0.250P_5(\mu)$ $+0.321P_7(\mu)-0.241P_9(\mu)-0.0882P_{11}(\mu)$ $+0.570P_{13}(\mu)-0.732P_{15}(\mu)+0.0377P_{17}(\mu)$ $+P_{19}(\mu)-0.537P_{21}(\mu)-1.27P_{23}(\mu)$ $+0.268P_{25}(\mu)+1.82P_{27}(\mu)+1.98P_{29}(\mu)$ $+1.29P_{31}(\mu)+0.610P_{33}(\mu)+0.225P_{35}(\mu)$ $+0.0677P_{37}(\mu)+0.0170P_{39}(\mu)+0.00299P_{41}(\mu)$

$P_1(\mu)$ are Legendre Polynomials.

Table 3.1. Eigenfunction and equivalent depth of each Hough mode for the zonal-mean annual cycle.

	T(ϕ , z, June 20) (K)			u(ϕ , z, June 20) (m/s)		
	30°N	45°N	75°N	30°N	45°N	75°N
10km	227.	228.	230.	-4.01	-2.01	-0.407
20km	217.	219.	228.	-6.64	-6.55	-3.19
30km	230.	232.	237.	-13.0	-14.6	-6.31
40km	259.	267.	276.	-30.0	-26.9	-9.21
50km	272.	277.	300.	-55.2	-52.4	-19.1
60km	252.	252.	262.	-57.6	-62.2	-35.5
70km	218.	215.	204.	-44.4	-64.0	-45.5

	v(ϕ , z, June 20) (m/s)			w(ϕ , z, June 20) (mm/s)		
	30°N	45°N	75°N	30°N	45°N	75°N
10km	-3.17E-2	4.12E-3	-1.04E-2	1.67E-1	6.94E-2	1.24E-1
20km	-9.45E-3	-6.88E-4	-7.37E-5	1.46E-1	1.76E-1	2.10E-1
30km	-7.93E-2	-7.11E-2	-2.86E-2	5.09E-1	4.59E-1	4.18E-1
40km	-1.06E-1	-6.85E-2	-2.81E-2	1.35E00	1.17E00	9.50E-1
50km	-8.07E-1	-5.90E-1	-1.44E-1	2.21E00	2.21E00	3.13E00
60km	-1.40E00	-1.12E00	-5.05E-1	2.15E00	2.71E00	5.22E00
70km	-2.01E00	-2.05E00	-1.06E00	6.85E-1	2.23E00	7.22E00

Table 3.2. The values of temperature and anti-symmetric circulation at 30°N, 45°N, and 75°N on June 20.

1.	$O_2 + h\nu \rightarrow O + O$	J_{O2}	
2.	$O_3 + h\nu \rightarrow O_2 + O$	J_{O3}	
3.	$Cl_2 + h\nu \rightarrow 2\ Cl$	J_{Cl2}	
4.	$Cl_2O_2 + h\nu \rightarrow ClOO + Cl$	J_{Cl2O2}	
5.	$HNO_3 + h\nu \rightarrow OH + NO_2$	J_{HNO3}	
6.	$ClNO_3 + h\nu \rightarrow ClO + NO_2$	J_{ClNO3}	
7.	$O + O_2 + M \rightarrow O_3 + M$	$1.1 \times 10^{-34} \cdot e^{510/T}$	Hartmann(1978)
8.	$O + O_3 \rightarrow 2\ O_2$	$3.5 \times 10^{-12} \cdot e^{-1300/T}$	Hartmann(1978)
9.	$Cl + O_3 \rightarrow ClO + O_2$	$2.9 \times 10^{-11} \cdot e^{-260/T}$	
10.	$ClO + ClO + M \rightarrow Cl_2O_2 + M$	see JPL 90-1	
11.	$ClOO + M \rightarrow Cl + O_2 + M$	$(2.7 \times 10^{-33} \cdot (T/300)^{-1.5})/(5.7 \times 10^{-25} \cdot e^{2500/T})$	
12.	$ClO + NO_2 + M \rightarrow ClNO_3 + M$	see JPL 90-1	
13.	$ClO + O \rightarrow Cl + O_2$	$3.0 \times 10^{-11} \cdot e^{70/T}$	

Table 4.1. Photochemical reactions considered in the model with reaction coefficients recommended in JPL 90-1 (Jet Propulsion Laboratory, 1990).

85°S ClO mixing ratio (ppbv)

Day	8/08	8/18	8/28	9/07	9/17	9/27	10/07	10/17
z(km)								
12.5	0.00	0.00	0.00	0.087	0.20	0.25	0.26	0.21
15.0	0.00	0.00	0.00	0.15	0.33	0.41	0.44	0.40
17.5	0.00	0.00	0.00	0.23	0.50	0.62	0.67	0.62
20.0	0.00	0.00	0.00	0.31	0.63	0.74	0.75	0.65

85°S Cl_2O_2 mixing ratio (ppbv)

Day	8/08	8/18	8/28	9/07	9/17	9/27	10/07	10/17
z(km)								
12.5	0.00	0.00	0.00	0.26	0.20	0.17	0.11	0.066
15.0	0.00	0.00	0.00	0.37	0.28	0.23	0.17	0.12
17.5	0.00	0.00	0.00	0.48	0.34	0.28	0.20	0.15
20.0	0.00	0.00	0.00	0.44	0.27	0.20	0.13	0.082

85°S NO_2 mixing ratio (pptv)

Day	8/08	8/18	8/28	9/07	9/17	9/27	10/07	10/17
z(km)								
12.5	0.00	0.00	0.00	0.005	0.021	0.050	0.32	0.59
15.0	0.00	0.00	0.00	0.007	0.027	0.060	0.37	0.62
17.5	0.00	0.00	0.00	0.010	0.038	0.081	0.48	0.77
20.0	0.00	0.00	0.00	0.026	0.11	0.22	1.10	1.90

85°S HNO_3 mixing ratio (ppbv)

Day	8/08	8/18	8/28	9/07	9/17	9/27	10/07	10/17
z(km)								
12.5	2.00	2.00	2.00	2.00	2.00	2.00	6.00	6.00
15.0	2.00	2.00	2.00	2.00	2.00	2.00	6.00	6.00
17.5	2.00	2.00	2.00	2.00	2.00	2.00	6.00	6.00
20.0	3.00	3.00	3.00	3.00	3.00	3.00	7.50	7.50

Table 4.2a. Time-evolution of the mixing ratio of ClO, Cl_2O_2, N_2O, and HNO_3 at 85°S in the model.

75°S ClO mixing ratio (ppbv)

Day	8/08	8/18	8/28	9/07	9/17	9/27	10/07	10/17
z(km)								
12.5	0.00	0.14	0.17	0.20	0.22	0.23	0.22	0.20
15.0	0.00	0.23	0.28	0.33	0.36	0.39	0.39	0.37
17.5	0.00	0.36	0.44	0.50	0.55	0.60	0.60	0.58
20.0	0.00	0.46	0.55	0.62	0.67	0.71	0.67	0.60

75°S Cl_2O_2 mixing ratio (ppbv)

Day	8/08	8/18	8/28	9/07	9/17	9/27	10/07	10/17
z(km)								
12.5	0.00	0.23	0.21	0.19	0.18	0.16	0.12	0.073
15.0	0.00	0.33	0.30	0.28	0.25	0.23	0.18	0.13
17.5	0.00	0.42	0.37	0.34	0.30	0.27	0.22	0.16
20.0	0.00	0.37	0.31	0.27	0.23	0.20	0.14	0.088

75°S NO_2 mixing ratio (pptv)

Day	8/08	8/18	8/28	9/07	9/17	9/27	10/07	10/17
z(km)								
12.5	0.00	0.009	0.017	0.030	0.047	0.071	0.34	0.54
15.0	0.00	0.012	0.022	0.037	0.059	0.087	0.40	0.58
17.5	0.00	0.017	0.031	0.052	0.081	0.12	0.52	0.74
20.0	0.00	0.047	0.085	0.14	0.22	0.32	1.2	1.8

75°S HNO_3 mixing ratio (ppbv)

Day	8/08	8/18	8/28	9/07	9/17	9/27	10/07	10/17
z(km)								
12.5	2.00	2.00	2.00	2.00	2.00	2.00	6.00	6.00
15.0	2.00	2.00	2.00	2.00	2.00	2.00	6.00	6.00
17.5	2.00	2.00	2.00	2.00	2.00	2.00	6.00	6.00
20.0	3.00	3.00	3.00	3.00	3.00	3.00	7.50	7.50

Table 4.2b. Time-evolution of the mixing ratio of ClO, Cl_2O_2, N_2O, and HNO_3 at 75°S in the model.

85°S ClO mixing ratio (ppbv)

Day z(km)	8/08	8/18	8/28	9/07	9/17	9/27	10/07	10/17
12.5	0.00	0.00	0.00	0.068	0.16	0.20	0.21	0.17
15.0	0.00	0.00	0.00	0.12	0.26	0.33	0.36	0.32
17.5	0.00	0.00	0.00	0.19	0.41	0.51	0.56	0.52
20.0	0.00	0.00	0.00	0.26	0.54	0.64	0.65	0.57

85°S Cl_2O_2 mixing ratio (ppbv)

Day z(km)	8/08	8/18	8/28	9/07	9/17	9/27	10/07	10/17
12.5	0.00	0.00	0.00	0.26	0.22	0.19	0.13	0.077
15.0	0.00	0.00	0.00	0.39	0.31	0.27	0.20	0.15
17.5	0.00	0.00	0.00	0.50	0.39	0.33	0.25	0.19
20.0	0.00	0.00	0.00	0.47	0.32	0.26	0.17	0.12

85°S NO_2 mixing ratio (pptv)

Day z(km)	8/08	8/18	8/28	9/07	9/17	9/27	10/07	10/17
12.5	0.00	0.00	0.00	0.004	0.016	0.037	0.24	0.43
15.0	0.00	0.00	0.00	0.005	0.020	0.044	0.26	0.43
17.5	0.00	0.00	0.00	0.008	0.028	0.058	0.33	0.51
20.0	0.00	0.00	0.00	0.021	0.078	0.15	0.72	1.2

85°S HNO_3 mixing ratio (ppbv)

Day z(km)	8/08	8/18	8/28	9/07	9/17	9/27	10/07	10/17
12.5	2.00	2.00	2.00	2.00	2.00	2.00	6.00	6.00
15.0	2.00	2.00	2.00	2.00	2.00	2.00	6.00	6.00
17.5	2.00	2.00	2.00	2.00	2.00	2.00	6.00	6.00
20.0	3.00	3.00	3.00	3.00	3.00	3.00	7.50	7.50

Table 4.3a. Same as Table 4.2a, but temperature at 12.5 km, 15.0 km, 17.5 km, and 20.0 km between 70°S and 90°S is fixed at 192 K from June 19 to October 18.

75°S ClO mixing ratio (ppbv)

Day	8/08	8/18	8/28	9/07	9/17	9/27	10/07	10/17
z(km)								
12.5	0.00	0.11	0.13	0.16	0.17	0.19	0.18	0.16
15.0	0.00	0.18	0.23	0.26	0.29	0.32	0.31	0.30
17.5	0.00	0.29	0.36	0.41	0.46	0.49	0.49	0.48
20.0	0.00	0.40	0.48	0.54	0.58	0.61	0.58	0.52

75°S Cl_2O_2 mixing ratio (ppbv)

Day	8/08	8/18	8/28	9/07	9/17	9/27	10/07	10/17
z(km)								
12.5	0.00	0.24	0.23	0.21	0.20	0.18	0.13	0.084
15.0	0.00	0.36	0.33	0.31	0.29	0.27	0.21	0.16
17.5	0.00	0.45	0.41	0.38	0.35	0.32	0.26	0.21
20.0	0.00	0.40	0.35	0.31	0.28	0.24	0.18	0.12

75°S NO_2 mixing ratio (pptv)

Day	8/08	8/18	8/28	9/07	9/17	9/27	10/07	10/17
z(km)								
12.5	0.00	0.007	0.013	0.022	0.035	0.052	0.25	0.40
15.0	0.00	0.009	0.016	0.027	0.043	0.063	0.28	0.42
17.5	0.00	0.013	0.024	0.039	0.059	0.084	0.36	0.51
20.0	0.00	0.038	0.066	0.11	0.16	0.22	0.81	1.2

75°S HNO_3 mixing ratio (ppbv)

Day	8/08	8/18	8/28	9/07	9/17	9/27	10/07	10/17
z(km)								
12.5	2.00	2.00	2.00	2.00	2.00	2.00	6.00	6.00
15.0	2.00	2.00	2.00	2.00	2.00	2.00	6.00	6.00
17.5	2.00	2.00	2.00	2.00	2.00	2.00	6.00	6.00
20.0	3.00	3.00	3.00	3.00	3.00	3.00	7.50	7.50

Table 4.3b. Same as Table 4.2b, but temperature at 12.5 km, 15.0 km, 17.5 km, and 20.0 km between 70°S and 90°S is fixed at 192 K from June 19 to October 18.

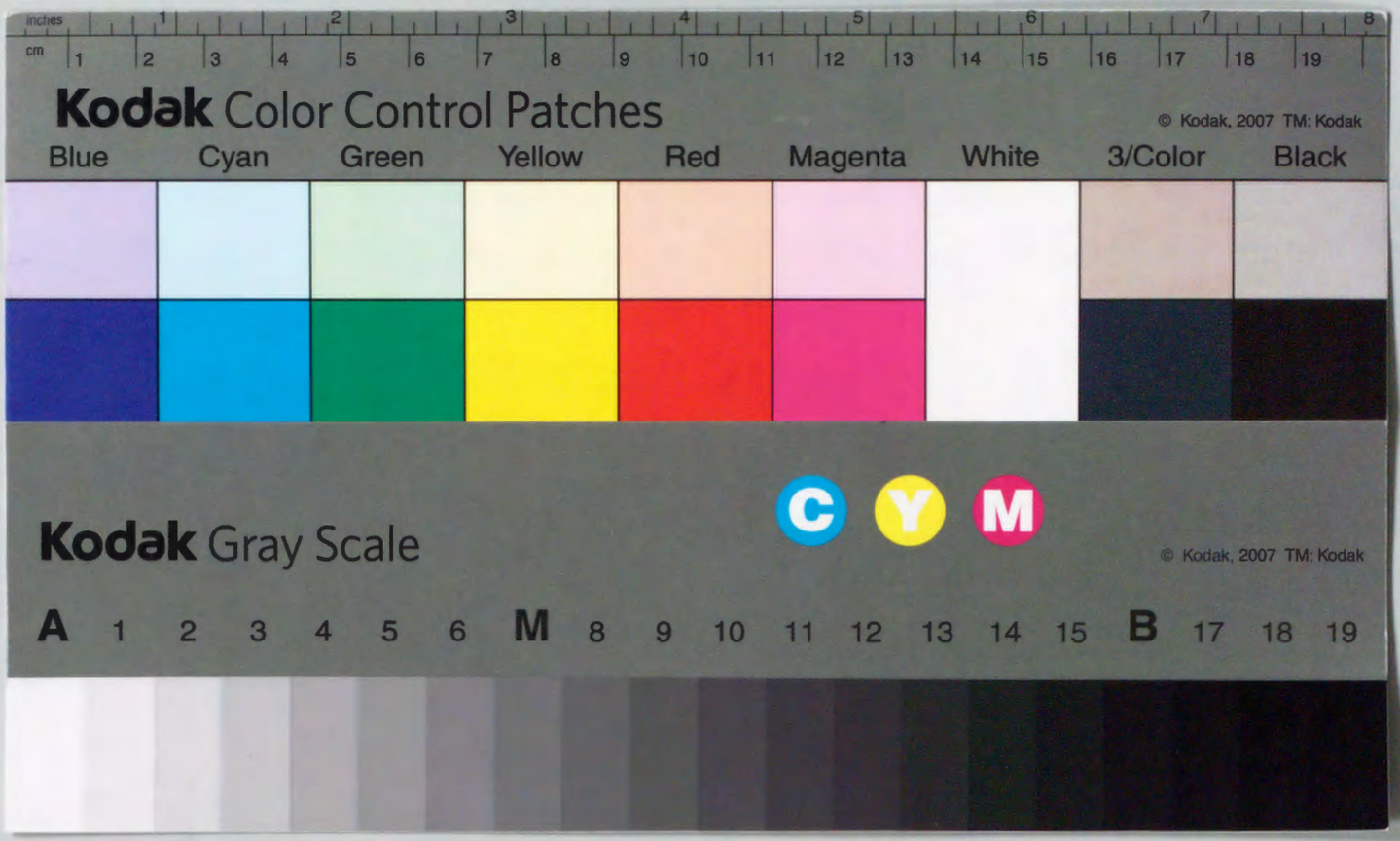
inches
cm
Kodak Color Control Patches
© Kodak, 2007 TM: Kodak
Blue
Cyan
Green
Yellow
Red
Magenta
White
3/Color
Black
Kodak Gray Scale
C
Y
M
© Kodak, 2007 TM: Kodak
A 1 2 3 4 5 6 M 8 9 10 11 12 13 14 15 B 17 18 19